FHR 2901-5
1 December 1966

FINAL REPORT

RESEARCH ON MICROMINIATURE PASSIVE TELEMETRY FOR BIOLOGICAL MEASUREMENTS

Contract NASw-789

Prepared for

Office of Advanced Research & Technology
National Aeronautics and Space Administration
Washington, D. C.

FAIRCHILD HILLER
Republic Aviation Division
Farmingdale, L.I., New York 11735

TABLE OF CONTENTS

TABLE OF CONTENTS (Cont'd)

LIST OF ILLUSTRATIONS

LIST OF ILLUSTRATIONS (Cont'd)

SECTION I
SUMMARY

A. PROGRAM DESCRIPTION

The work conducted under Contract NASw-789 and described in this Final Report had an objective which is best described by quoting parts of the Work Statement:

"A research program shall be undertaken to develop physiological passive telemetry devices. These devices are to be used in living organisms to monitor vital biological functions by telemetering. No batteries or other internal power sources will be used on these devices. In operation, external radio frequency energy is beamed on the device which re-radiates a portion of the received energy. Biological signals as sensed by electrodes attached to the device will modulate the radio frequency and thus be observed at an external receiver. The main emphasis of the program is to ascertain those parameters which would limit the capabilities of passive telemetry and to specify the parameters giving reliable operation for the most useful applications. This should result in an accurate picture of the future capabilities of passive telemetry, its fields of usefulness and details of operation which would make possible specific new applications."

The initial contract work, described in Paragraph B, spanned the period 1 October 1963 to 30 September 1964. The second phase of the contract was funded for a period extending from 15 February 1965 to 30 June 1966. This phase called for continuing the research with the objective of increasing the useful range by employing a closed loop frequency modulation system. The range of operation was to be sufficient to transmit information within a cylindrical region 8 feet in length and 5 feet in diameter. Waveforms such as heart muscle potentials were to be transmitted with good fidelity, avoiding the distortion produced by the transformer used in the implant in the initial study phase.

Eight quarterly reports were issued in the course of this research having the following dates and numbers:

First Phase

Quarterly Status Report		Report Number
#1	1 October 1963 to 31 December 1963	RAC 2044
#2	1 January 1964 to 31 March 1964	RAC 2256
#3	1 April 1964 to 30 June 1964	RAC 1729-3
#4	1 July 1964 to 30 September 1964	RAC 1729-4

Continuation Phase

#1	15 February 1965 to 31 May 1965	RAC 2901-1
#2	1 June 1965 to 31 August 1965	RAC 2901-2
#3	1 September 1965 to 30 November 1965	FHR 2901-3
#4	1 December 1965 to 31 March 1966	FHR 2901-4

B. RESULTS ACHIEVED AND PRESENT STATUS

The initial investigation used a single transmitted frequency and a simple tuned circuit implant whose absorption was varied by the desired intelligence to produce amplitude modulation. A range of 4 to 5 inches only was obtained and waveform distortion was severe. A new system was invented which employed two transmitted frequencies and received a third (sum) frequency modulated by the physiological parameter signal.

Following a demonstration of this multifrequency system over a range of several feet using amplitude modulation, funding for the second phase was received to develop a frequency modulation system to improve the signal to noise ratio and range. This system has been constructed and works to the point where phase modulation can be demonstrated, i.e., an antenna excited with 8 and 12 megacylces receives the sum frequency of 20 megacycles which has been phase modulated by an audio frequency signal. The system processes the phase modulated signal, and both the phase modulation itself can be displayed on an oscilloscope or the modulating signal recovered in a phase detector and displayed as the desired intelligence waveform. This, of course, falls short of demonstrating a frequency modulation system but is a very key step since the phase variation is determined by the tuning of a LC resonant circuit in the implant and by means of a phase lock loop it will be possible to track the changing resonant frequency and thereby develop a Δf which when applied to an FM discriminator will produce the desired signal waveform. While

complete circuits have been built (for the FM system) they have not been operated and debugged. Completion of this FM system debugging would require funding for another period of investigation.

C. PROPOSED APPLICATIONS

Some applications for which the battery-less implant would be particularly suitable are the following:

- Studies involving animals where implants must be used because external probes or transmitting packages would not be tolerated by the animals.
- Studies of orbiting primates where a battery powered implant might be too short lived if launch dates were postponed some months after implanting was performed.
- Where it is not necessary to have freedom of motion throughout a volume of space and when telemetry data is needed only for short intervals of time, the antenna may be shrunk down to a configuration of pickup coils only a few inches in diameter which can be placed close to the body. The battery-less implant could be monitored for many, many years in very long term experiments in this manner.
- A location device or beacon which would be powered by external radiation is an interesting modification which does not make use of the implantable feature of this device but which expolits the fact that the life is indefinite. Atomic warheads or the like could identify themselves (when not shielded by metal enclosures or a layer of water) in response to illumination.
- Astronauts exploring the moon might use this technique to provide a battery-less beacon mounted externally on their space suit. It would serve as a back-up device for communicating with their space ship should they suffer a power loss in the prime communication link. Beamed energy at higher frequencies than discussed in this report would be needed.

D. RECOMMENDATIONS

It is recommended that work be continued to finish the present feasibility or laboratory model with one of the applications just mentioned in mind. The steps to be taken would include the following:

- The phase locked loop should be closed and debugged. Complete FM operation can then be demonstrated and performance parameters measured.
- A redesign of the present antenna to increase efficiency, or development of a smaller configuration, depending upon the chosen future application, should be undertaken so that the implant circuitry can then be made compatible with the antenna field strength.

- With antenna and receiving system operation well established, the implant circuit can be firmed up and oriented toward the simplest realization in microcircuits. A microcircuit implant should then be developed in cooperation with an organization having the necessary experience and capabilities.

At the conclusion of these steps a first engineering model of this system would be in existance. Users of the system could test its application to their problem quickly, or make duplicate systems for longer tests. The design of flyable models could then follow on a well established engineering base.

SECTION II
CONTRACT INITIAL PHASE INVESTIGATIONS

A. SINGLE FREQUENCY SYSTEM

1. Description

The basic, single frequency direct-coupled voltage telemetry system consists of three inductively coupled electric circuits: a transmitting coil circuit, an animal-implanted circuit, and a receiving coil circuit (Figure 1). The transmitting and receiving coil circuits may or may not be tuned, but the implanted circuit is always adjusted to be at or near resonance at the transmitted frequency. Magnetic energy from the transmitter is coupled simultaneously to the implant coil and the receiving coil. The magnetic energy which is coupled through an r-f coil in the implant circuit induces a voltage in that circuit. This induced voltage causes currents to flow in the implant. The instantaneous magnitudes of these currents are dependent on:

- The overall Q of the implant circuit
- The magnitude of the induced voltage
- The nearness to resonance of the implanted circuit

A re-radiated field caused by these currents is coupled to the transmitter and receiver coils. The magnitude of this re-radiated field is controlled by the physiological voltage to be telemetered since it varies the closeness to resonance of the implanted circuit. A voltage sensitive capacitor (varicap) is used to tune the implanted circuit via the physiological voltage which varies as a continuous low audio frequency function of time. The variation in the implant's re-radiated field appears as an audio modulation at the receiver input.

Energy that is coupled directly from the transmitter to the receiver is an unwanted quantity since it can cause saturation of the receiver or reduce the percentage modulation at the receiver coil. These effects mask the telemetry

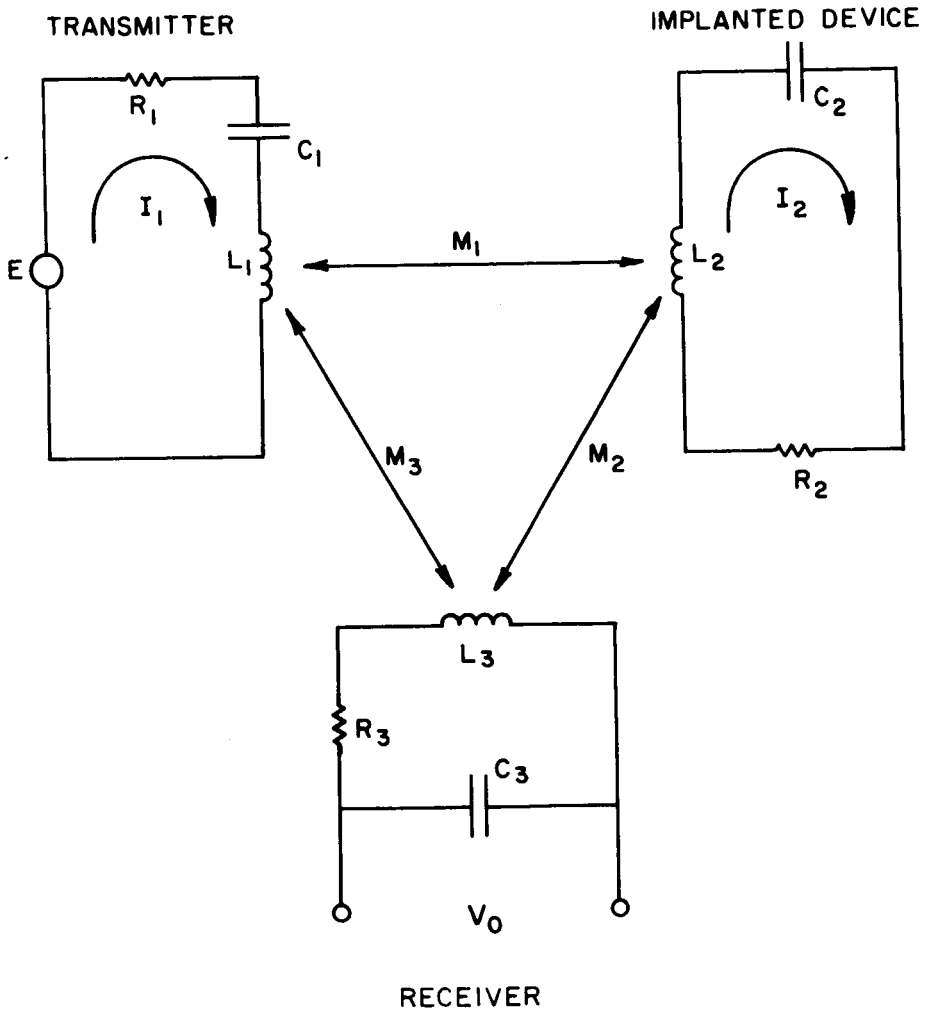

Figure 1. Single Frequency Passive Telemetry System, Schematic Diagram

information. In an optimum system it is desirable to maximize the ratio:

$$\frac{\text{induced voltage at receiver due to implant}}{\text{induced voltage at receiver due to direct couple with transmitter}}$$

2. Problems Encountered

Tests and analysis for different telemetry schemes based on the single frequency principle were conducted using a radio frequency of 7 megacycles. Of the schemes considered, the most promising arrangements involved the coupling of the transmitter r-f induction fields directly to the receiver inductor which considerably reduced the sensitivity of the receiver to small changes in r-f level. These arrangements were:

a. Orthogonal Scheme - In this method, the r-f induction fields of the inductors are approximately dipole fields and the transmitter and receiver inductors are arranged so that their fields are orthogonal and direct coupling is minimized. This may reduce the coupled voltage by a factor of 200 - 1000 compared to the case when the axes of the transmitter and receiver inductors are parallel. In this arrangement, the orientation of the implant device inductors (and their dipole fields) must be intermediate between the transmitter and receiver inductors. The implant inductor must be coupled to the transmitter magnetic field in order to get r-f power; and it must also be coupled to the receiver inductor in order to cause an effect at the receiver. This effect is also dependent on the distances between transmitter, receiver, and implanted device.

b. Double Receiver-Inductor Nulling Scheme - In this method, there are two receiver-tuned circuits whose outputs are subtracted from each other and then applied to the receiver. The implant must be located in positions which are closer to one of the receiver inductors in order for a net signal to appear at the receiver input. High level signals due to coupling from the transmitter to the receiver do not cause receiver saturation because such voltages are nulled at the receiver input by so locating the two receiver inductors that their voltages cancel. This requires that the phase and the amplitude of

the voltages to be nulled be closely controlled. This method reduces the transmitter to receiver coupled voltages by a factor of 200 - 1500 compared to the case of a single transmitter and a single receiver coil.

c. Single Receiver-Inductor Nulling Scheme - In this method there is a single transmitter and a single receiver coupler. The induced voltage in the receiver coupler consists of the high level signal coupled from the transmitter coupler and the small change in that signal level due to the operation of the implant. This may be considered as a high level signal with an extremely small percentage of modulation. Circuitry at the receiver couple is arranged so as to put this signal into two separate channels. One of the channels contains an r-f limiter which levels the output and eliminates the small percentage of modulation due to the implanted device signal The output of this channel is then subtracted from the other unleveled channel. The difference would ideally be a 100% modulated r-f signal whose modulation is due to the device. This method may reduce the transmitter coupled voltage by a factor of 200 or more compared to the case of a single transmitter and single simple transmitter coil.

Tests have indicated that all these methods have disadvantages. The orthogonal and double nulling schemes are extremely sensitive to small changes in the position of the couplers, such as due to vibration, but are relatively insensitive to the presence of small amplitude variations on the r-f transmitter signal. The single inductor nulling scheme is inherently not sensitive to small changes in position, but is sensitive to the presence of small amplitude variations on the r-f transmitter signal. The efficiency of this method is also relatively low.

3. Results Achieved

Turtle, rabbit, and cat heart voltage waveforms and impedance levels were measured and recorded for use in telemetry tests. It was found that rabbit heart voltages obtained on the operating table have the following characteristics:

Amplitude:	10 - 20 millivolts
Source Impedance	2500 ohms
Pulse Width:	70% pts 5-15 milliseconds
Rise Time:	2 - 6 milliseconds
Pulse Repetition Rate:	5 pulses per second

Cat heart voltage pulses are similar, but the repetition rate is slower. Once these measurements were made it was decided to simulate these waveforms for experiment with the telemetry system. A battery operated transistorized pulse generator was fabricated and by appropriate R, L, and C loading, was made to simulate heart voltages in the determined characteristics.

The problem of meeting the range requirements was considered prime in the simulated setup. While minimizing the direct coupling with the transmitter is one way of increasing the ratio given previously, it is also possible to achieve a similar effect by increasing the numerator. To this end it was found that the Q of the implanted circuit and the cross-sectional area of the r-f implant coil were important parameters. The Q of the implant r-f coil was increased from early values of 20 to 40 to values of 150 to 190 by means of single layer windings that tend to reduce distributed capacitance. The implanted r-f coils used in early experiments were fabricated on ferrite bobbins manufactured by Indiana General Corporation. A Q-1 material bobbins with a pole diameter of 0.157 inch was typical. The cross-sectional area was thus 0.019 in.^{2}. Such a coil gave a telemetry range of $3\frac{1}{2}$ - 4 inches. By increasing the size of the coil cross section to 1.5 in.^{2}, ranges up to 10 - 12 inches from the implant to the nearest coupler were obtained.

B. MULTI-FREQUENCY SYSTEM

Based on the results of the early experiments conducted, it was evident that a more sophisticated approach would be required to achieve desirable operational ranges of several feet. To avoid having the small signal of the implant swamped by the signal generator power, received directly at the same frequency, a new scheme was investigated using generator and receiver frequencies which differed widely.

1. Description

As shown in Figure 2, the transmitting system consists of two sources at f_1, f_2 which by virtue of the antenna system generates voltages in the implant coils

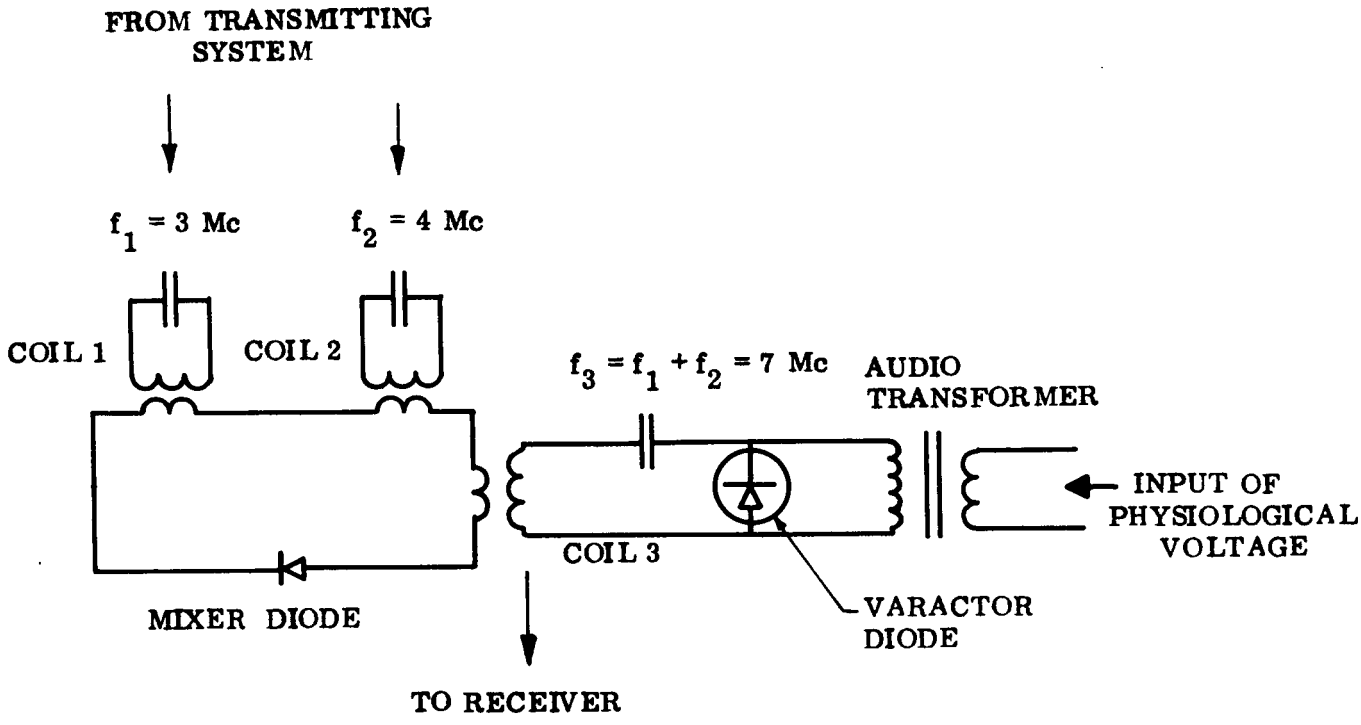

Figure 2. Multi-Frequency Amplitude-Modulation Implant Circuit

1 and 2. In the mixer circuit a signal of frequency $f_3 = f_1 + f_2$ is generated. This is applied to coil 3 whose resonant frequency is controlled from the input voltage through change of the capacitance of the varactor diode. Radiation from coil 3 at f_3 is received at the receiver as an AM signal via the antennas. The antennas are designed to handle the three frequencies simultaneously and efficiently.

The method of establishing the radio frequency fields at the frequencies f_1 and f_2 is shown in the block diagram of the generator - radiator - receiver system (Figure 3). The purpose of the band pass filters is to prevent mixing of the frequencies f_1 and f_2 at any part of the system other than in the implant circuit. This is important for achieving maximum range, as it preserves the degree of modulation on f_3 (7MC) imposed by the physiological voltage being telemetered, and allows a large overall gain to be used in the system.

2. Test Apparatus and Results

The multi-frequency system was built into operating equipment on company funds in the period between the initial funding of the contract and the continuation phase of the contract. Figure 4 shows the implant assembly before potting in silastic; this assembly does not represent the minimum size possible. Figure 5 shows the loop antenna laid out around the edge of an 8' by 4' piece of plywood. Prominent in the foreground are capacitors and coils which tune the antenna for multi-frequency use. In operation, this plywood board is turned upside down and an animal cage fastened to the unencumbered other side. An implant in an animal was not used, tests being by simulation only.

A test of this system gave operation throughout a volume defined by the the extent of the loop antenna, 6' by 3', times a range in the normal direction of about two feet above or below the plywood. The normal direction range would be exploited by having the loop around the middle of a cage four feet high. Simulated heart voltages were used for modulation of the implant device.

At various times considerable noise obscured the signal at the extremes of the indicated range (2' above antenna); this was believed to be due to outside noise sources and possibly incipient corona produced by high RF voltages on the antenna.

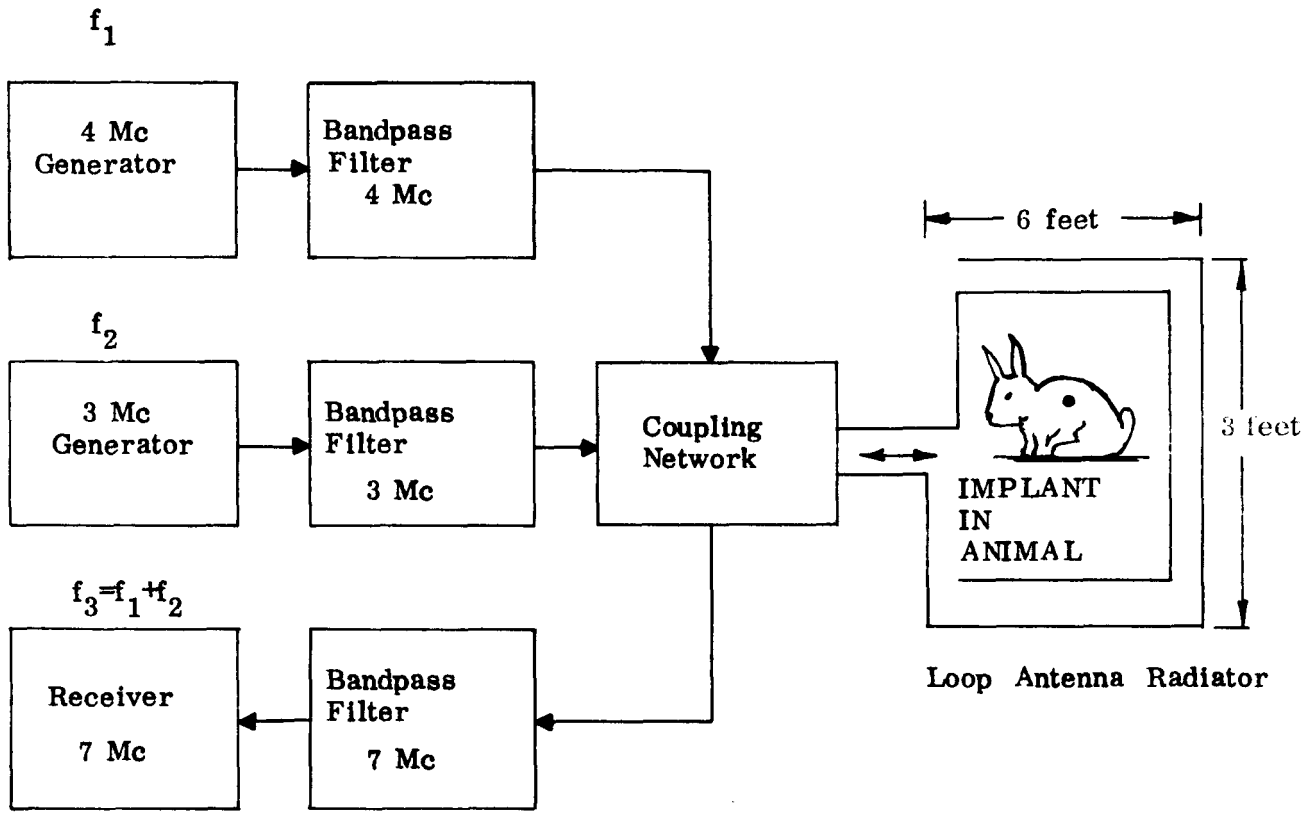

Figure 3. Block Diagram of Generator-Radiator-Receiver System

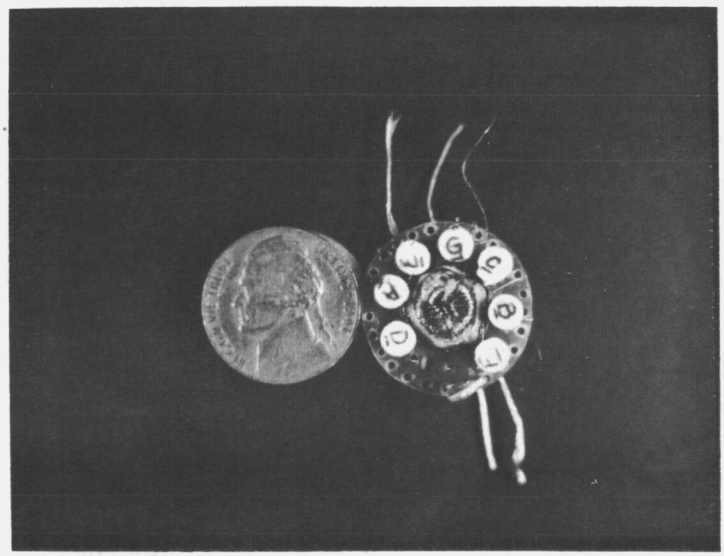

Figure 4. Implant Assembly, Multifrequency AM System

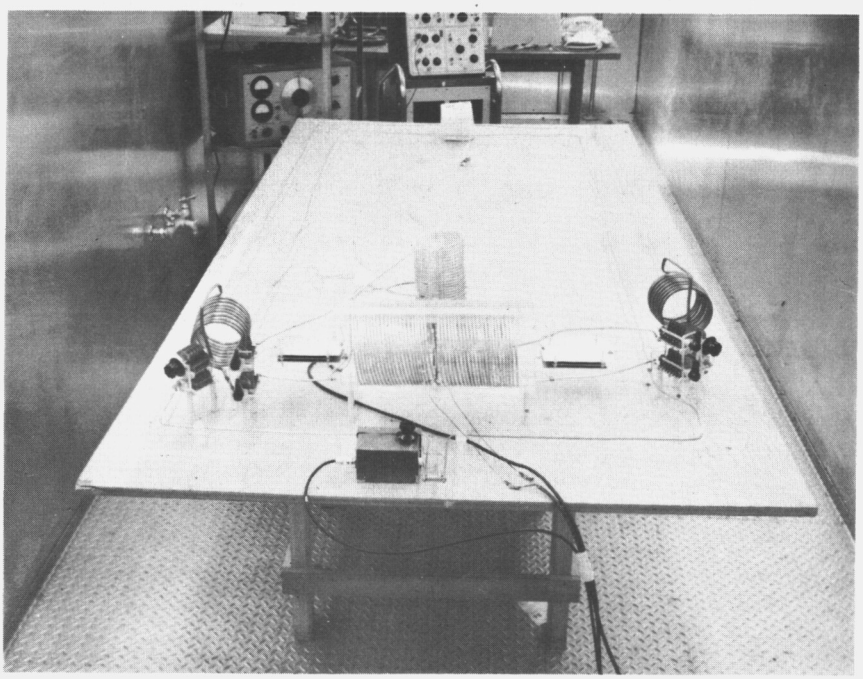

Figure 5. Loop Antenna and Tuning Elements

3. Batteryless Low Frequency Amplifier For Implant Use

A problem of considerable concern is the fidelity with which heart voltages or other physiological voltages can be telemetered. A toroidal transformer with a core of supermalloy was used in early experiments to raise the level of the heart voltage to the level needed for modulation of the varicap, the capacitor which tunes the implant. Due to the low input reactance of the transformer, and high internal tissue source impedance, the low frequency components of the heart waveform are heavily attenuated, and the heart waveform is effectively differentiated in the step-up process. Fourier analysis shows that a typical heart waveform has its strongest frequency components in the 0-200 cps region.

Elimination of the audio frequency transformer with its low input impedance and poor low frequency response was accomplished by development of a batteryless audio amplifier (RF powered), having high input impedance and a flat response from DC to 300 cps. A future integrated microcircuit version of this amplifier can occupy less volume than the transformer it replaced. It was demonstrated that EKG signal and impedance level requirements are met by this amplifier.

C. MEDICAL ACTIVITY

Early medical experiments under this contract with turtles and rabbits were of an acute nature due to the lack of a sterile environment for operation. Since chronic experiments would be needed to observe telemetry over long periods of time, Republic purchased and had outfitted an air conditioned animal trailer (Figure 6) designed to house small animals in a sterile atmosphere. Several successful chronic experiments were performed within the trailer and animals were kept alive and healthy with electrodes attached to their hearts for indefinite periods (Figure 7).

Difficulty was at first experienced in getting a stable cardiac potential electrode implant. Better techniques in making the electrode lead assembly and the surgical procedures ultimately greatly improved matters. One experimental animal preparation showed a decrease of cardiac muscle potential from 25 millivolts to 17 millivolts occurring in the first few weeks. Subsequently the voltage remained practically constant at 17 millivolts for a period of six weeks. This was considered a significant improvement over earlier techniques, with which a decrease to a few millivolts typically occurred.

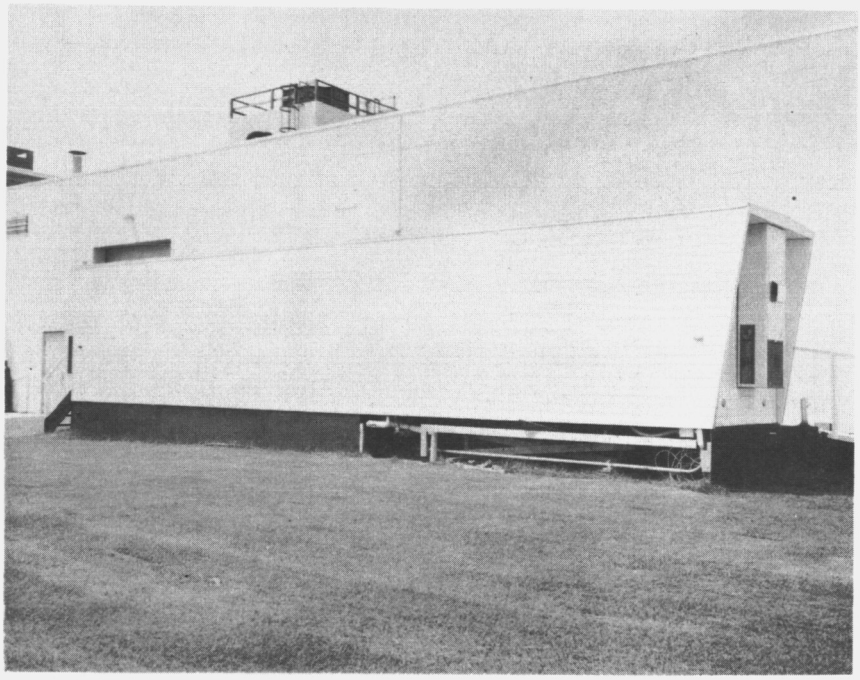

Figure 6. Republic's Animal Trailer

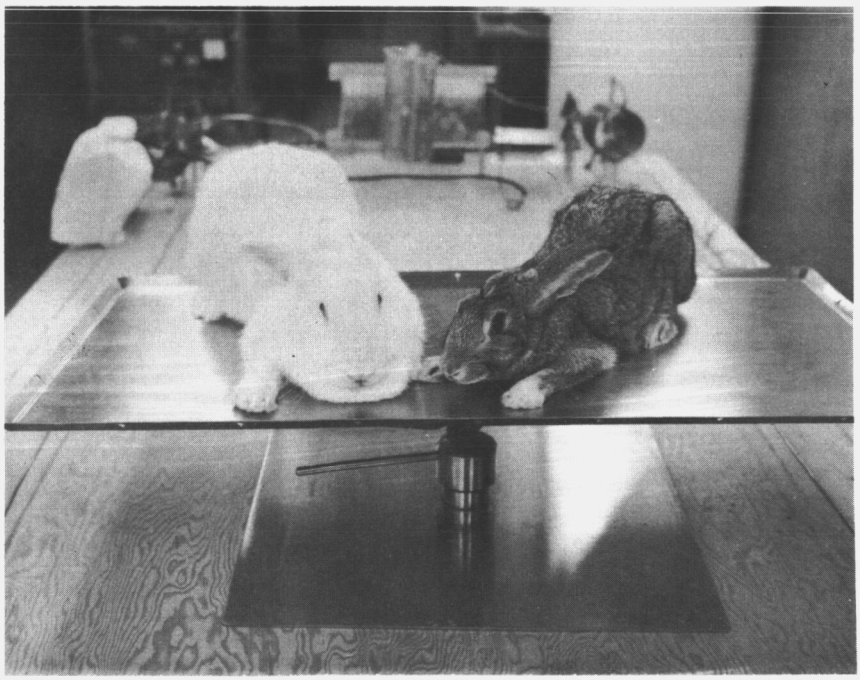

Figure 7. Rabbits with Implanted Electrodes

adjusted so that $f_o + f_2^{(m)} = f_{implant}^{(m)}$ where: $f_{implant}^{(m)}$ is approximately the the frequency at which the tuned circuit of implant m is resonant, as a result of the physiological input to that implant.

There may be m separate, transmitters of $f_2^{(m)}$ and receivers of $f_{implant}^{(m)}$, or a single broadband transmitter and receiver may be used if the implants are sampled sequentially rather than observed simultaneously. In Figure 8, simultaneous observation is assumed and thus separate transmitters and receivers are used and shown.

The common source of frequency, f_o, powers all n implants. This is advantageous, since it avoids the need of n sources which might cause excess irradiation and excessive complexity.

The n low power generators are matched to the corresponding implants, each implant tuned to the corresponding signal of frequency $f_2^{(m)}$.

At the implants, and in a similar manner to that of the amplitude modulation system, the received signals of f_o and $f_2^{(m)}$ are added and frequency shifting of $f_2^{(m)}$ is achieved. A tank circuit in the implant is now approximately tuned to $f_2^{(m)} + f_o = f_{implant}^{(m)}$ which in turn, as in the amplitude modulation implant, re-radiates the time shifted and phase modulated signals. The signal $f_{implant}^{(m)}$ is now received at the multiplex receiver simultaneously with all other (n-1) signals, where they are amplified so that they can be demultiplexed and further processed through the pulse shaper which delivers the corresponding synchronizing pulses to the $f_2^{(m)}$ respective generators.

Thus each of the n single loops is closed. The operation may now be seen in its entirety: the generated $f_2^{(m)}$ frequency signals will be locked to that frequency for which the received synchronized pulse has the proper phase and time relations, which, in turn, is governed by the implant's tuning, $f_{implant}^{(m)}$. By modulating this tuning frequency with the information to be transmitted, frequency modulation of the $f_2^{(m)}$ is achieved. Demodulation is readily achieved through n discriminators, the frequency modulation detectors in Figure 8, and the n signal outputs required are delivered after amplification. Appendix I explains in detail how phase-locking the

signal frequency $f_2^{(m)}$ results in a frequency modulated signal.

As stated before, the n transmitters tuned to $f_2^{(m)}$, and receivers tuned to $f_{implant}^{(m)}$, may be combined. A single transmitter and receiver, each capable of operating over the band of all the implants, may be used. This modification of Figure 8 may be visualized as follows: it is required to add an electronic switch to the band pass filters and demodulator unit. Thus the transmitter would sequentially be caused to operate at frequencies corresponding to implants 1 . . .m. . .n, the system being otherwise identical.

B. SYSTEM COMPONENTS

1. Block Diagram

A block diagram of the system is presented in Figure 9. Each component of the system having a significant overall function has been broken out on this diagram and given a number which will be used in subsequent discussion. Certain of the blocks, such as elements of the antenna system, may require more discussion than other discrete but somewhat simpler elements such as circuit boards whose function is to multiply or divide frequency.

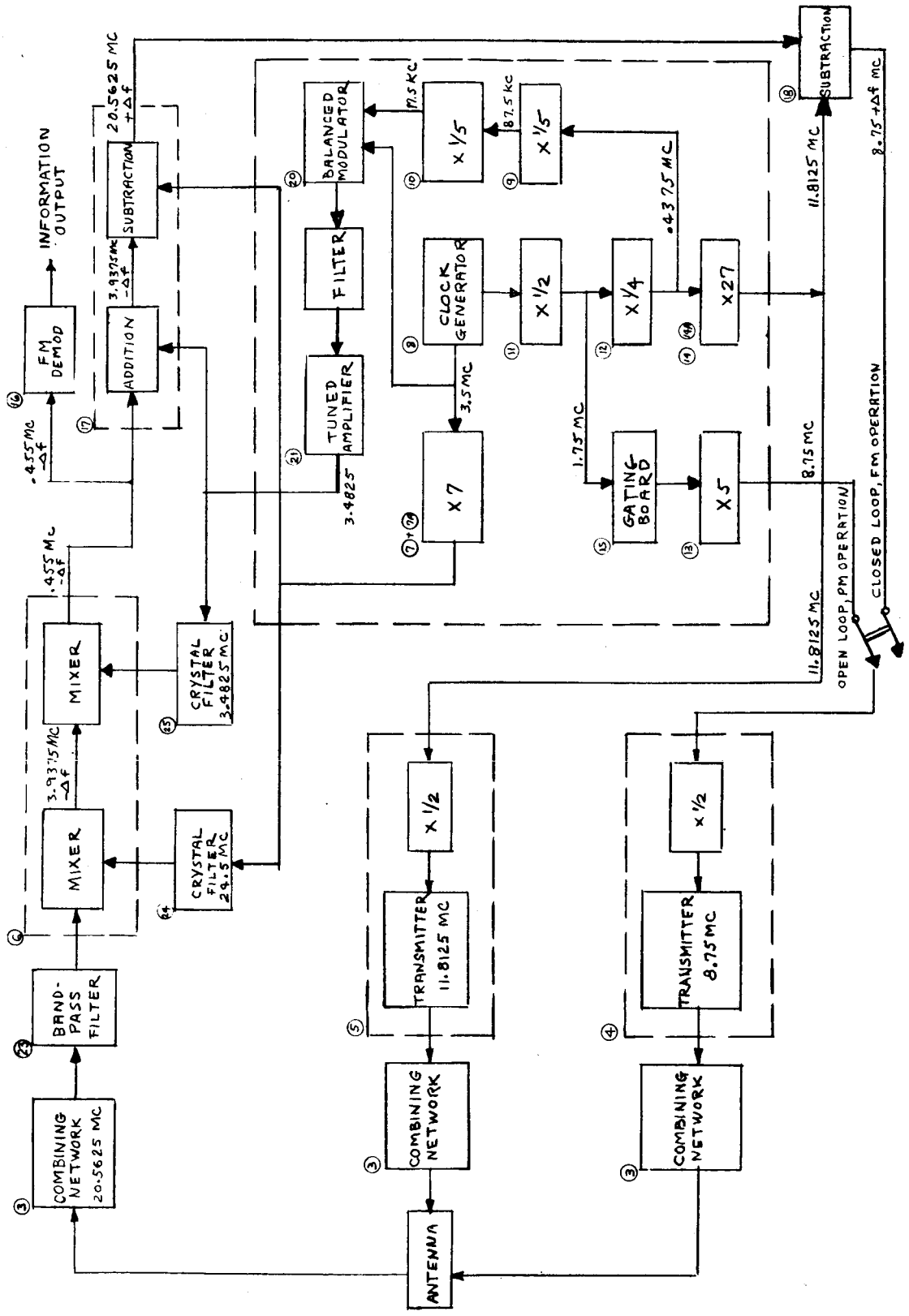

Figure 9. System Block Diagram as Constructed

2. Antenna System Design (Block No. 1)

a. Antenna Configuration

It is desired to telemeter from any point within a 5 foot by 5 foot by 8 foot volume. A three turn antenna configuration as in Figure 10 has been selected.

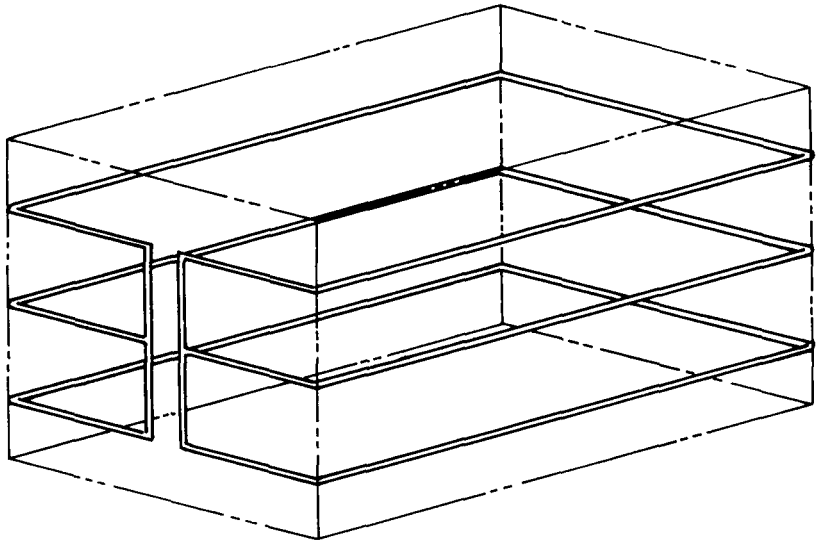

Figure 10. Antenna Configuration

The primary purpose of the transmitting antenna is to build up the required field strength at every point within the volume of telemetry. To this end, high currents within the antenna conductor are needed. Further increase in field strength may be accomplished by maintaining uniform in-phase currents along the antenna; in this manner the superposition of all elemental current contributions to the field strength at any point will be practically additive. For the received signal to be most independent of location of the implant, within the telemetry volume a uniform current is again dictated. From these considerations design goals for the antenna can be stated:

1) the antenna should present a low impedance at each of the transmitting frequencies of operation so that high currents can be tolerated without excessive voltage buildup to avoid unwanted corona effects; 2) uniform in-phase currents for all antenna conductors at each of the three carrier frequencies of operation, two being transmitted and one being received.

The approach was to consider each of the three turns in Figure 10 separately. A computation was made to justify this simplification. It was determined[1] that the self inductance of one of the turns in Figure 10 is 9.2 μh. while the mutual inductance between any turn and its nearest neighbor is 1.5 μh. Since the mutual inductance is only 16% of the self inductance it was considered acceptable to design the antenna as three non-coupled antennas in parallel feed and any adjustments would be made at the antenna terminals after fabrication. Each turn of the antenna was considered to be made up of sections of a balanced transmission line. Starting with one end of the antenna, Foster reactance networks were added to compensate the inductive reactances of each transmission line segment at the three frequencies of operation. The filters were placed electrically close enough 1) to insure practically uniform current over sections, and 2) to prevent excessive reactance buildup which would lead to high voltages in the compensating filters. The result is an antenna which can be readily made resonant at 8.47 mc., 11.53 mc, and 20.00 mc (See Figure A-7, Appendix II).

Simultaneous with the design of the antenna a laboratory program was initiated to develop the capability to construct the high Q low valued inductances required for the filter sections of the antenna. Various sizes and types of conductors, open and closed ferrite cores, and a transmission line technique were among the approaches tried. The best results (Qs) were obtained with 3/16" diameter copper tubing coils with an air core. A facility for fabricating precise numerical values of inductance by shaping the coils was also developed. A Booton Model 260A Q Meter was employed for measuring inductances and higher frequency Qs. A special fixture was constructed to measure Qs at 8.47 mc and 11.53 mc. Table I shows typical values for coil Qs at the three frequences of operation first selected.

---

(1) See Appendix II, Part A

Table I

Inductance h	Frequency mc	Q
	8.47	210
.239	11.53	234
	20.00	301
	8.47	170
.158	11.53	190
	20.00	247
	8.47	150
.131	11.53	166
	20.00	213

In accordance with design values and expected losses in the wires of the antenna and the filter circuits, an expected impedance of the antenna at each frequency of operation has been evaluated[2]. These single and three turn impedances (which should be a reasonable measure of the practical values) are shown in Table II.

Based on the values of Table II, an estimate of the currents in the antenna conductors can be given in terms of the power available. The existing transmitters have r-f power capabilities of approximately 35 watts. If the 50 ohm transmitters are matched efficiently to the load, an rms current of $1/3\sqrt{35/R}$ amperes will be produced in each turn of the antenna where the resistance R is that for three turns taken from Table II. At 8.5 mc we have $I_{rms} = 1.13$ amps and at 11.5 mc $I_{rms} = 1.08$ amps. The magnetic flux density at a remote point of the telemetry volume due to currents in the conductors has been computed[3] to be 6.16×10^{-3} gauss.

(2) See Appendix II, Part C

(3) See Appendix II, Part D

Table II

Frequency (mc)	Design Impedance single turn	Design Impedance three turns
8.47	9.03 + j0	3.01 + j0
11.53	9.89 + j0	3.30 + j0
20.00	24.7 + j0	8.23 + j0

As outlined in the second quarterly status report, the tuning of the individual loops of the three loop antenna did not agree exactly with system requirements; nor could they be expected to as various approximations were necessary in the design approach. In addition the three loops did not possess identical characteristics as designed for due to component tolerances in the compensating networks and the small departures from the design configurations at the interconnection end of the antenna. Indeed it was not necessary that the individual loops matched the system requirements, because intercoupling between turns would affect the overall tuning of the antenna and make adjustments necessary anyway.

The fine tuning of the antenna was accomplished by a cut and try process in the laboratory. The three frequencies at which the three loop antenna is required to be series resonant are 8.75 mc, 11.8125 mc, and 20.5625 mc. Initially, the individual loops were designated east, middle, and west and the individual impedances were measured using a Wayne Kerr Balanced Admittance Bridge at the three system frequencies and also at their individual resonant frequencies. It was found that the resonant frequencies of all three loops were lower than the system frequencies, with the 20.5625 mc impedances off most, the 8.75 mc impedances next, and the 11.8125 mc impedances closest to the resonance point. There were also differences between the individual loop impedances at any frequency of measurement. The approach used is as follows: The compensating reactance networks of each of the three loops of the antenna were modified to 1) make each of the three loops as nearly the same electrically as possible and 2) to raise the individual loop resonant frequencies to be close to the required system resonant frequencies. This amounted to removing a portion of the series capacitance from each of the reactance networks and introducing a tuning slug to one of the inductances in each reactance network for the purpose of

lowering these inductances. When this homing-in procedure was completed to what was believed to be a satisfactory point, the following individual turn impedance characteristics were measured:

Loop Designation	Loop Impedances		Loop Resonant Frequencies
East	8.75 mc	31.2 + j 231	8.398 mc
	11.8125 mc	10 + j 40	11.625 mc
	20.5625 mc	46.8 + j 34.7	20.480 mc
Middle	8.75 mc	29.4 + j 277	8.42 mc
	11.8125 mc	7.73 + j 60.2	11.447 mc
	20.5625 mc	54.3 + j 76.2	20.432 mc
West	8.75 mc	33.8 + j 255	8.41 mc
	11.8125 mc	12.1 + j 93.6	11.472 mc
	20.5625 mc	57.7 + j 75.1	20.420 mc

Then, under these conditions of individual loops tuning, the three loops were connected in parallel and the impedances of the composite antenna measured:

@ 8.75 mc Z = 12.5 + j 150

@ 11.8125 mc Z = 5.33 + j 118

@ 20.5625 mc Z = 41.4 + j 183

While it was intended that the composite antenna be resonant (0 reactive components) at these frequencies, the individual loop reactances as shown in the table are low enough so that excessive voltages would not be developed in series tuning reactances added to achieve these resonances (i.e. when transmitting currents of the order of 1 ampere are passed.

In addition to achieving overall antenna resonance, it is required that when a voltage is applied across the antenna terminals at one of the three main frequencies of system operation the currents through all three loops are divided equally. The method used to achieve this result was to attach small incandescent lamps across identical sections of all three loops of the antenna and add compensating

reactances to the individual turns as required to make all three lights glow equally when the three-loop paralleled combination was powered. This was done at 8.75 mc, 11.8125 mc, and 20.5625 mc. It was determined over a period of several days of laboratory work, that the following set of reactances were required to make a) the overall antenna resonant and b) the currents through the three loop approximately equal at the three frequencies of interest.

Frequency	Total Loop Reactances Required (Ohms)		
	West Turn	Middle Turn	East Turn
8.75 mc	- j 445	- j 670.2	- j 445
11.8125 mc	- j 357	- j 357	- j 266
20.5625 mc	- j 475.4	- j 602.9	- j 441

In keeping with the balanced line approach to the design of the antenna the reactances shown in this table were divided by 2 and reactance networks were designed for each of the three loops in accorance with these values. The networks are of the form of the earlier (see Quarterly Status Report #1 Appendix Part B) treated antenna reactance networks (2 poles, 2 zeros) and two are evidently required per loop. The networks have been constructed and mounted at the 3 loop antenna terminals. See Figure 11. Note that since air core coils were used (for constant L and high Q over the band) care had to be exercised in the construction to have mutual coupling effects between coils reduced to a minimum. Neighboring coils were constructed with their respective axes orthogonal. Figures 11A and 11B are views of the antenna and system components.

Upon completion of the above, the total 3 turn antenna was again powered at the 3 frequencies of interest. Aside from a slight difference in brightness of one of the indicating lamps at 11.8125 mc, this compensated antenna worked and in view of time and money limitations is being used as is. The uniformity of current along the antenna conductors was, as predicted in Quarterly Status Report #2, verified by positioning the indicating lamps along different sections of the antenna conductors of any one loop and observing no noticeable difference in brightness between them. The final stage of antenna development was the measurement of the input impedances at 8.75 mc, 11.8125 mc, and 20.5625 mc. The Wayne Kerr admittance bridge used for the measurements had an upper limit for shunt conductance of

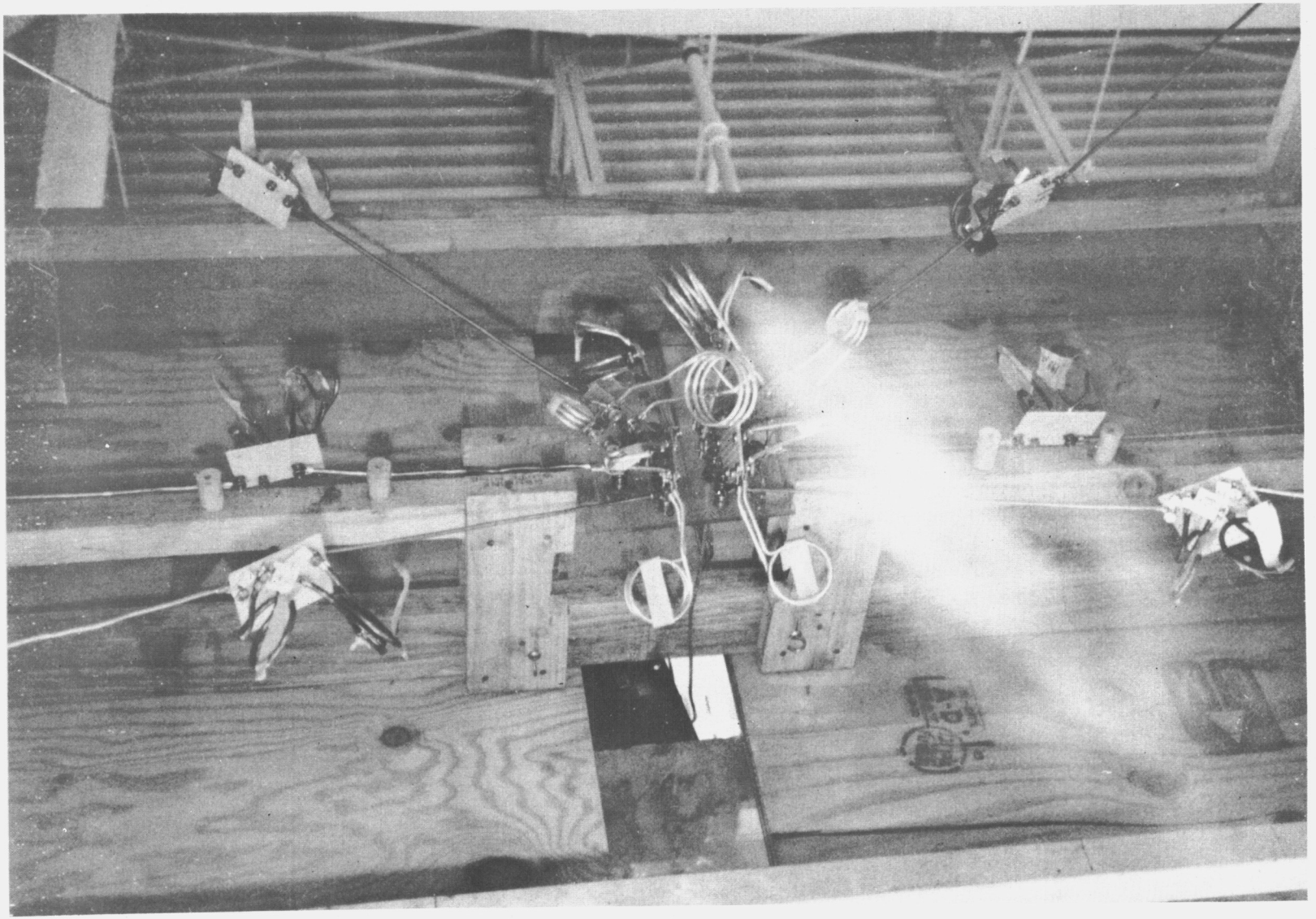

Figure 11. Antenna Terminal Reactance Network (RD-5263)

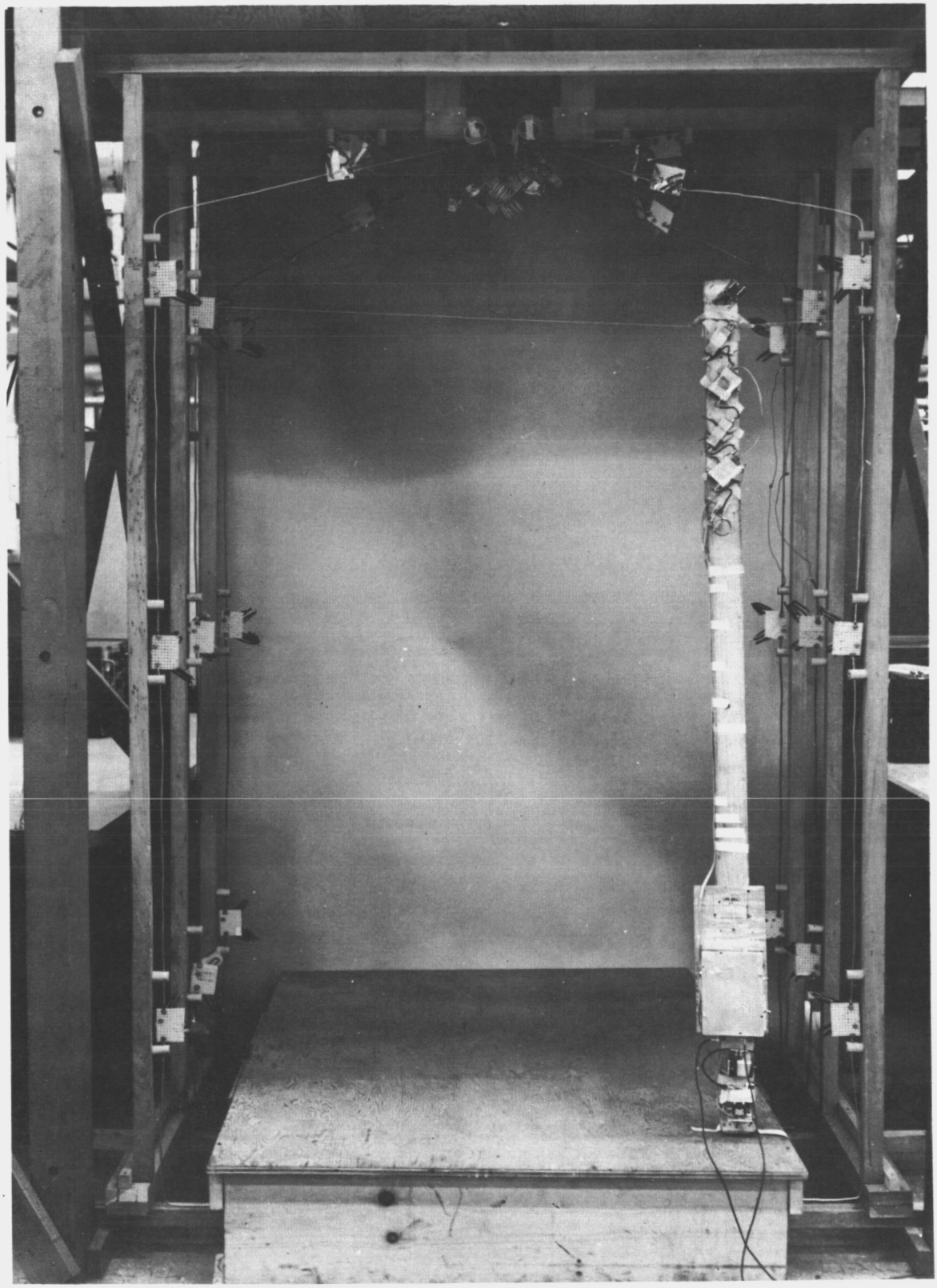

Figure 11a. Antenna, Overall View (RD-5696)

Figure 11b. Antenna and System Components (RD-5695)

100 milliohms. This necessitated the taking of readings on either side of the operating frequencies of 8.75 mc and 11.8125 mc and interpolating these readings to the desired points as in Figures 12 and 13. The results of these final antenna measurements are the input impedances to which the combining network and bandpass filters must be matched:

@ 8.75 mc $\quad Z = 21.0 + j\,6$

@ 11.8125 mc $\quad Z = 21.2 - j\,20$

@ 20.5625 mc $\quad Z = 51.6 + j\,2$

A full detailed schematic of the antenna loop can be found in Appendix II Part B.

b. Evaluation of Phase Shift with Respect to Frequency

In the design of the antenna, expressions were developed for the reactances of various sections symmetrically located with respect to the ground plane. These can be used in connection with the impedance functions of the compensating Foster reactance networks to determine expressions for the derivative with respect to frequency of the impedance function for the antenna[4]. The rate of change of current phase with respect to frequency can be obtained from this expression and the impedance function itself.

The numerical results obtained for the frequencies 8.47 mc and 20.00 mc (the 11.53 mc frequency is not frequency modulated) are:

$$\left|\frac{\partial \phi}{\partial f}\right|_{8.47\ \text{mc}} = 2.6 \times 10^{-3} \ \frac{\text{degrees}}{\text{cycle/sec}}$$

$$\left|\frac{\partial \phi}{\partial f}\right|_{20.00\ \text{mc}} = 1.04 \times 10^{-3} \ \frac{\text{degrees}}{\text{cycle/sec}}$$

The predominant influences affecting the rate of phase change with frequency were the compensating reactance networks. Since these networks are closer to a singularity at 8.47 mc (a pole at about 9.5 mc) than at 20 mc (a pole at

(4) See Appendix II, Part G

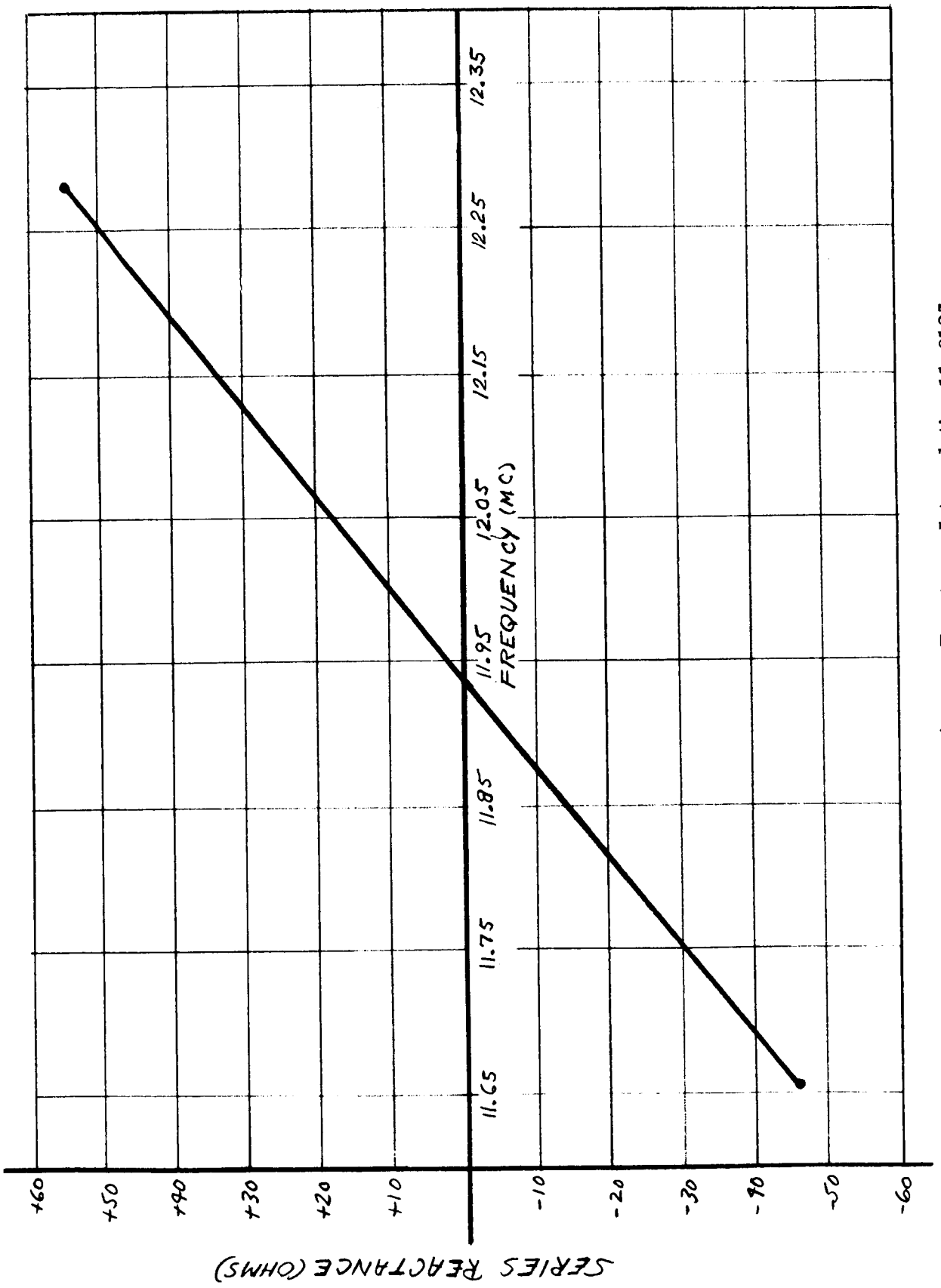

Figure 12. Antenna Reactance Interpolation 11.8125 mc

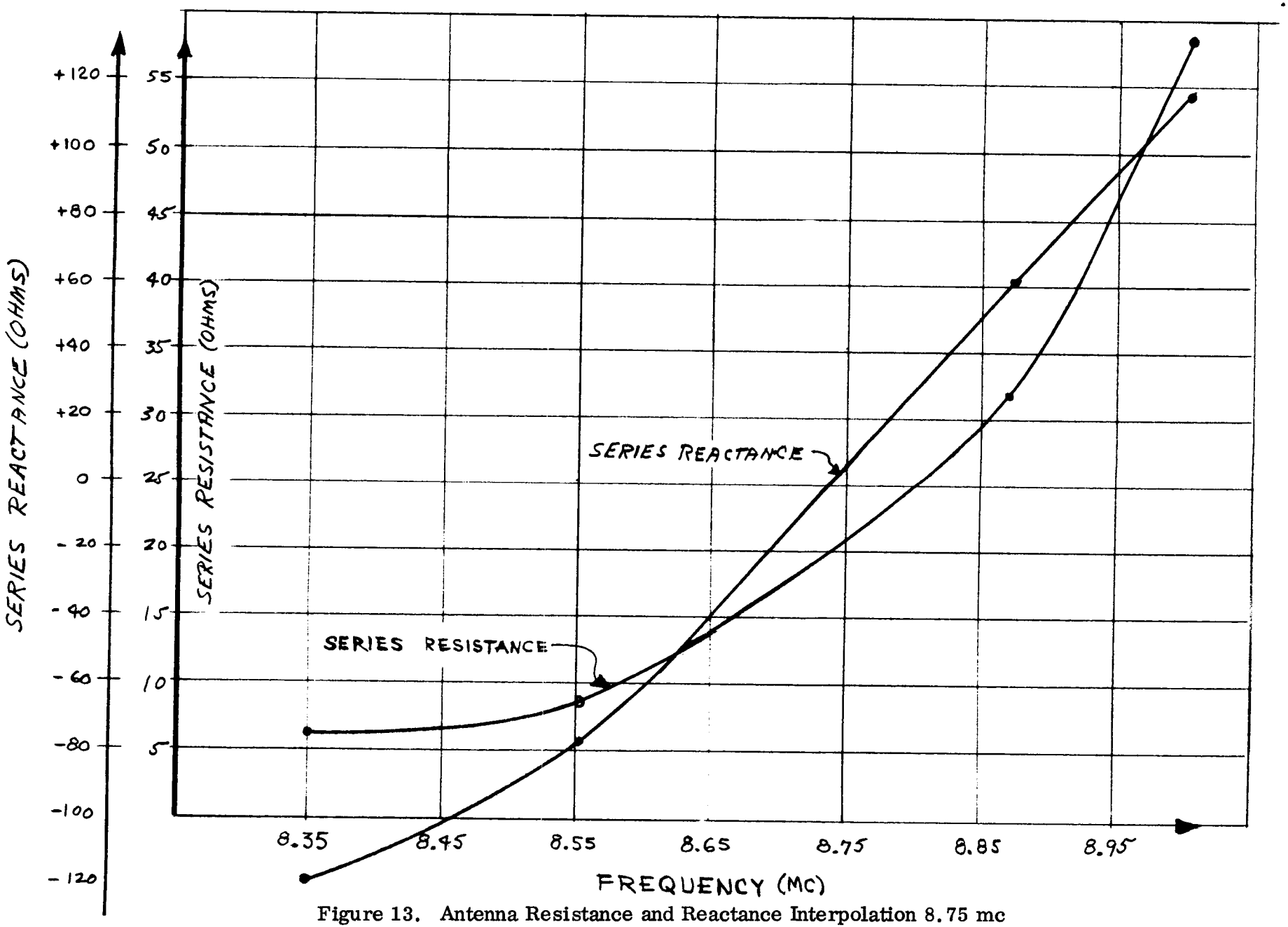

Figure 13. Antenna Resistance and Reactance Interpolation 8.75 mc

about 17.3 mc) the observed phase change is greater at 8.47 mc than at 20.00 mc.

c. Design of Coupling Networks and Bandpass Filters for the Antenna (Block 3 Figure 9)

The transmitter amplifiers to be used at 8.75 mc and 11.8125 mc are designed to drive a 50 ohm load. The real part of the input impedance of the receiver to be used at 20.5625 mc is 50 ohms. Therefore, the problem of the coupling networks and bandpass filters becomes one of matching the antenna impedances as determined above to 50 ohms. This must be done in separate isolated networks for each of the three channels. The configuration which was decided upon consists of three channels similar to the one shown below.

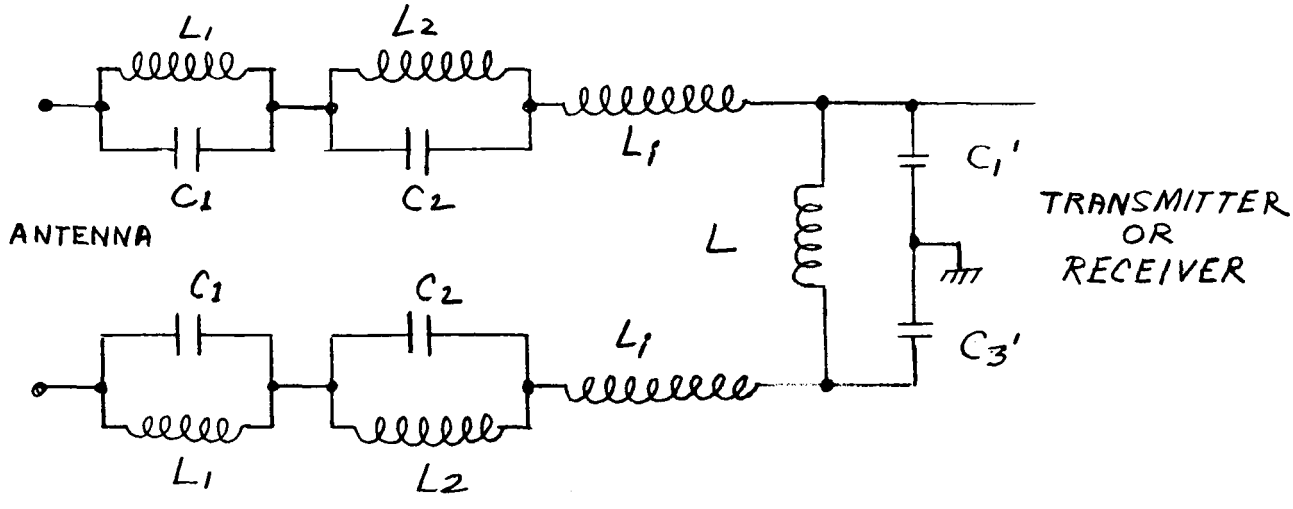

Figure 14. Combining Networks

Values used in constructing the three combining networks may be tabulated as follows:

	20.5625 mc pass	11.8125 mc pass	8.75 mc pass
L_1	1.348 uh	.776 uh	1.348 uh
C_1	135 pf	77.3 pf	135 pf
L_2	1.82 uh	1.82 uh	.776 uh
C_2	181.8 pf	181.8 pf	77.3 pf
L_i	1.32 uh	.608 uh	95.6 pf (capacitor)
C_1'	1295.5 pf	2330.5 pf	3256 pf
C_3'	1295.5 pf	2330.5 pf	3256 pf
L	.1032 uh	.134 uh	.242 uhy

3. Electronic Circuit Components

This section will cover the detailed circuitry of remaining components shown on the overall block diagram, Figure 9, by reference to the Block Number.

a. 8.75 MC Transmitter, Block No. 4

This part of the system generates the high power R.F. signal of frequency 8.75 mc/s. It is phase controlled by a locking signal generated by Block #18 through a multiply by 1/2 stage.

For Block No. 4, a modified Viking Transmitter, Figure 15, has been utilized with circuit modifications as follows:

- 50 pf trimmer in parallel with 39 pf fixed capacitor from junction of L7 and C13 to position 9 of Switch 1A
- trimmer capacity of 47 pf across R30
- 400 pf ceramic capacity across position 1 and 3 of Switch 1B

The transmitter operates on the second harmonic of the excitation frequency (to avoid the tendency to oscillate) so a multiply by 1/2 circuit was designed and built; this is shown in Figure 16.

For system operation in open loop, where phase modulation of the implant RF can be demonstrated, the drive frequency for the transmitter is obtained from the clock generator after being multiplied by 2.5 (in two steps, divide by 1/2, multiply by 5.)

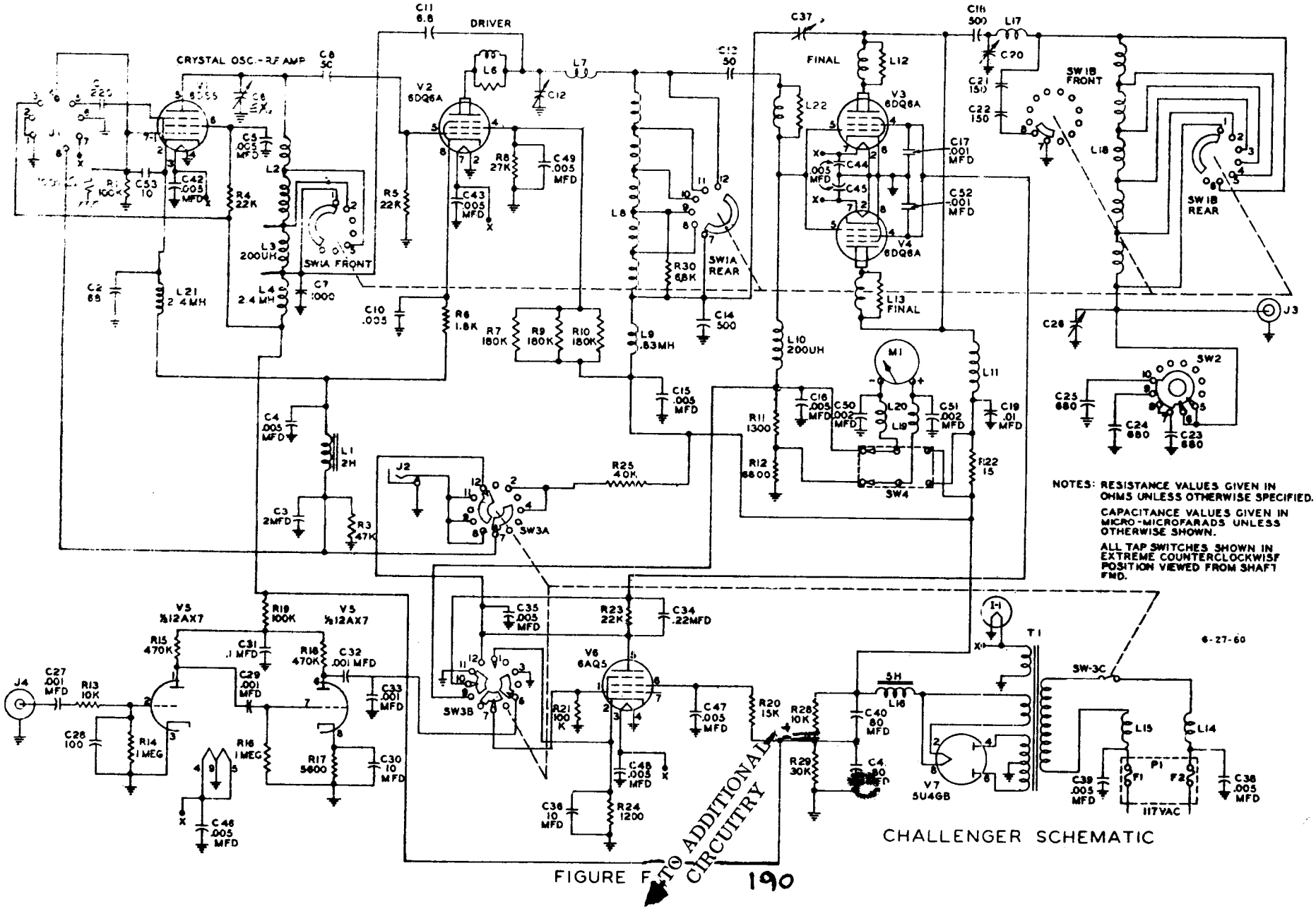

FIGURE F 190

Figure 15. Viking Challenger Schematic Transmitter, 8.75 mc

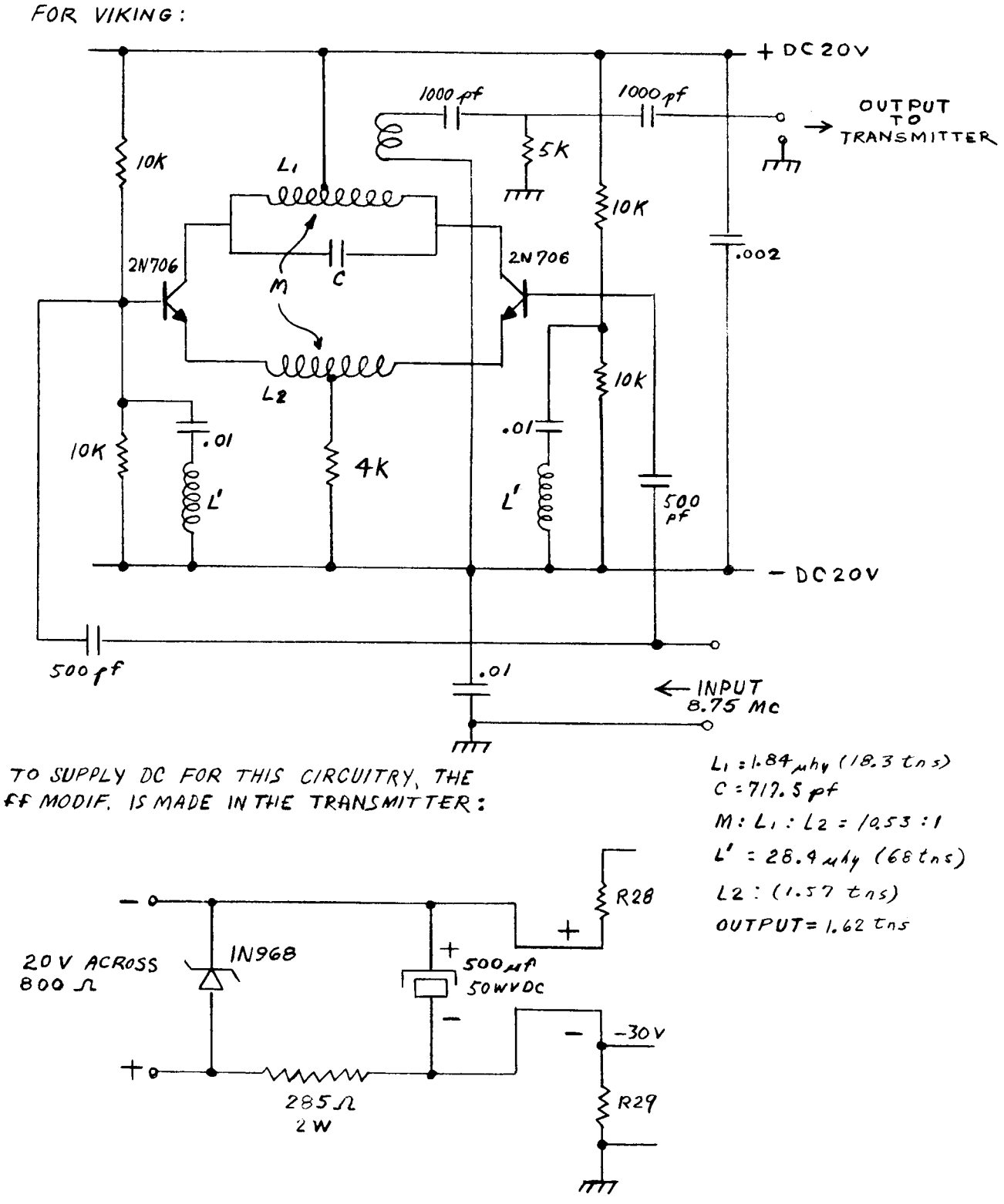

Figure 16. Additional Circuits used with 8.75 mc Transmitter

b. 11.8125 MC Transmitter, Block No. 5

This block is the transmitter which provides the 11.8125 MC power to the antenna. It is excited at half this frequency, again to avoid oscillation, so a multiply by 1/2 stage is used at the input.

The circuit diagram for the original transmitter is presented in Figure 17. A 20 pf capacitor was added across positions 1 and 3 of switch BS-2.

The multiply by 1/2 circuitry is shown in Figure 18.

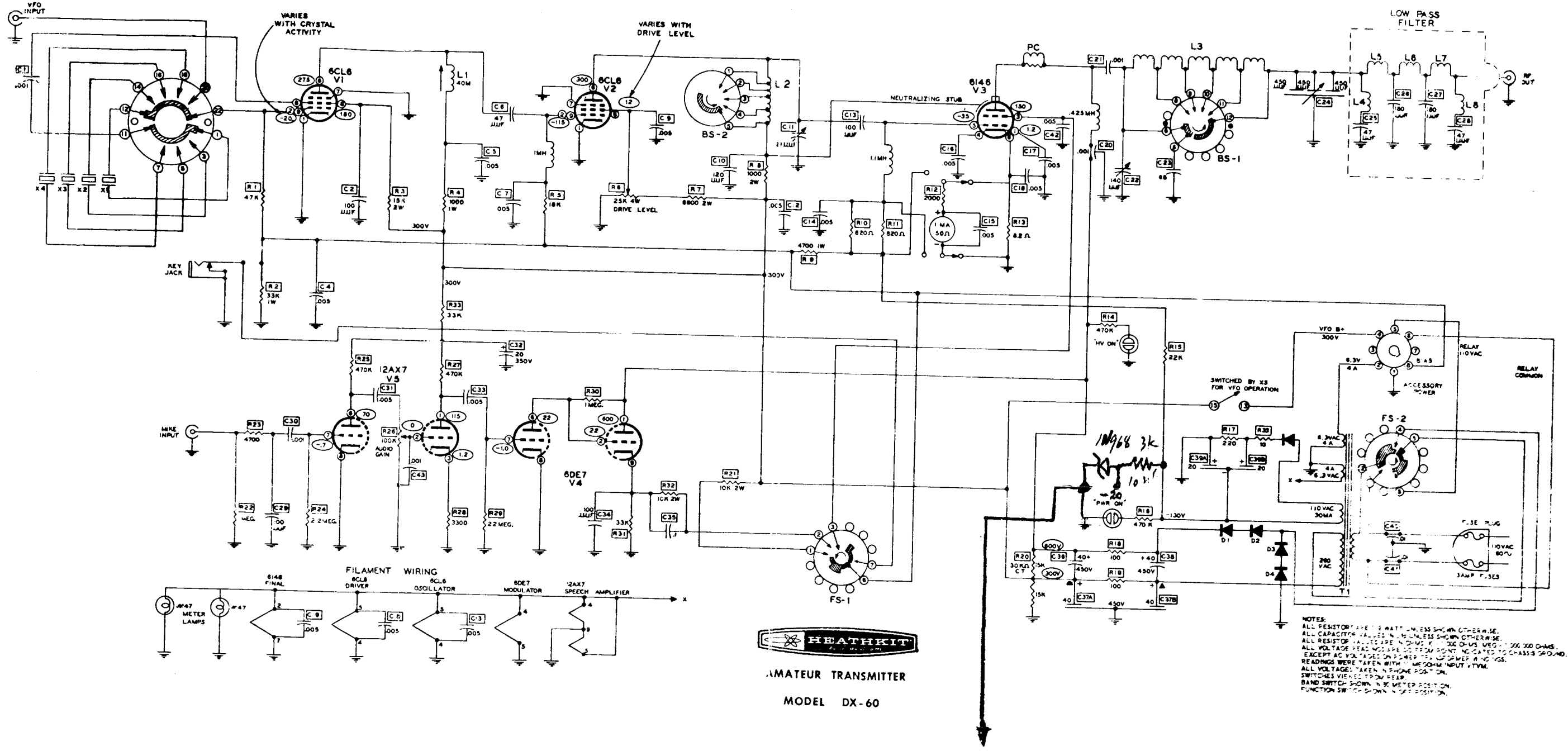

Figure 17. Heathkit Transmitter Schematic, 11.8125 mc

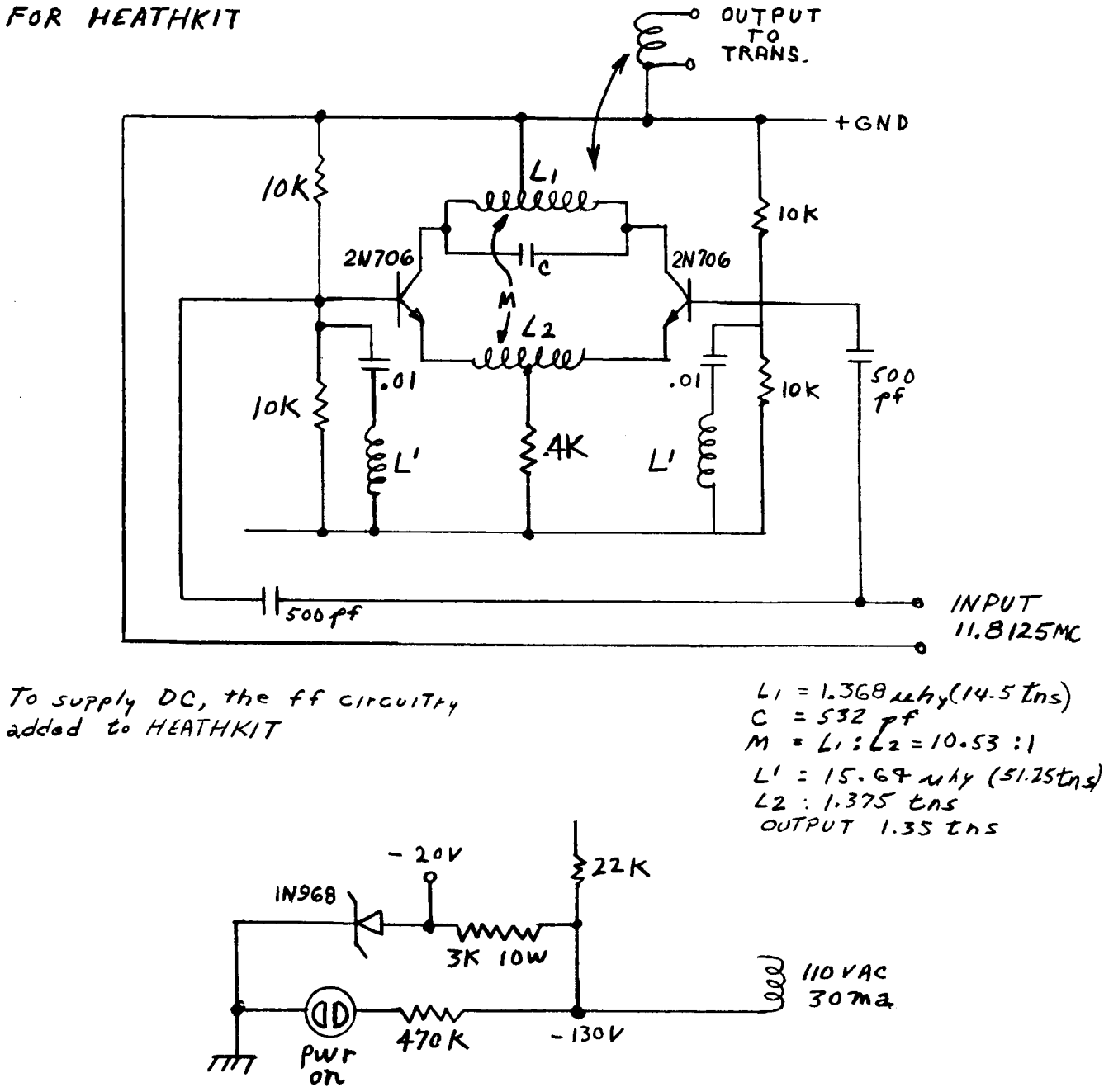

Figure 18. Additional Circuits used with 11.8125 Transmitter

c. Fixed Tuned 20.5625 MC Receiver, Block No. 6

This receiver is a modified Technical Material Corporation Model GPR-90-RX in which the envelope detector is not used so that the output is the 0.455 MC intermediate frequency. The two mixers of the receiver are supplied with local oscillator frequencies of 24.5 MC and 3.4825 MC, phase locked to the clock generator. This double conversion brings the input frequency of 20.5625 MC down to 3.9375 MC in the first step and then to 0.455 MC as shown in Figure 9. Limiting is provided in the IF stages to eliminate amplitude modulation, and as a result the output waveform seen on an oscilloscope reveals only phase modulation (for open loop operation) when the implant is modulated by the signal it is desired to transmit.

For closed loop operation, phase locking will transform this phase modulation into frequency modulation as demonstrated in Appendix I of this report. At present the bandwidth of the loop is about 1,500 cycles, but a wider bandwidth could be beneficial and should be tried in future work.

The circuit for the unmodified receiver is given in Figure 19, and modifications are given in Figure 20.

BAND	TUNING RANGE
1	.54 — 1.4 MC
2	1.4 — 3.3 MC
3	3.2 — 5.6 MC
4	5.4 — 9.7 MC
5	9.4 — 17.8 MC
6	17.3 — 31.5 MC

S1 - RANGE SELECTOR SWITCH

SEE DETAIL A (FIG 20)

SEE DETAIL B (FIG 20)

ANTENNA

MAIN TUNING

BAND SPREAD

AVC

RF GAIN

+250 V.

+150 V.

CRYSTAL FILTER

S12 - HFO SWITCH

1. ALL RESISTORS ARE 1/2 WATT, UNLESS OTHERWISE NOTED.
2. ALL CAPACITORS IN MMF EXCEPT—
   (A) ALL DECIMAL CAPACITORS, WHICH ARE IN MF.
   (B) ALL OTHERS AS NOTED.
3. (S1) BANDSWITCH SHOWN IN BAND 1.
4. (S2) SELECTIVITY SWITCH SHOWN IN NON-XTAL POSITION.
5. (S5) AUDIO SELECTIVITY SWITCH SHOWN IN NORMAL POSITION
6. (S12) HFO SWITCH SHOWN IN VARIABLE POSITION.
7. (S13) SWITCH
   A. S13 IS IN POSITION 4 WHEN HFO SWITCH (S12) IS IN POSITION "VAR."
   B. S13 IS IN POSITION 5 WHEN HFO SWITCH (S12) IS IN POSITION "EXT." AND "XTALS."

Schematic Diagram, Model GPR-90-RX

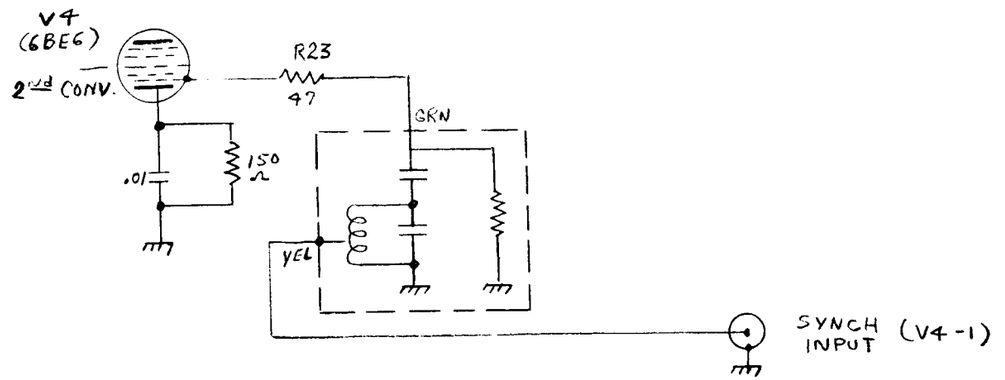

DETAIL A

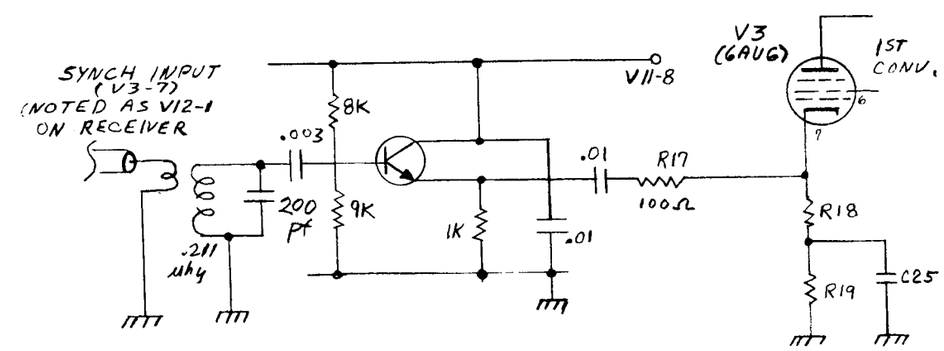

DETAIL B

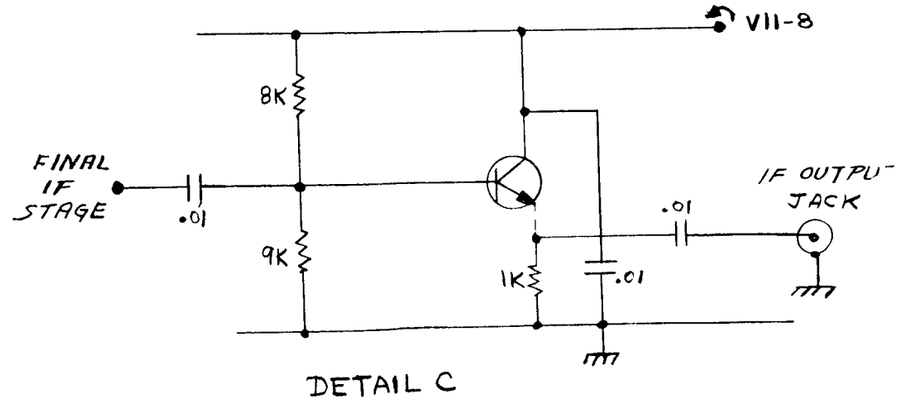

DETAIL C

Figure 20. Modifications to Receiver

d. Crystal Controlled Clock Signal Generator and Locked Frequency Circuits, Blocks 7-15, 20, and 21.

The frequencies required for the transmitters are generated from a crystal controlled oscillator and combinations of multiplying and dividing stages. Besides these frequencies of 8.75 and 11.8125 MC, the local oscillator frequencies of 24.5 MC and 3.4825 MC are also generated in a similar manner, except that the latter frequency involves a subtraction of 17.5 KC from 3.5000 MC by mixing in a balanced modulator and subsequent filtering.

The blocks enclosed in the large dotted box of Figure 9 are here listed with detailed circuits presented in the following Figures:

Block No.	Description	Figure No.
7	Multiply by Seven Circuit, 3.5 MC Input	21
7A	Tuned Amplifier for 24.5 MC	22
8	Crystal Controlled 3.5 MC Oscillator	23
9	Divide by Five Circuit, 0.4375 MC Input	24
10	Divide by Five Circuit, 87.5 KC Input	25
11	Divide by Two Circuit, 3.5 MC Input	26
12	Divide by Four Circuit, 1.75 MC Input	27
13	Multiply by Five Circuit, 1.75 MC Input	28
14, 14A	Multiply by Twenty-seven Circuit, 0.4375 MC Input	29
15	Gating circuit for Block 13	29a
20	Balanced Modulator	30
21	Tuned Amplifier for 3.4825 MC	31

e. FM Demodulator, Block 16

As the receiver being used (partially) in Block 6 is an AM receiver, a discriminator circuit or FM demodulator had to be constructed. This is part of Block 16 which also provides more amplification of the IF frequency (455 KC -Δf)

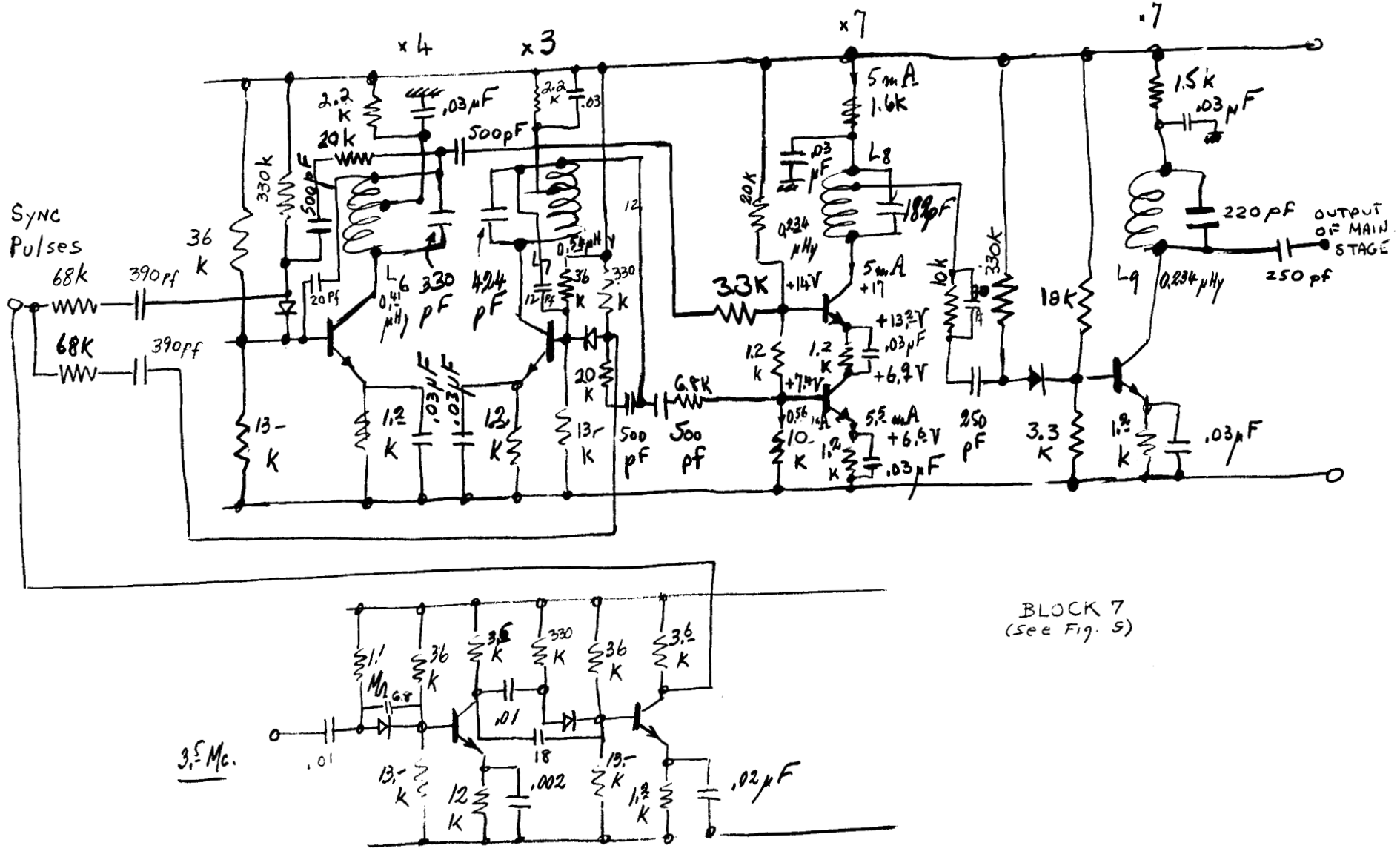

Figure 21. Multiply by Seven Circuit, 3.5 mc Input

BLOCK 7A

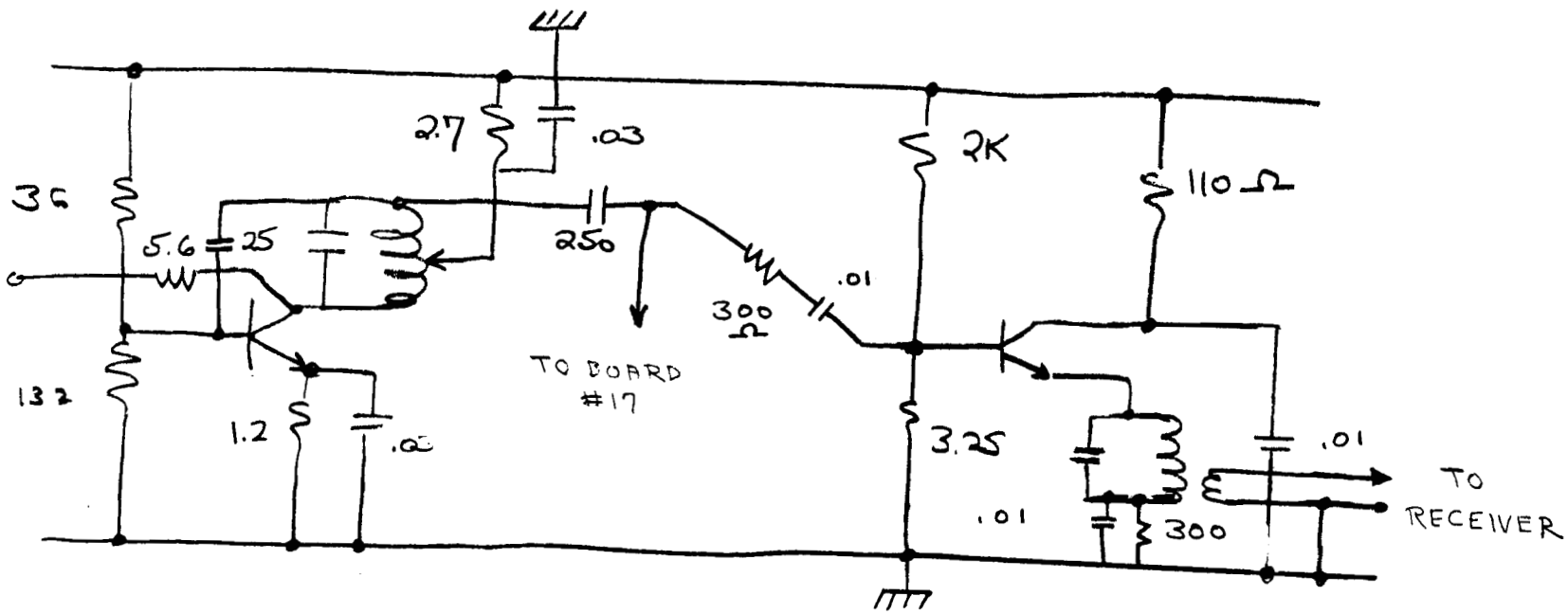

Figure 22. Tuned Amplifier for 24.5 mc

BLOCK 8
(See Fig. 9)

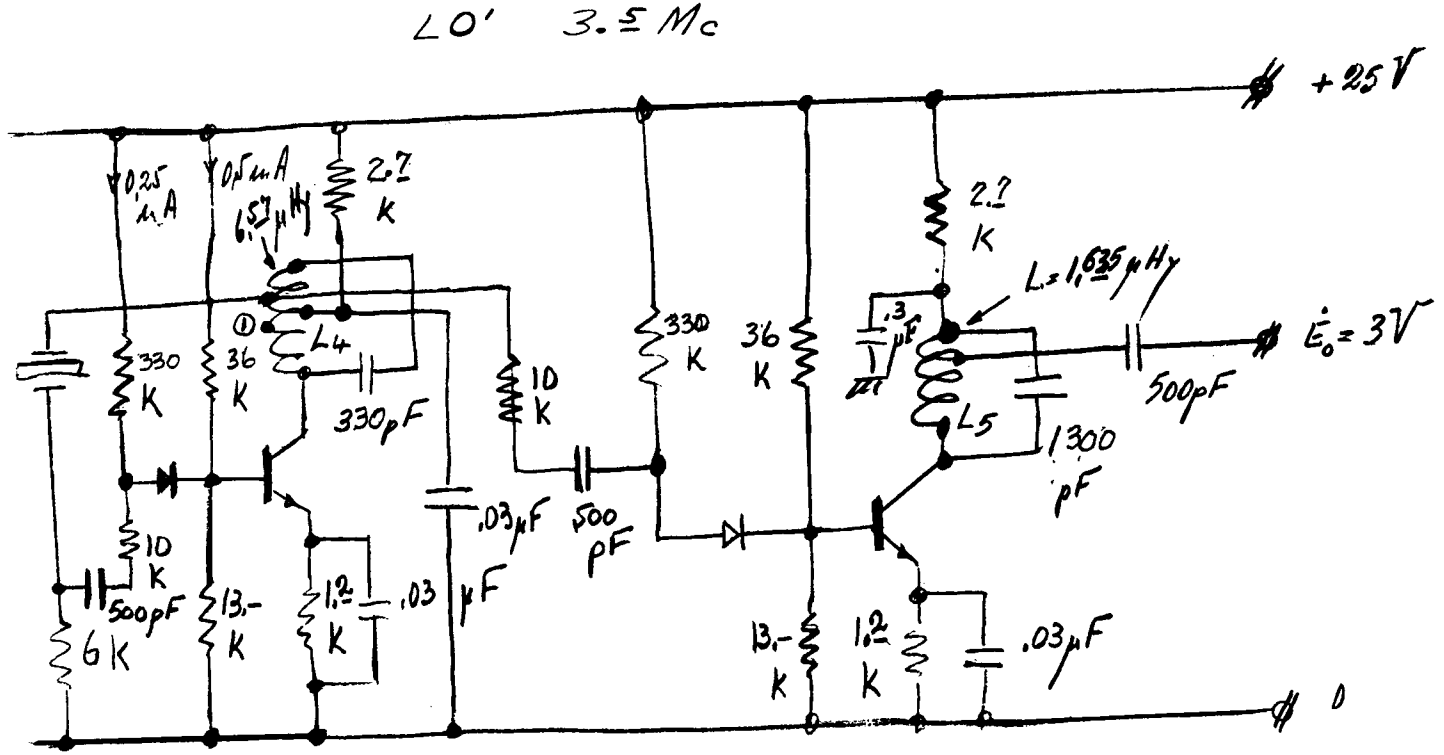

TRANSISTORS - 2N 706
DIODES - 1N 276

Figure 23. Crystal Controlled 3.5 mc Oscillator

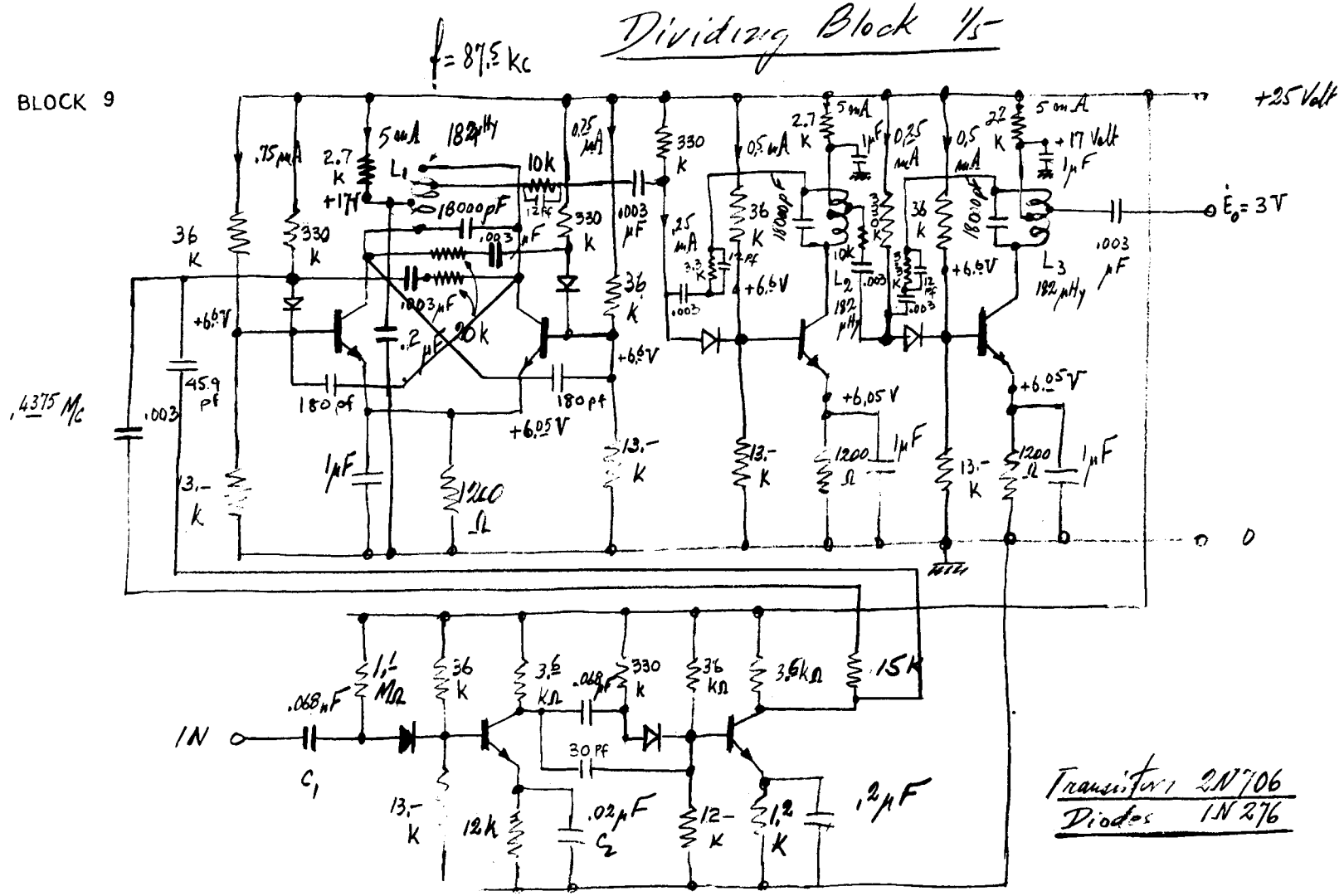

Figure 24. Divide by Five Circuit, 0.4375 mc Input

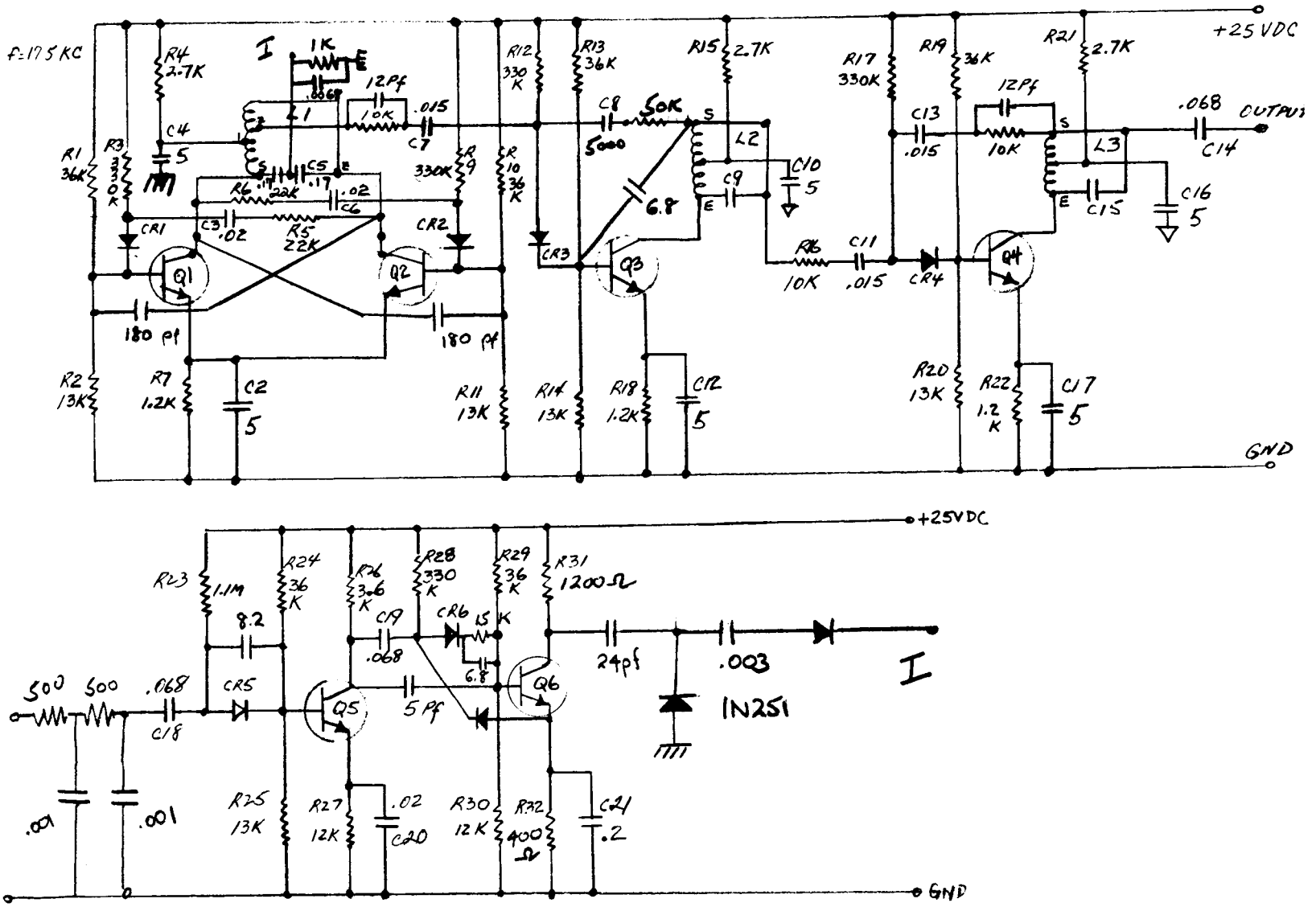

Figure 25. Divide by Five Circuit, 87.5 kc Input

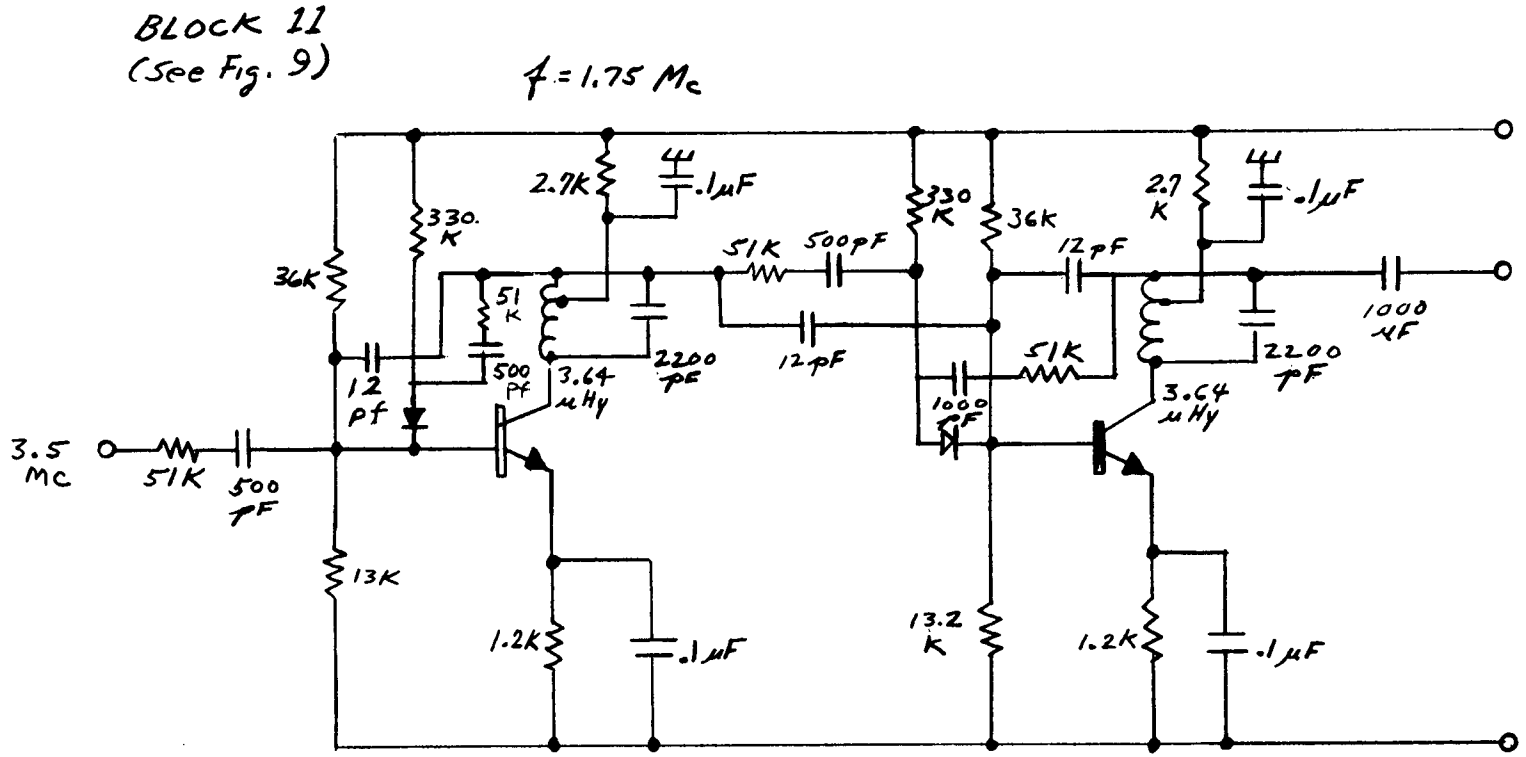

Figure 26. Divide by Two Circuit, 3.5 mc Input

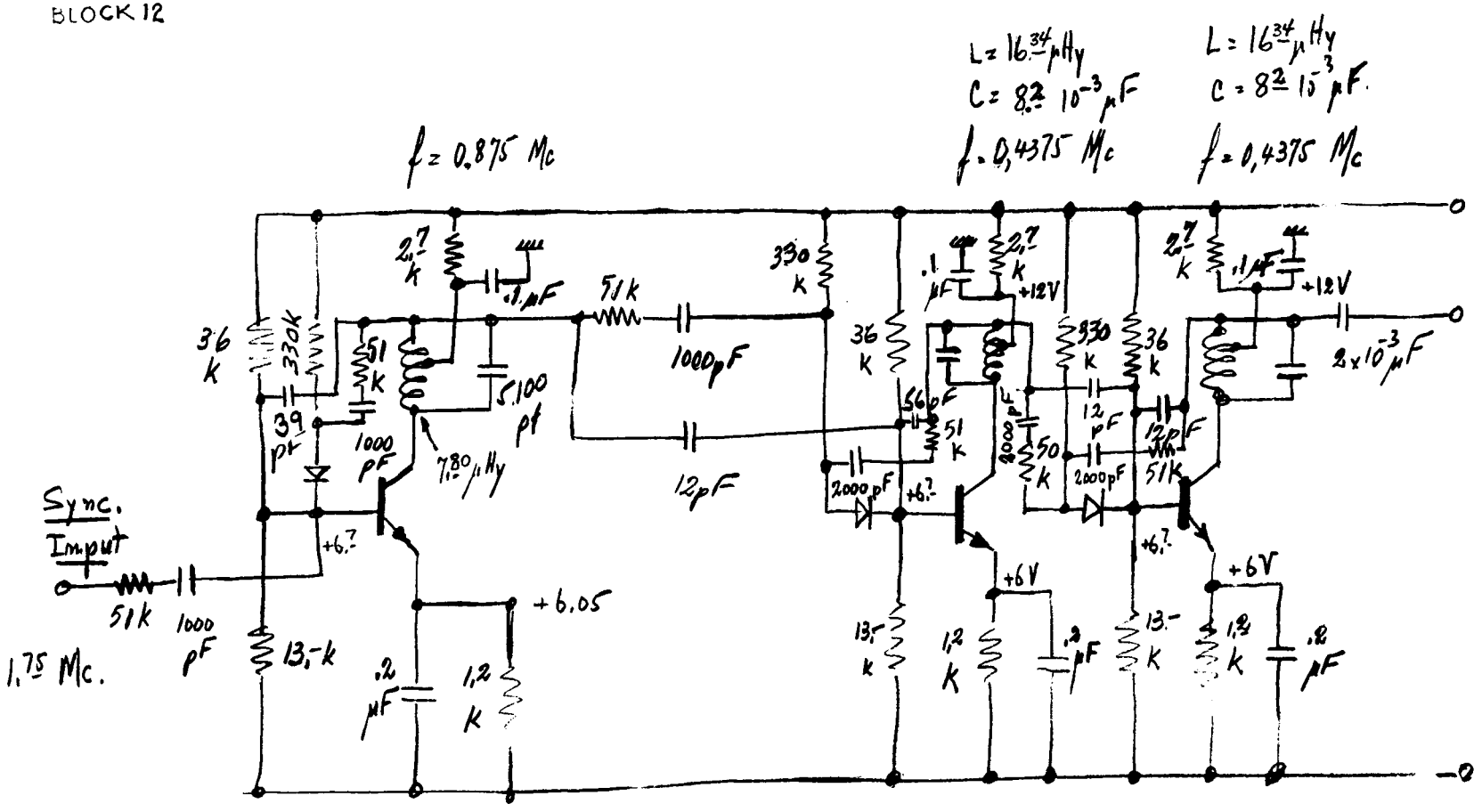

Figure 27. Divide by Four Circuit, 1.75 mc Input

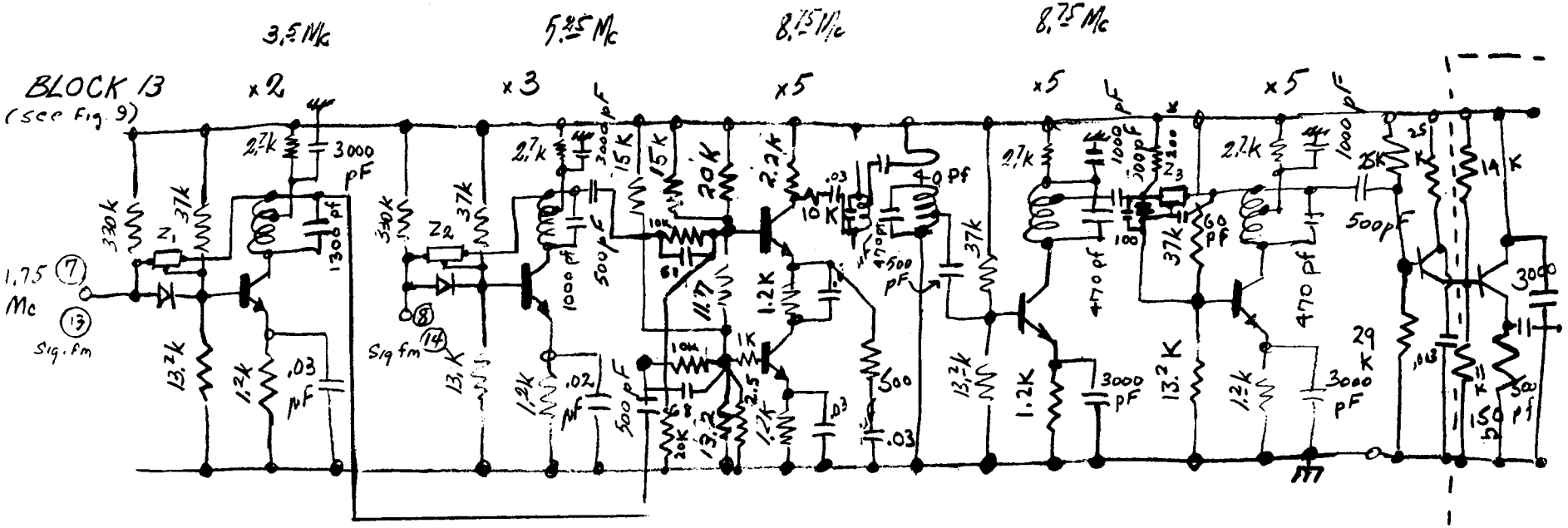

Figure 28. Multiply by Five Circuit, 1.75 mc Input

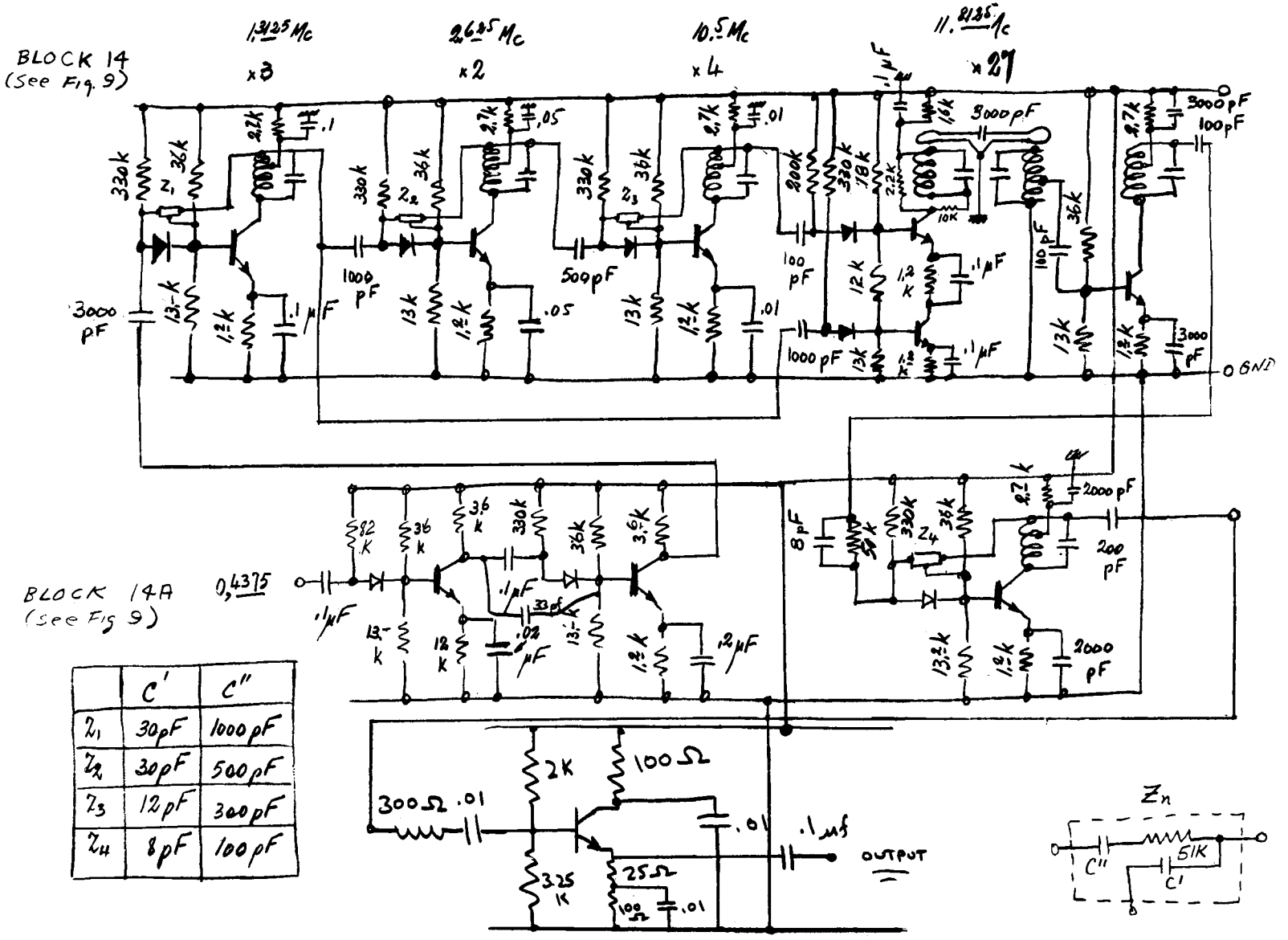

	C'	C''
Z_1	30pF	1000 pF
Z_2	30pF	500 pF
Z_3	12 pF	300 pF
Z_4	8 pF	100 pF

Figure 29. Multiply by Twenty-Seven Circuit, 0.4375 mc Input

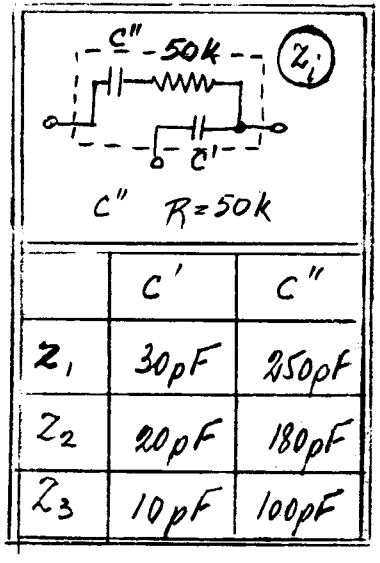

	C'	C"
Z_1	30pF	250pF
Z_2	20pF	180pF
Z_3	10pF	100pF

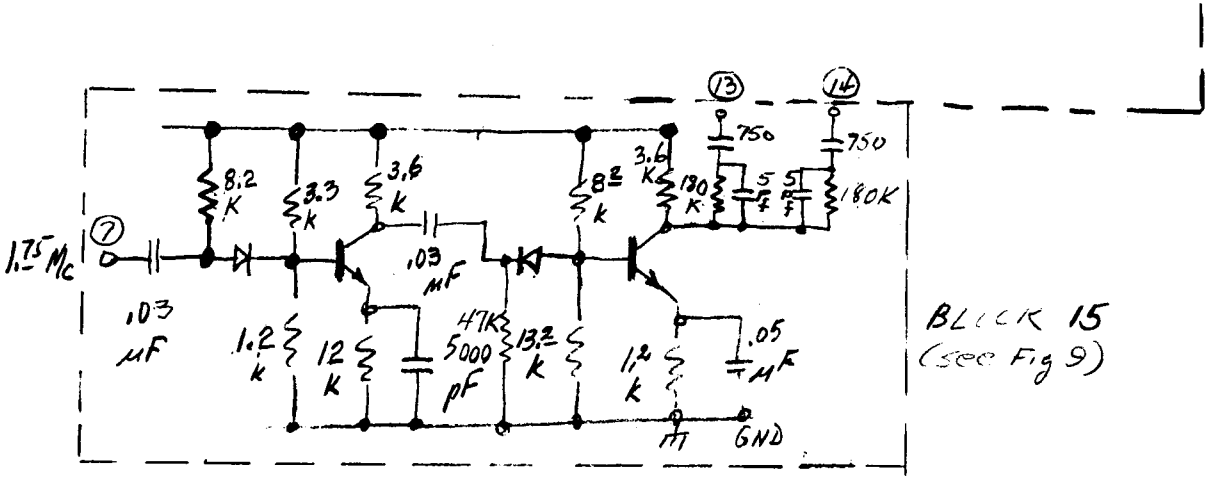

Figure 29a. Gating Circuit for Block 13

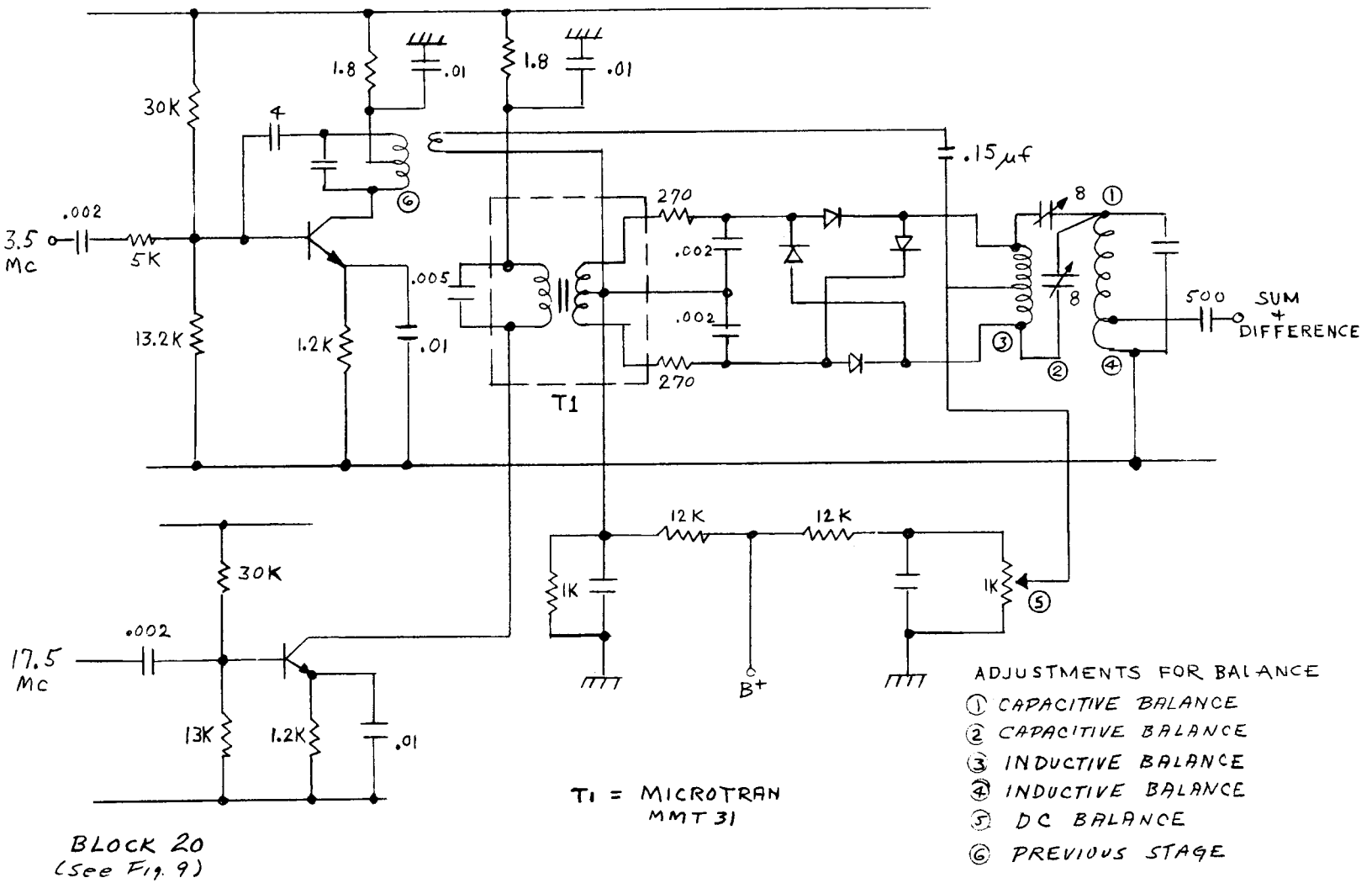

Figure 30. Balanced Modulator

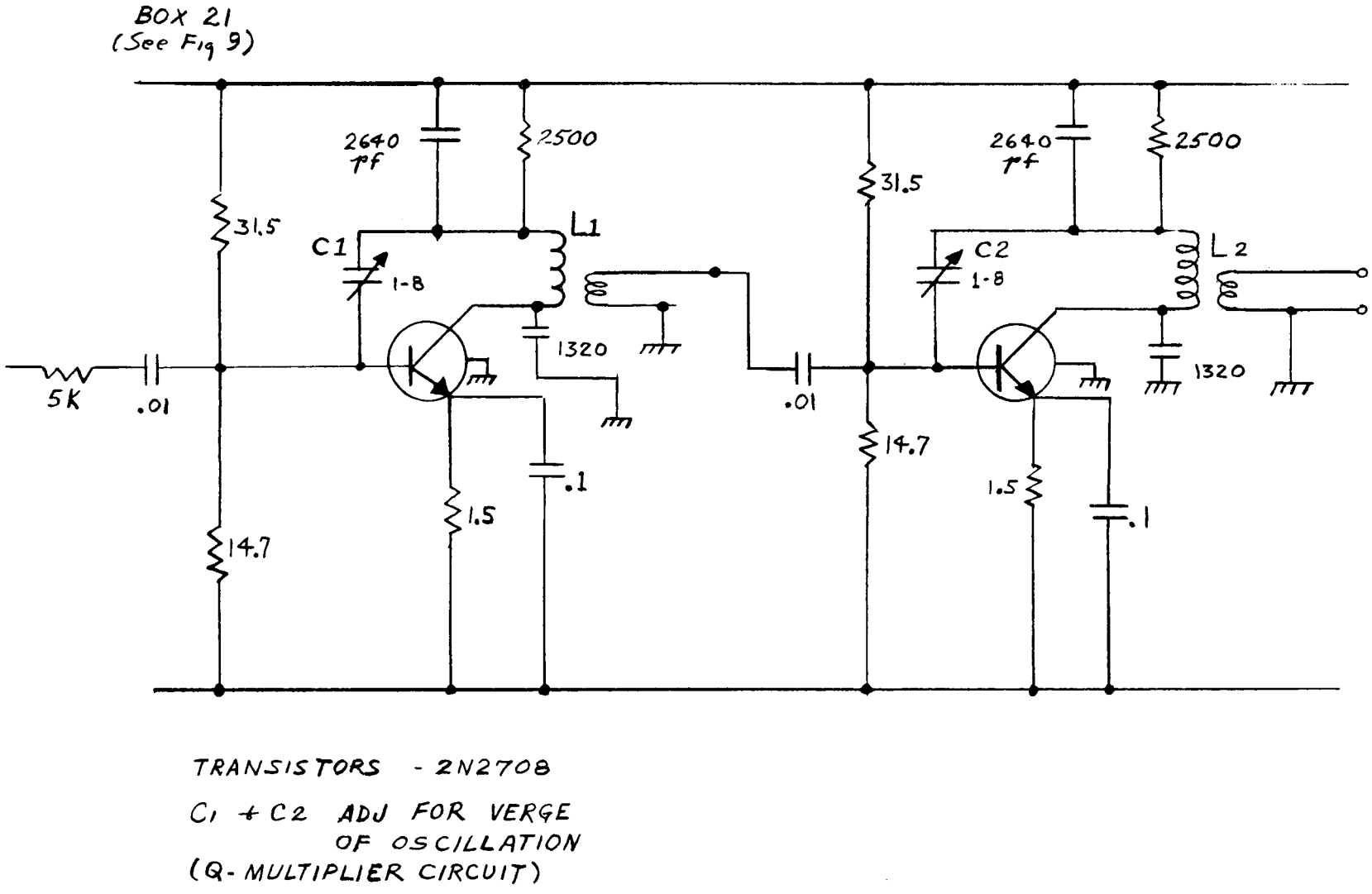

Figure 31. Tuned Amplifier for 3.4825 mc

plus amplitude limiting prior to demodulation, as shown in Figure 32.

f. Feedback Mixing Circuits, Blocks 17 and 18

Referring again to the System Block Diagram, Figure 9, the closed loop FM operation requires that the frequency (.455 - Δf) MC fed to the demodulator be raised to (8.75 + Δf) MC to excite that particular transmitter which will be phase locked to the tuning of the implant. The following circuits are used for this purpose:

Block No.	Description	Figure No.
17	Addition - Subtraction Circuits, 0.455 MC Input, 20.5625 MC Output	33
18	Subtraction Circuit, 20.5625 MC Input 8.75 MC Output	34

g. Added Filter Circuits, Blocks 22, 23, 24, and 25

Filters, Figure 35, were used in the 60 cycle line supplying power to the receiver, Block 6, and to the clock generator and associated circuits. Each of these identical filters rejected 8.75 MC and 11.8125 MC. Additionally the circuits were provided with shielding enclosures.

A bandpass filter, Figure 36, centered at the wanted 20.5625 MC was used to reject the other frequencies existing in the antenna at high levels (Block 23 Figure 9).

Block 24 is a crystal filter, Figure 37, used to clean up the 24.5 MC supplied as a local oscillator signal to the receiver. Figure 38 is also a crystal filter used with the receiver for the second L.O. signal of 3.4825 MC (Block 25).

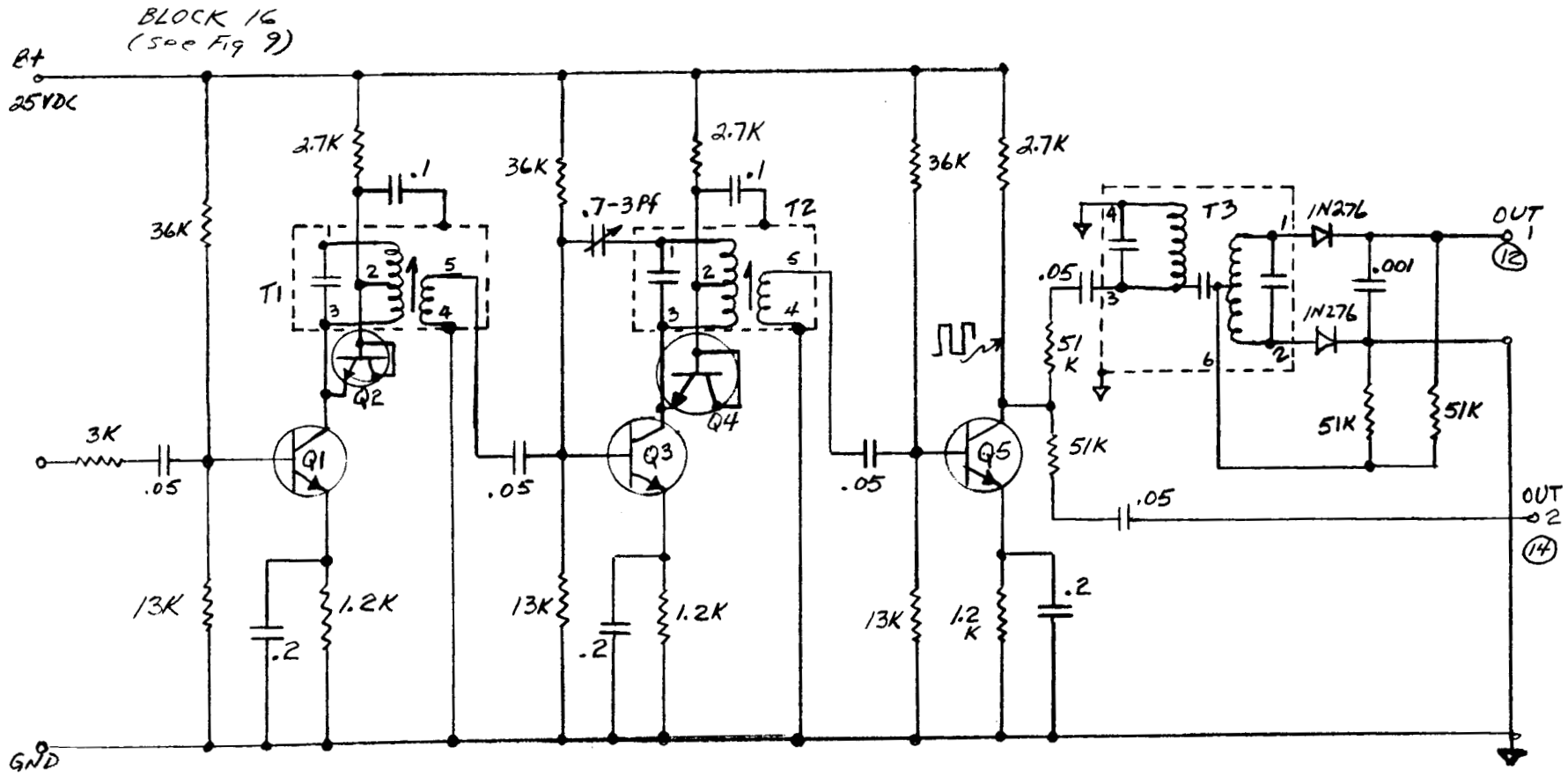

Figure 32. FM Demodulator

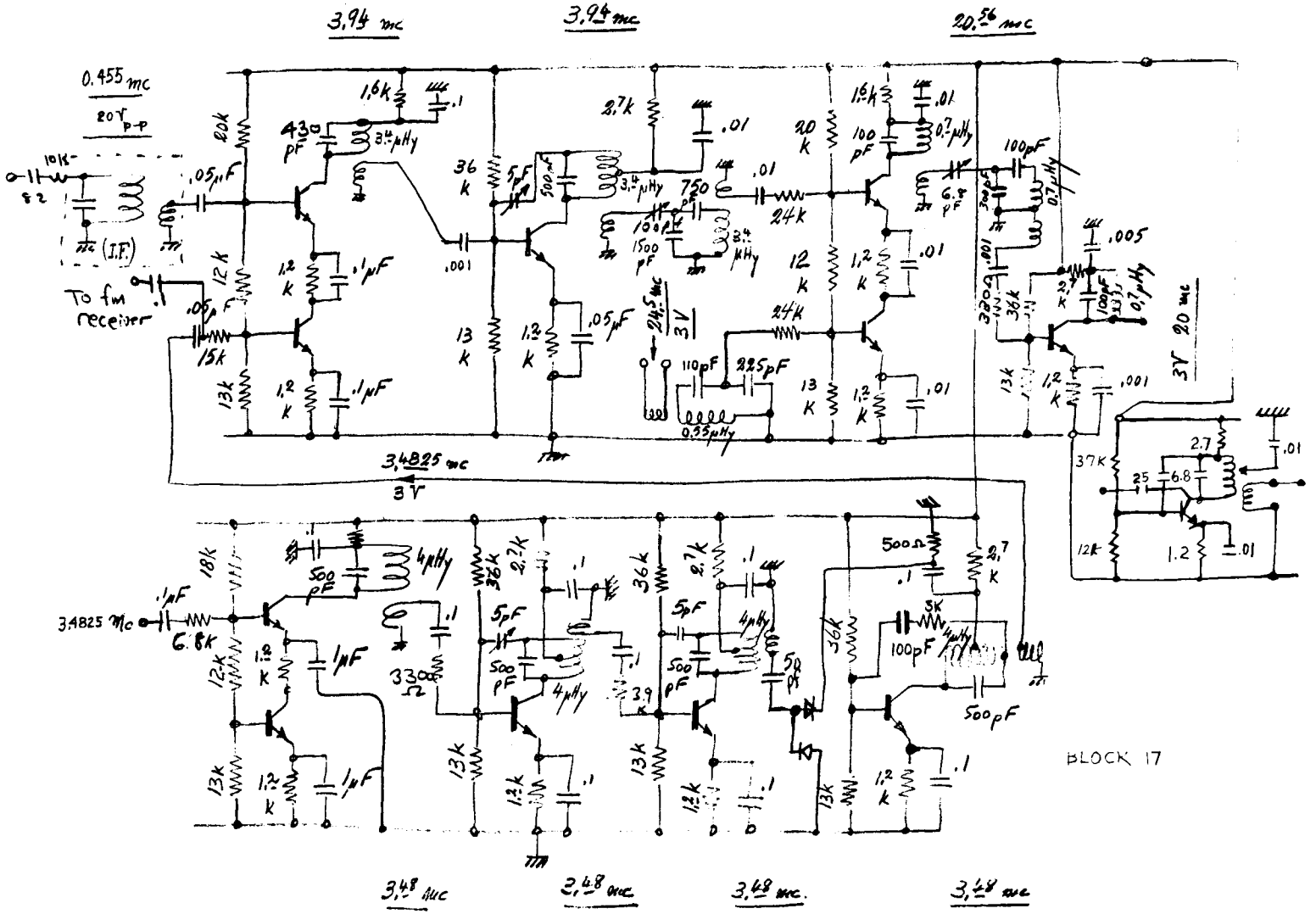

Figure 33. Addition - Subtraction Circuits, 0.455 mc Input, 20.5625 mc Output

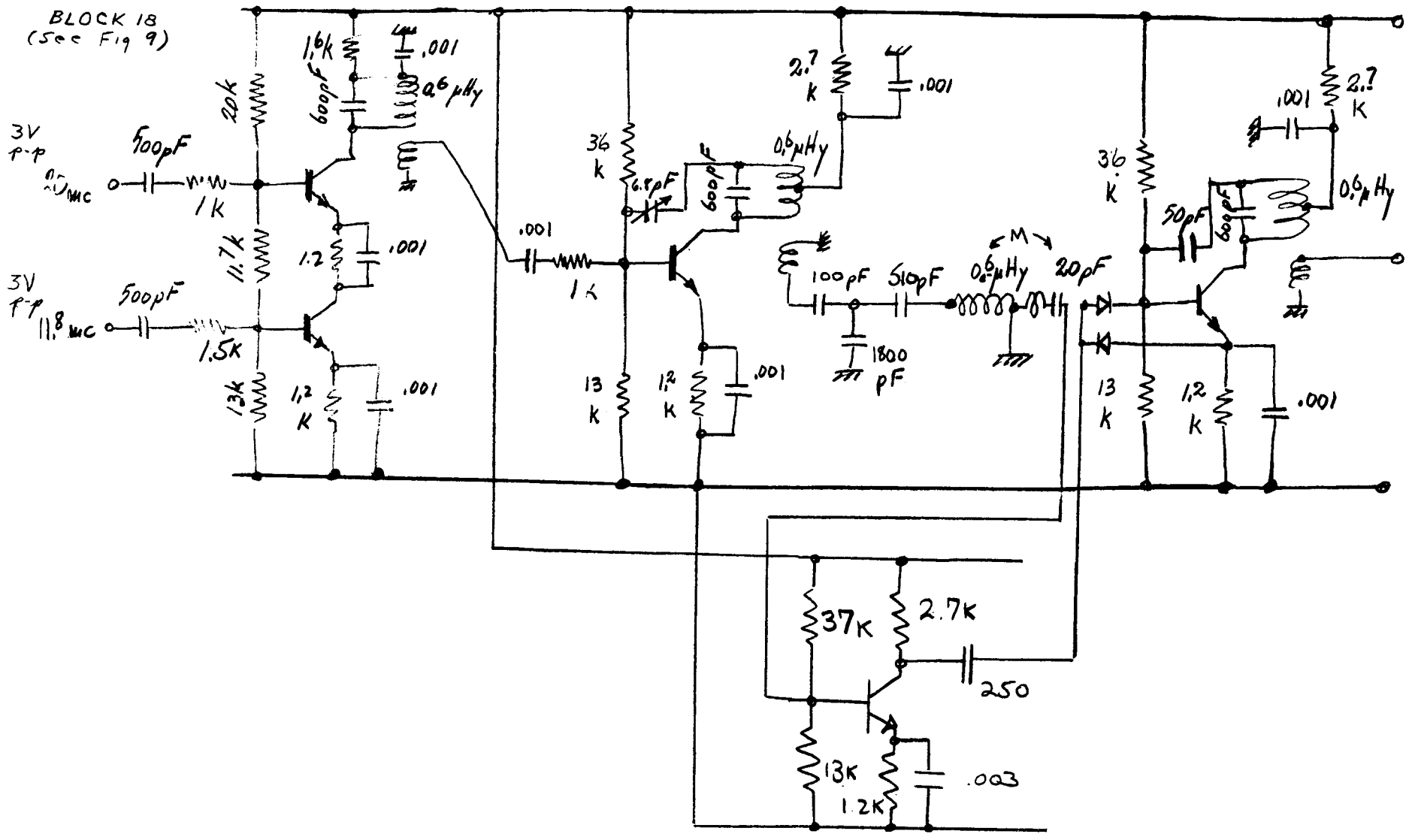

Figure 34. Substraction Circuit, 20.5625 mc Input, 8.75 mc Output

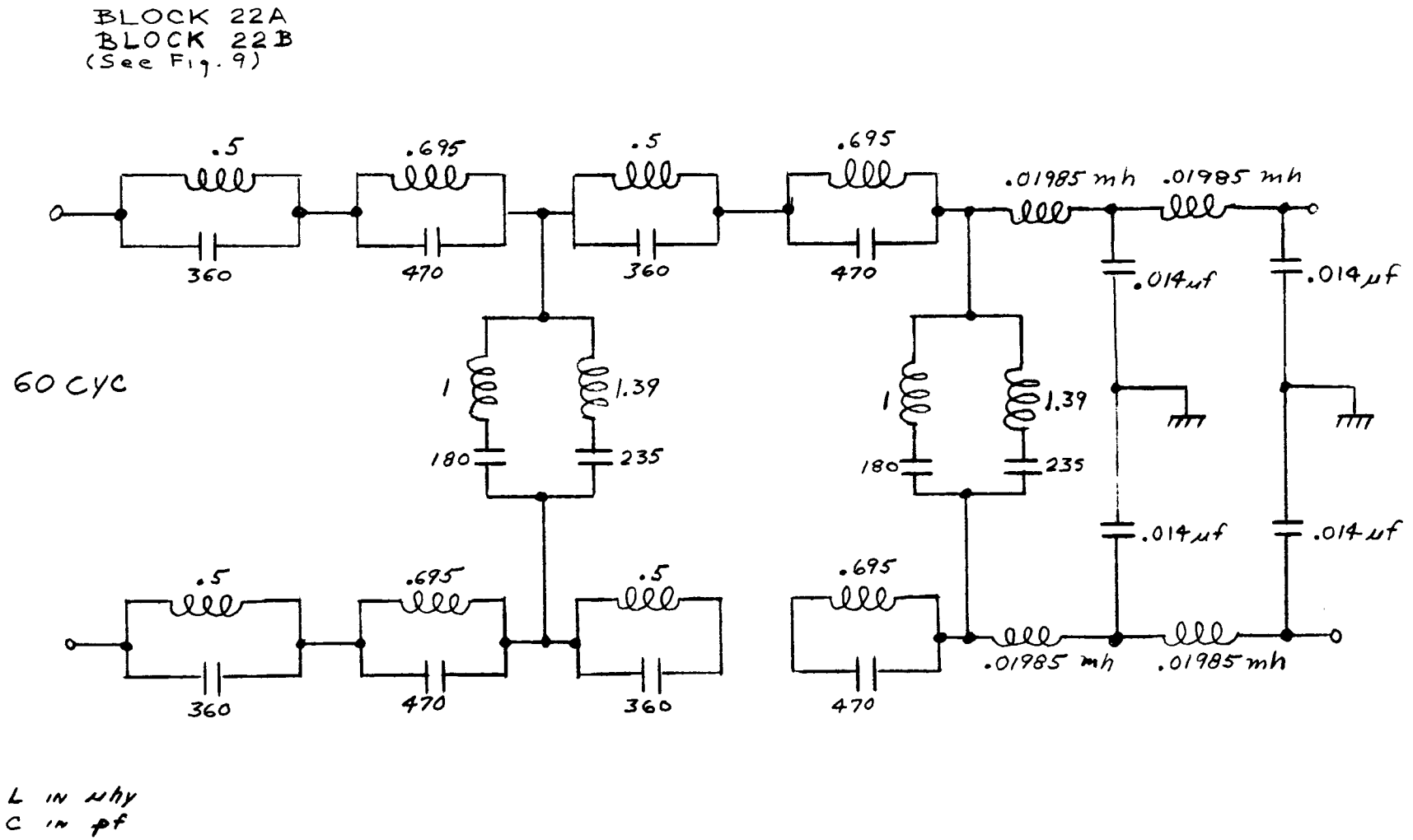

Figure 35. Sixty (60) Cycle Line Filters Rejecting 8.75 mc and 11.8125 mc

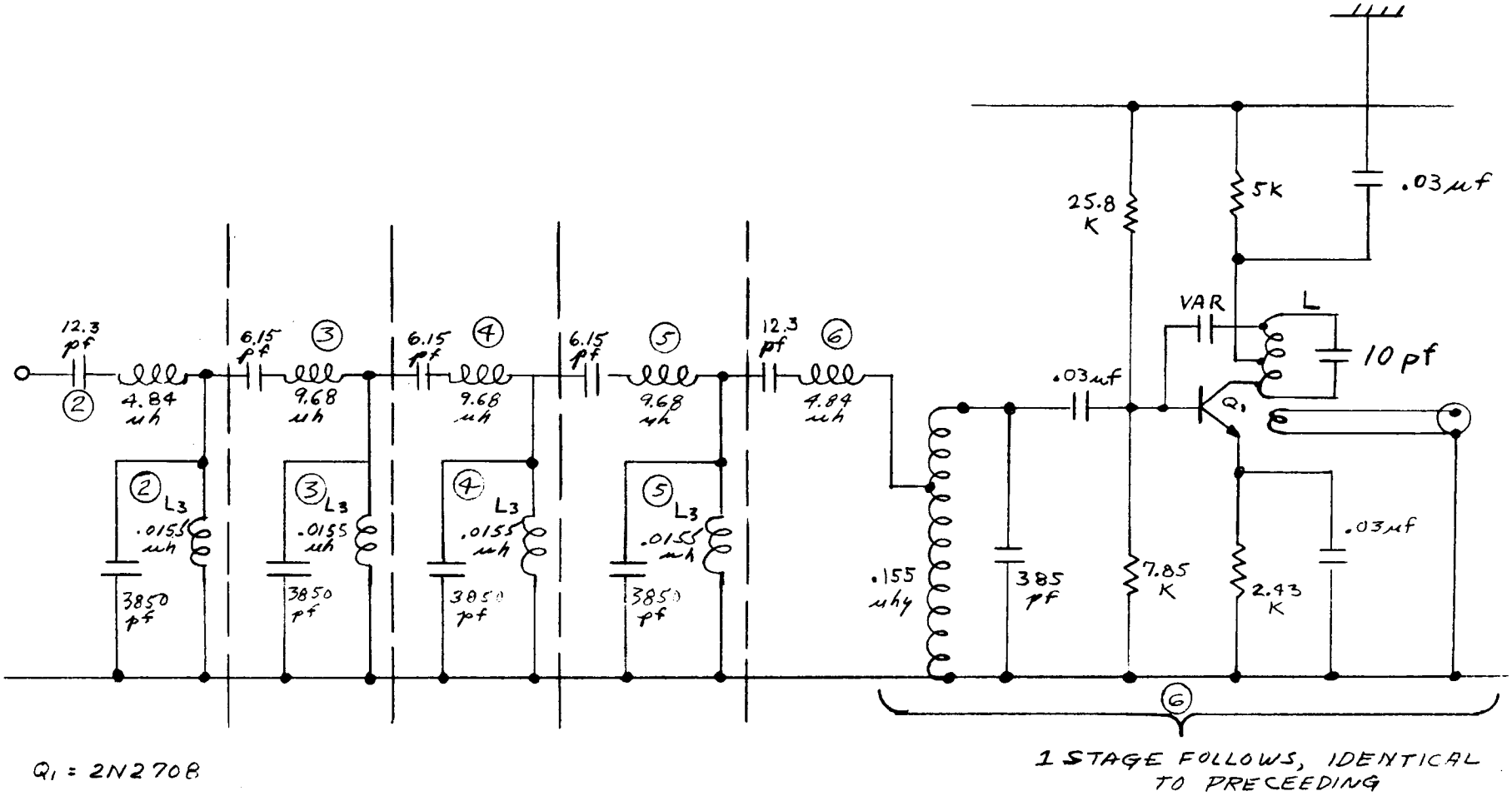

Figure 36. Bandpass Filter Amplifier Centered at 20.5625 mc

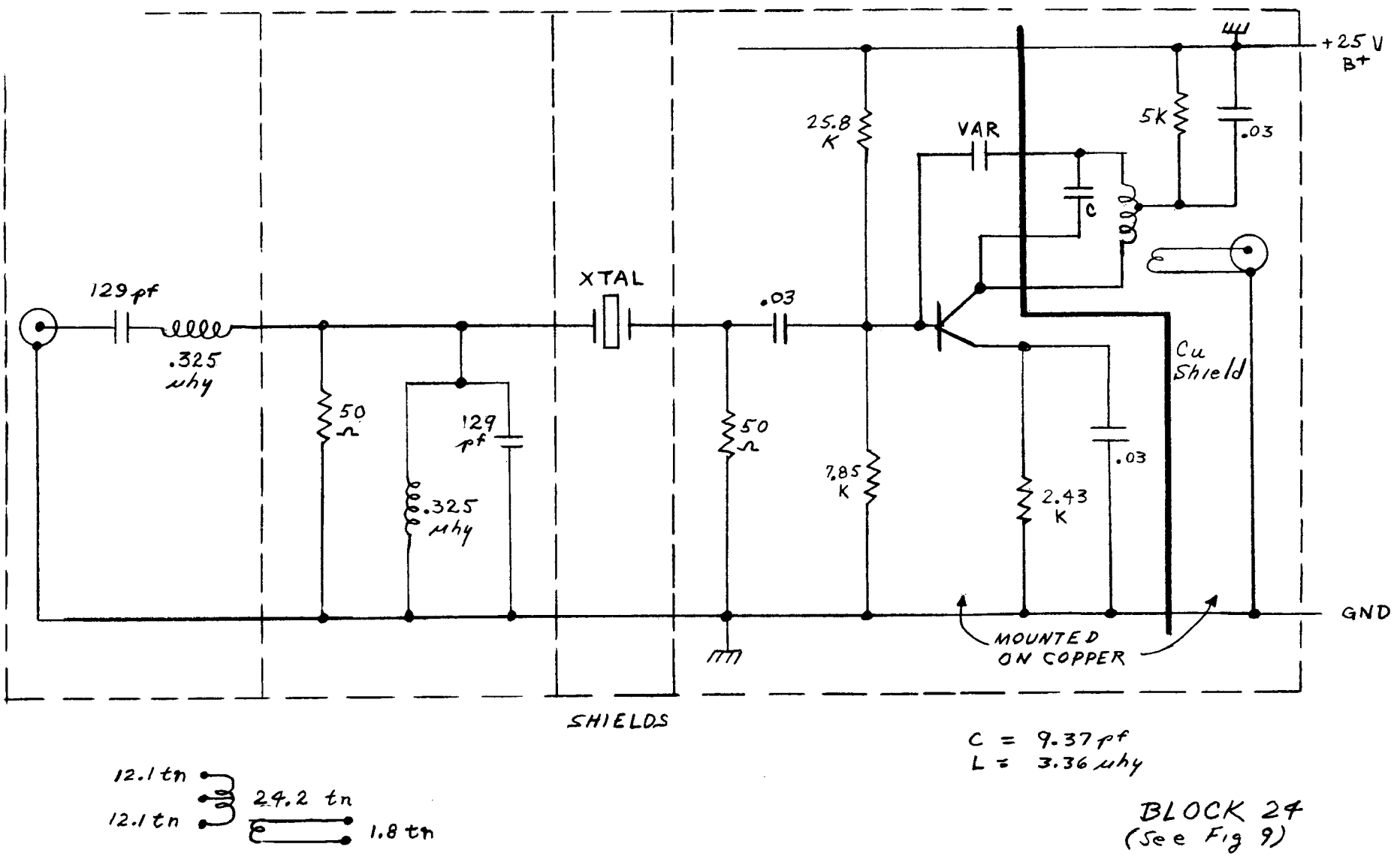

Figure 37. Crystal Filter Centered at 24.5 mc

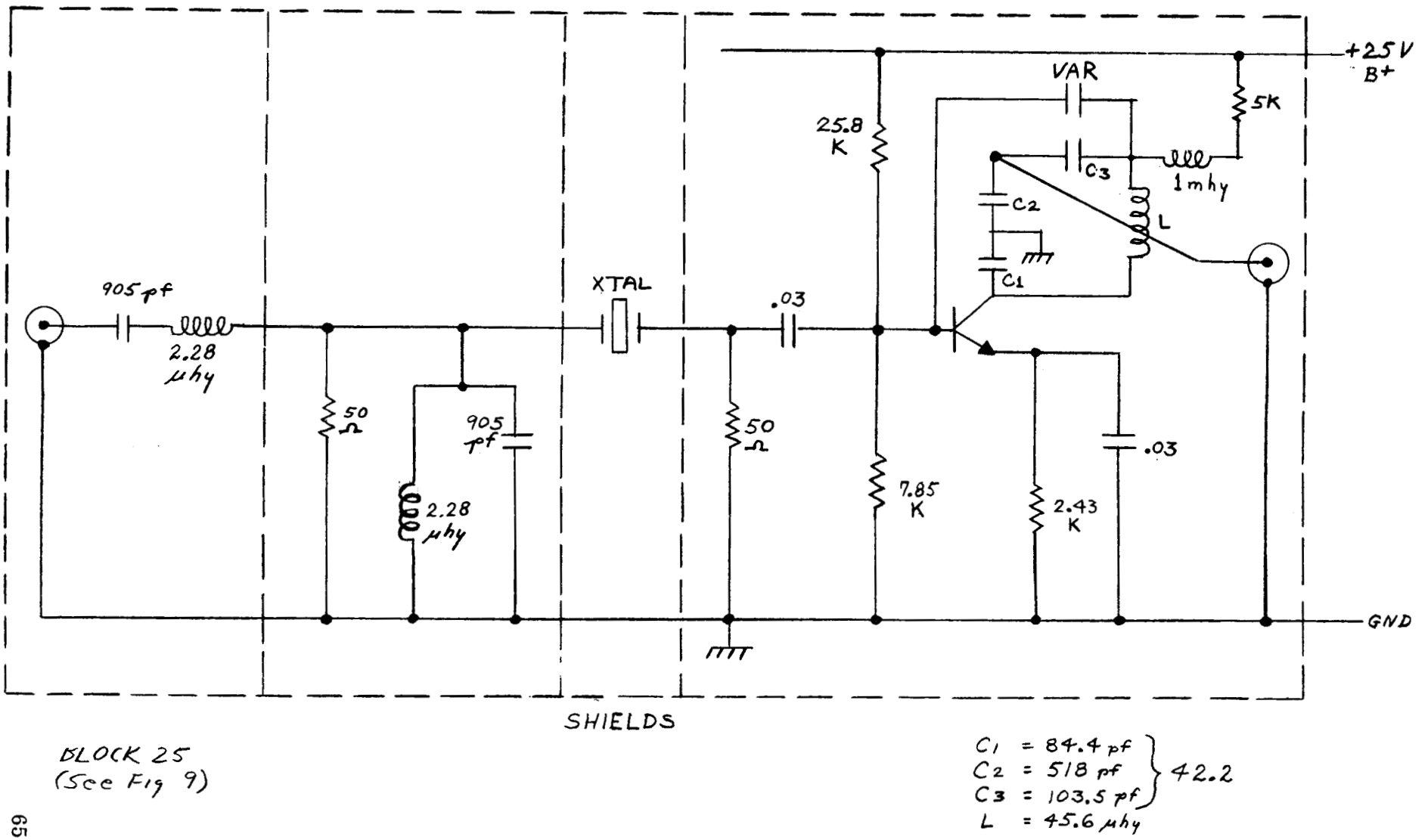

Figure 38. Crystal Filter Centered at 3.4825 mc

4. The Implanted Device Design

a. Introduction

This portion of the report will deal with the design considerations of the Implanted Device, which we will call the Implant, and its realization. We shall begin by making a thorough Systems Analysis, then discuss the actual implant design, and finally give data on the results obtained.

b. System Analysis to Determine Implant Power Budget

We shall obtain the necessary power levels at inputs and output of the implant, by making a study of the FM system based on the following assumptions:

Receiver Bandwidth	B.W.	= 3 kc
Receiver Noise Figure	N.F.	= 10 db
Receiver Base Band	B.B.W.	= 300 cps
Receiving Antenna Losses	A	= 10 db

The average Base Band frequency can be evaluated, considering a uniform spectral distribution, to be approximately the geometric average frequency between 10 cps and 300 cps, that is:

$$f_{av} = \sqrt{10 \times 300} \cong 50 \text{ cps}$$

For the resultant FM system the average index of modulation, $\beta = \frac{\Delta F}{f}$, will be, if the peak deviation is defined to be $\Delta F = 1.2$ kc:

$$\beta = \frac{1,200}{50} = 24$$

Thus, the expected signal to noise ratio improvement factor relative to AM becomes[5]

$$\frac{S}{N}\Big|_{FM} = 3\beta^2 \times \frac{S}{N}\Big|_{AM} \therefore \frac{S/N\,|FM}{S/N\,|AM} = 3\beta^2 = 1700 = 32 \text{ db}$$

Since for proper operation of the FM system, the AM S/N would be 32 db, the total S/N expected would be 64 db.

(5) "Radio Engineers Handbook", F. E. Terman, 1st Ed. pg. 671

At this point and for comparison purposes it may be noted that the phase modulation (PM) system resulting from open loop operation may be compared with an AM system by means of the same relationship, where β = radians of phase modulation.

$$\frac{\left.\frac{S}{N}\right|_{PM}}{\left.\frac{S}{N}\right|_{AM}} = 3\beta^2 \cong 0.6 = -2 \text{ db}$$

This is based on a PM modulation of 0.45 radian peak duration. Using these results overall improvement between the open loop or PM system and the closed loop or FM is in favor of the FM by 34 db.

This will be so if the system meets the conditions of the following analysis. By defining parameters of bandwidth, noise figure, etc., as above, the threshold for the receiver is defined, and for proper operation the following should be met at the IF of the receiver:

$$\frac{\text{Signal carrier Power}}{\text{Noise over IF BW}} = 3\beta = \frac{S_c}{N_{IF\ BW}}$$

or

$$S_c = 3\beta \left[N_{IF\ BW}\right] \tag{1}$$

where: $N_{IF\ BW}$ = is the noise referred to the input of the receiver for the IF Bandwidth of the receiver

Evaluating we obtain:

$$N_{IF\ BW} = KT\,(BW)\,NF = -204 + 34.8 + 10 = -159.2 \text{ dbW}$$

for $KT = -204$ dbW

$BW = 3 \times 10^3$ cps = 34.8 db

substitution in (1) for $\beta = 24$ results in, if $3 \times \beta = 3 \times 24 = 72 = 18.6$ db,

$$S_{c_{(db)}} = -159.2 \text{ db} + 18.6 = -140.6 \text{ dbW}$$

corresponding to 0.66 μ $Volt_{rms}$ input to the receiver at its ohm input terminal. Thus, allowing 10 db losses for the antenna, we get that the voltage induced at the antenna has to be, for threshold receiver conditions, at least

$$E_{ant_{rms}} = 0.66 \times (+10 \text{ db}) = 2.1 \ \mu V_{rms}$$

Since the antenna of the implant is within the near field of the receiver antenna, for practical purposes the evaluation of the induced voltages can be made as for two normally coupled coils, that is the output voltage at receiver antenna coil can be expressed as:

$$E_a = j \omega M I_{imp} \qquad (2)$$

where: E_a = voltage at receiver's antenna coil (2.1 μV_{rms} required)

M = mutual inductance between inductances L_{ra}, the receiver antenna, and L_i the implant's transmitting antenna

$M = K\sqrt{L_i L_{ra}}$, K being the coupling factor

The coupling factor K is the relation of field coupling which can be considered to be approximately equal to the area ratios of the smaller coil to the larger, that is:

$$K = \frac{5 \text{ cm}^2}{3.6 \times 10^4} \cong \frac{1}{7 \times 10^3} \text{ for the relative sizes}$$

considering for the receiver's antenna the 5 x 8 foot dimensions and for the implant's transmitting antenna the size of 1" in diameter.

The inductance for these antennas are:

- for the receiver's antenna:

$$L_{ra} \cong \frac{0.01 \ \phi \ N^2}{0.45 + \frac{\ell}{\phi}} \cong 10^{-2} \ \frac{183}{1.28} \cong 1.4 \ \mu Hy$$

ϕ = 6 ft = 183 cm average

ℓ = 5 ft = 152 cm

N = 1 turn

- for the implant:

$$L_i = 0.01 \frac{2.54 \times 144}{0.64} = 5.75 \ \mu Hy$$

$\phi = 1'' = 2.54$ cm

$\ell \cong 1/5'' = 0.485$ cm

N = 12 turns

Q = 250 $\therefore$ $r_\ell = 2.96\ \Omega$ measured

Thus current required in the implant antenna becomes, substituting in (2) $M = K\sqrt{L_i L_{ra}}$,

$$I_{imp} = \frac{2.1 \times 10^{-6} \times 7 \times 10^{3}}{6.28 \times 2 \times 10^{7}\ 2.84 \times 10^{-6}} = 4.1 \times 10^{-5} \text{ Amp}_{rms}$$

and the voltage across the implant antenna is

$$E = r_\ell \times I_{imp} = 2.96 \times 4.1 \times 10^{-5} = 120\ \mu V$$

If the receiving antenna circuit of the implant is as follows:

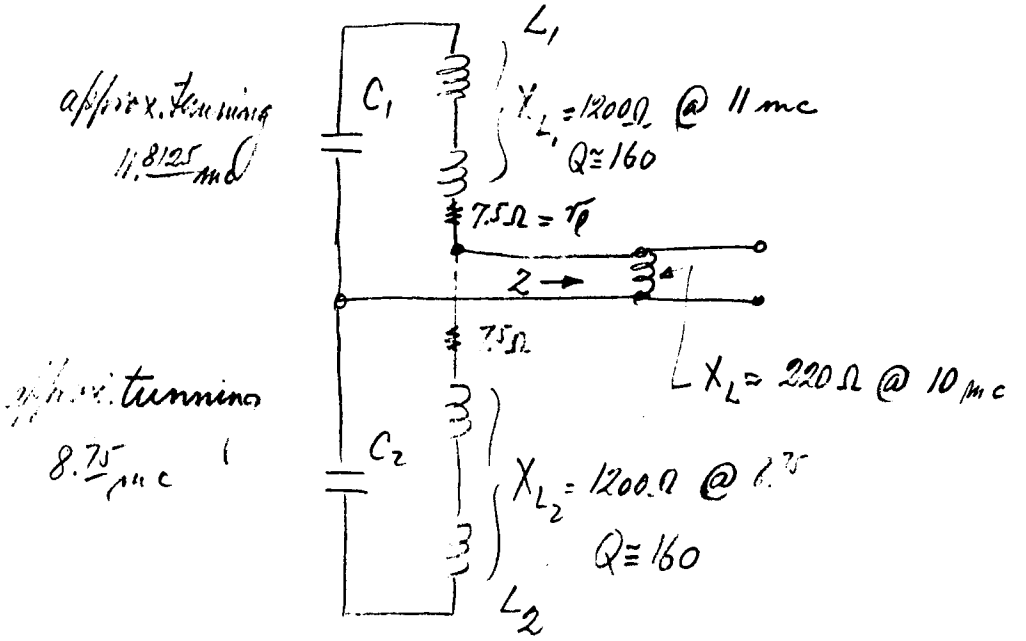

where: Z = 7.5 Ω + jX

X = is tuned out at the frequencies of interest by C_1 and or C_2

This condition for Z implies that the antenna circuit is optimally loaded and the energy available will be

$$W_a = \frac{1}{2} \frac{E_i^2}{2 r_\ell} \qquad (3)$$

L_1 is formed by two coils of an inductance of $\frac{L_1}{2} \approx 10\ \mu$Hy made with 20 turns on a ferrite core of a cross section area of $A \approx 0.08\ cm^2$.

The voltage induced in one of the two coils in the field of $B_{rms} = 6.16 \times 10^{-3}$ gauss, for N = 20 turns is

$$E = N \left|\frac{d\phi}{dt}\right|_{rms} 10^{-8} = N\ \omega\ \frac{\phi\ max}{\sqrt{2}} \times 10^{-8} = N\ \omega\ B_{rms} S\ 10^{-8} =$$

$$= 20 \times 6.28 \times 10^7 \times 6.16 \times 10^{-3} \times 8 \times 10^{-2} \times 10^{-8} =$$

$$= 6.18\ 10^{-3}\ \text{Volt rms}$$

For the two coils in series we have

$$E = 12.36 \times 10^{-3}\ V_{rms}$$

The Power available becomes by equation (3):

$$W_a = \frac{1}{4} \frac{144 \times 10^{-6}}{7.5} \quad 4.8\ \mu\text{Watt}$$

c. Implant Design

(1) Implant Transmitting Antenna Circuit

In accordance with the data utilized for the Power Budget evaluation the following comprises the antenna transmitting circuit for a 50 Ω input impedance:

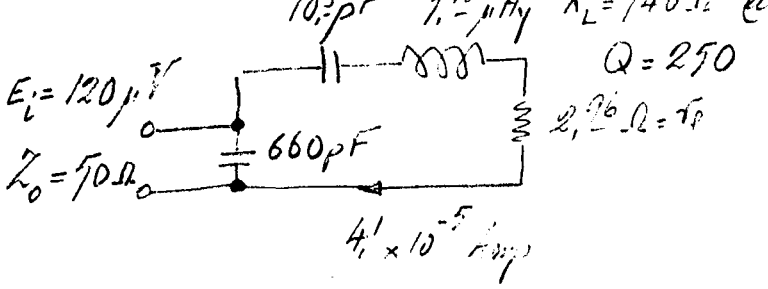

(2) Modulator Circuit

Evaluation of the Modulator Circuit results in the following equivalent circuit; all values and parameters are indicated:

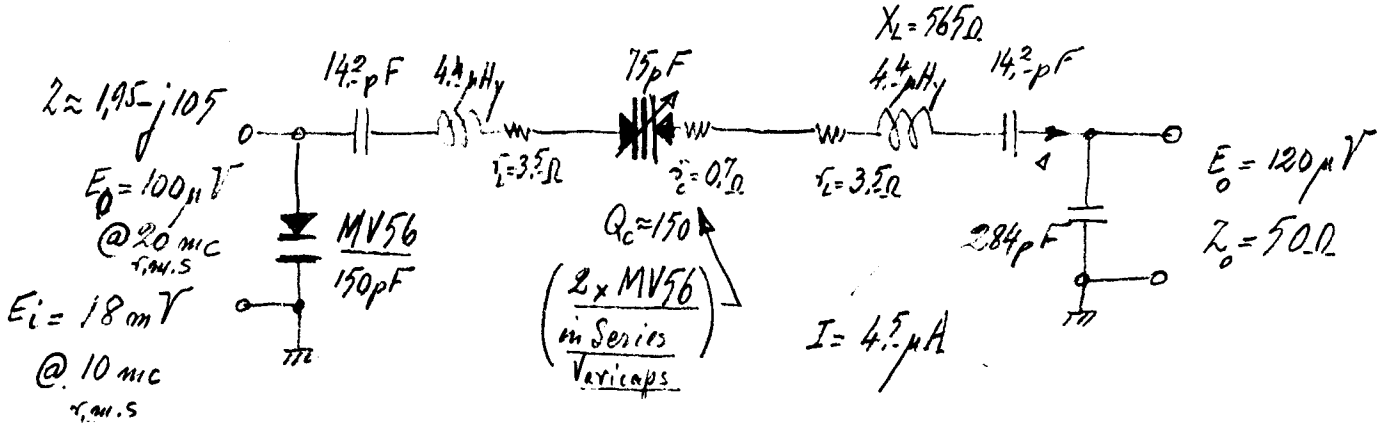

$$E_O = 0.31\ E_1 E_2 \approx 0.31\ E_i^2 \quad \therefore E_i = \sqrt{\frac{100 \times 10^{-6}}{0.31}} = 18\ \text{m V}$$

@ 20 mc @ 8 & 11 mc @ 10 mc

(3) Evaluation of Varicap Converter Constant

The varicap is a nonlinear capacitance of value

c(v) and reactance $X_c(v)$

where: $c = \frac{K}{V^{\frac{1}{2}}}$

$V = (v + V_o)$

K is a constant

V_o is a constant

and so

$$X_c(v) = \frac{V^{\frac{1}{2}}}{\omega K}$$

differentiation gives:

$$\frac{\partial X_c}{\partial V} = \frac{1}{2} \frac{1}{\omega K V^{\frac{1}{2}}}$$

In the circuit that follows, E_1 and E_2 are the signals to be converted:

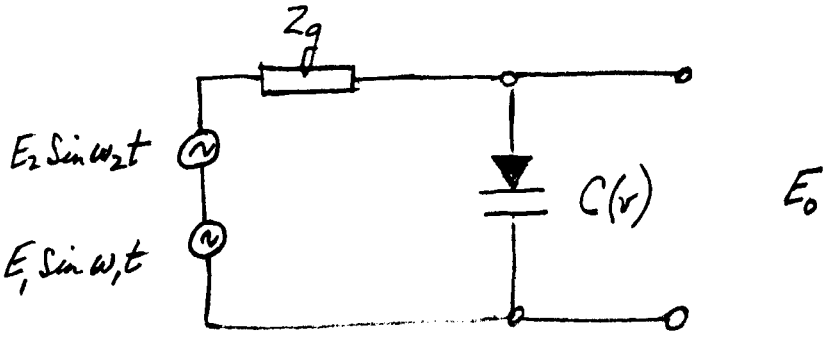

The output voltage E_o can be readily expressed by the following cross products

$$E_o = \frac{\partial X_c}{\partial V} \left\{ X_{c_{\omega_1}} I_1 \operatorname{Sin} \omega_1 t \, I_2 \operatorname{Sin} \omega_2 t + X_{c_{\omega_2}} I_2 \operatorname{Sin} \omega_2 t \, I_1 \operatorname{Sin} \omega_1 t \right\} =$$

$$= 2 \frac{\partial X_c}{\partial V} X_c \frac{1}{2} I_1 I_2 \left\{ \operatorname{Sin} (\omega_1 + \omega_2) t + \operatorname{Sin} (\omega_1 - \omega_2) t \right\}$$

since $X_{c_{\omega_1}} \approx X_{c_{\omega_2}} \approx X_c$ and also $I_1 \approx I_2 \approx I \approx \frac{E}{\sqrt{2}Zg}$

If for best matching $Zg = Rg = X_c$ then we can write, if only interested in the sum component

$$E_o = \frac{1}{2} \frac{\partial X_c}{\partial V} \frac{E^2}{Rg} \operatorname{Sin} (\omega_1 + \omega_2) t$$

The value for $\frac{\partial X_c}{\partial V}$ turns out to be 66 Ω/Volt for Varicap Type MV 56 and and $Rg \approx X_{MV56}$ @ 10 mc/s ≈ 105 Ω for 150 pF at $v = 0$.

These values give $E_o = 0.31 E^2$ peak value of converted signal for peak value of input signals.

(4) Receiving Antenna for Implant

The receiving antenna parameter evaluation results in the following circuit values:

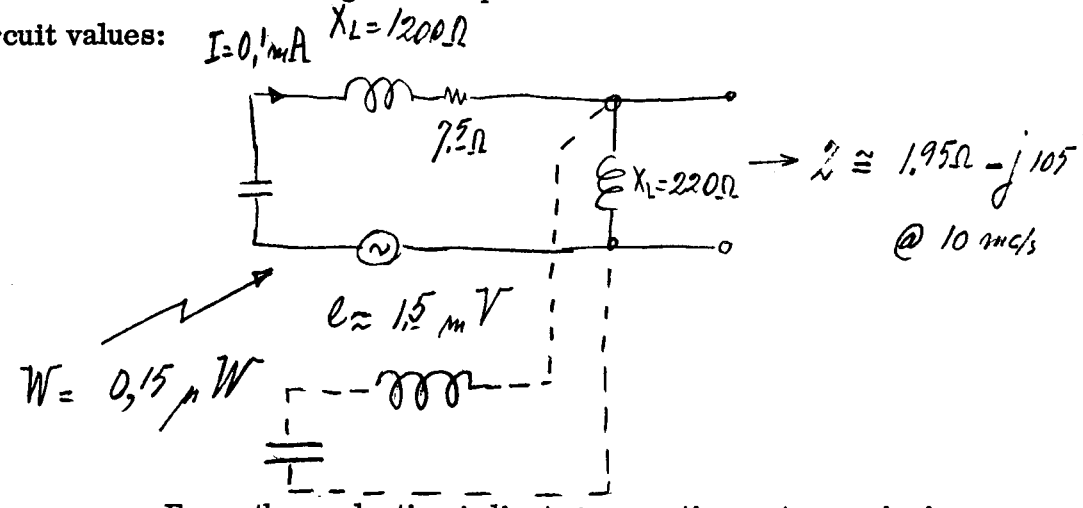

From the evaluation indicated for optimum transmission conditions there is a favorable balance of power of around 15 db to guarantee optimal performance.

The operation of the closed loop is analyzed in Appendix I; the operation in open loop follows.

The phase modulation at the implant is obtained by varying the reactance in the series branch of Figure 39 by the modulating voltage applied simultaneously to the two varicaps in a series connection through decoupling 10 KΩ resistors and an RF choke of 30.5 μHy inductance.

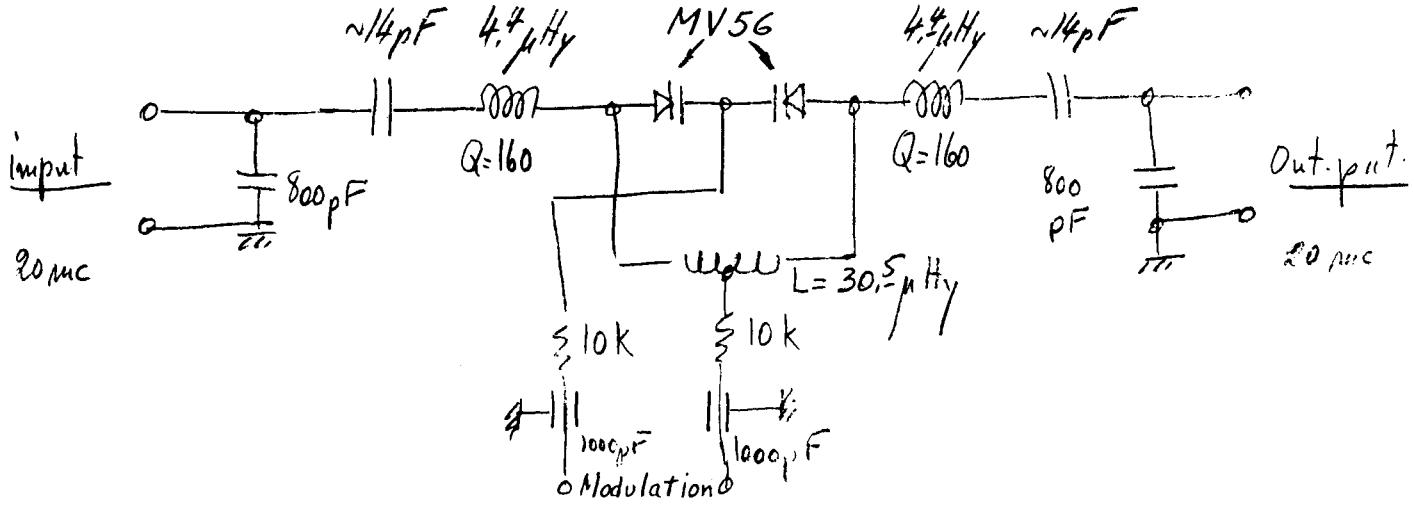

Figure 39. Modulator Circuit in Implant

For the above circuit it can be written:

$V = (v + v_o)$ $$\frac{\partial \varphi}{\partial V}\Big|_v = \frac{\partial \varphi}{\partial c}\Big|_v \frac{\partial c}{\partial V}\Big|_v \qquad (4)$$

where: ϕ = phase angle in radians

For near resonance for the above circuit

r_s = series resistance

$$\frac{\partial \varphi}{\partial c} = \frac{\partial}{\partial c} \frac{\Sigma X_\ell - \Sigma X_c}{r_s}$$

Because only the varicaps are dependant on V it reduces to:

$$\frac{\partial \varphi}{\partial c} = \frac{1}{r_s} \frac{\partial X_c (v)}{\partial c (v)}$$

substitution in (4) gives

$$\frac{\partial \varphi}{\partial V} = \frac{1}{r_s} \frac{\partial X_c}{\partial c}\Big|_v \frac{\partial c}{\partial V}\Big|_v = \frac{1}{r_s} \frac{\partial X_c}{\partial V}\Big|_v$$

and since $\frac{\partial X_c}{\partial V}$ = 33 Ω/Volt @ 20 mc/s for one varicap, for two in series we obtain $\frac{\partial X_c}{\partial V}$ = 66 Ω/Volt and so finally, with r_s = 11.7 Ω

$$\frac{\partial \varphi}{\partial V} = \frac{66\ \Omega/\text{Volt}}{11.7\ \Omega} = 6 \text{ radians/Volt}$$

For 150 mV peak to peak amplitude, obtained by 10 times gain through amplification of the 15 mV heart voltage, there results a phase deviation peak to peak of

$$\Delta\varphi = 6 \times 0.150 = 0.9 \text{ radians}$$

$$\cong 52° \text{ peak to peak}$$

C. FM/PM SYSTEM TEST RESULTS

1. Implant Device Construction

The Implant circuitry was constructed according to the evaluated data of the previous chapter and its output verified within the antenna fields.

Measurements indicated too low a voltage output to make the system operable. This confirmed the extra losses introduced by the increased measured resistance of the antenna at its input.

In order to get the system into operation, and to prove the principle involved, two small amplifiers were designed and constructed with a total power consumption of 0.75 Volt x 300 μA = 225 μ Watts. It is important to state here that the analysis made previously indicates that power should be available for the system to work. That this was not so is due only to the excessive antenna losses found. The amplifiers added for test just supply the losses of the antenna system. They could be RF field powered due to their very low power requirements, if they should be found to be necessary.

The amplifier schematic is as follows:

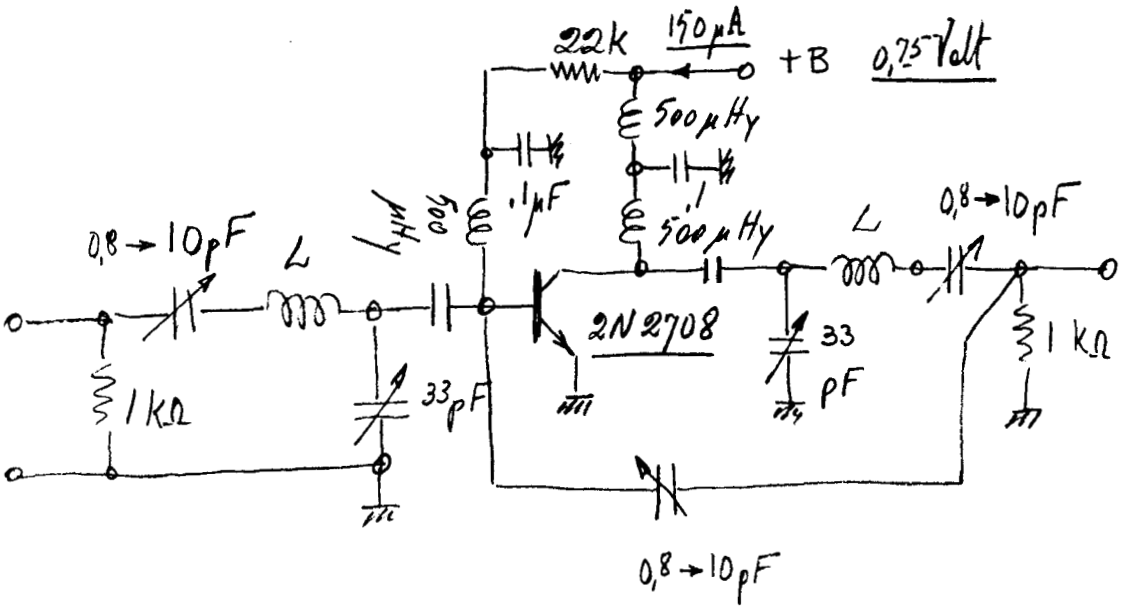

The inductances L were made to tune to 20 Mc with an approximate setting of the series condensers at 7 pF in the circuit shown.

One of the above amplifiers was introduced at the imput to the modulator just following the converter stage. This point was selected because the signal coming out of the converter stage is dependent on the product of the two input signals (8.75 Mc + 11.8125 Mc) and if both are low the output drops as the square of the input.

The second amplifier was located at the output of the modulator stage. As the amplifier gain is on the order of 5 to 7, this is now sufficient to make possible the operation of the link, as was verified with measurements.

The following block diagram gives the disposition of all "Implant Device" components whose circuits and designs have been treated previously.

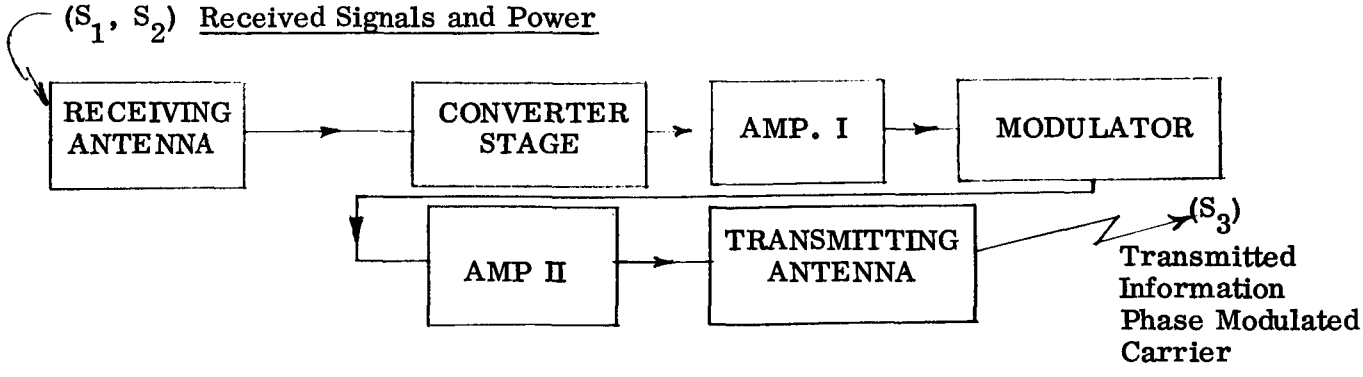

2. Measurement Results

Developing the antenna, the phase locked-loop circuitry of the FM receiving system, and the implant circuitry just described, represented a greater effort than was initially believed would be required. Consequently the program was running out of time and funds by the time it was possible to operate the system and verify the principles involved. Successful operation was achieved and demonstrated, to the extent of proving that phase modulation was being obtained in a very satisfactory manner; this was shown by displaying the 455 KC IF output of the receiver, Block 6, on an oscilloscope. The waveform was free of amplitude modulation (limiter stages were used) and could be made to phase shift back and forth about 40 to 50 degrees by turning on an audio frequency oscillator supplying 10 millivolts of signal to the modulator circuit in the implant.

A photograph of the waveform as it appeared on the oscilloscope is shown in Figure 40.

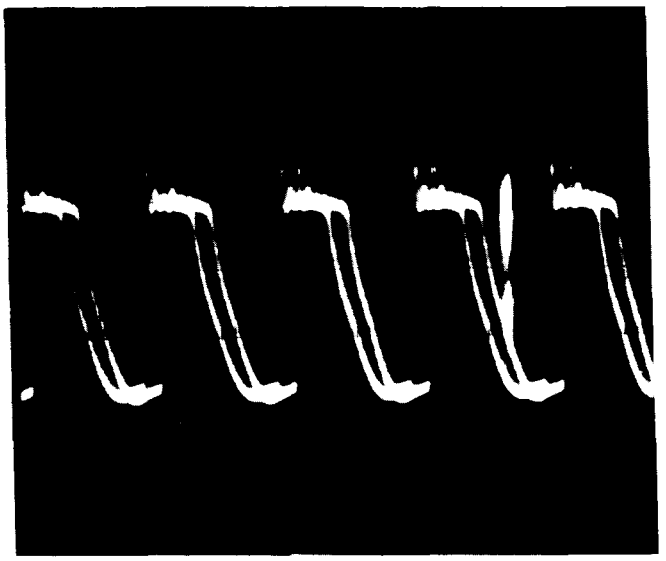

Figure 40. Phase Modulated Wave (455 KC)

While time did not permit complete operation of the FM system by closing the loop, a worthwhile demonstration was provided with the Phase Modulation signal by using a product detector to recover the audio modulation on the PM output. This modulation was made audible by using an amplifier and loud speaker after the product detector. It was then possible to vary the audio oscillator over a frequency range of 50 to 300 cycles and thereby demonstrate to a group of people that the intelligence signal modulating the 20 MC radio frequency wave was indeed being recovered from the phase modulated wave.

APPENDIX I

FREQUENCY MODULATION PRODUCED BY PHASE LOCKING TO RESONANT FREQUENCY OF IMPLANT

If the receiving coils at the implant have N_j turns and the received magnetic flux is $\phi\ (f_i^j)$, the induced voltage can be expressed as:

$$E_{f_i^j} = N_j \frac{\partial}{\partial t} \phi\ (f_i^j)$$

The wanted output of the conversion process can be expressed as:

$$E_{f_{imp}(n)} = \eta N_n \frac{\partial}{\partial t} \phi\ (f_2^{(n)}) \times N_0 \frac{\partial}{\partial t} \phi\ (f_o) = N \frac{\partial}{\partial t} \phi\ (f_{imp}^{(n)})$$

$$I_{imp} = \frac{E}{Z} = \frac{N \frac{\partial}{\partial t} \phi}{R + j\left[\omega L - \frac{1}{\omega c}\right]} = \frac{N \frac{\partial}{\partial t} \phi}{R + j\left[\omega L - \frac{1}{\omega c\ (E_m)}\right]}$$

where $c\ (E_m)$ is the value of the capacitance as a function of the applied modulation E_m.

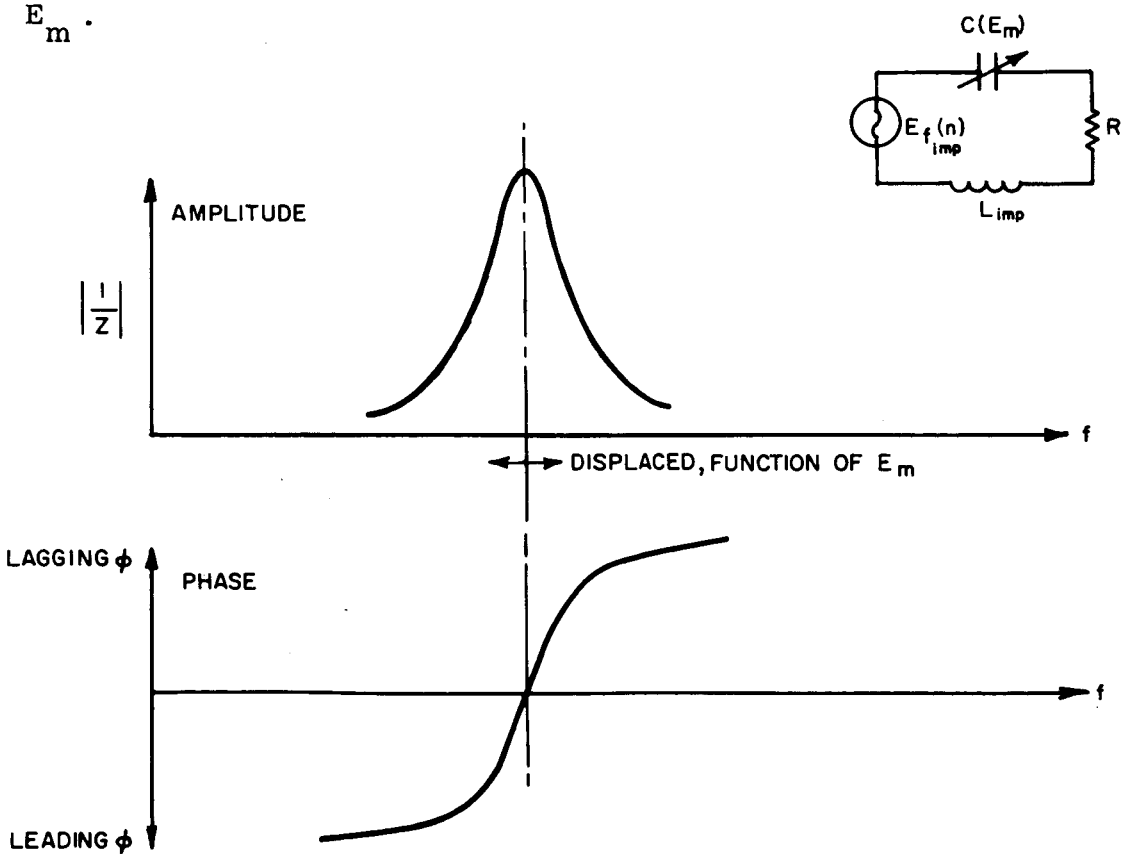

Figure 3. Amplitude and Phase Relations for Series Circuit

If the tuning circuit is tuned to the frequency near the top of the resonant peak, Figure 3, we can write the following approximation for the modulated current:

$$I_{imp} = N \frac{\partial}{\partial t} \phi \left| \frac{1}{Z} \right| e^{j\left(\frac{\partial \varphi}{\partial e_m} E_m + \nu\right)}$$

where $\left| \frac{1}{Z} \right| \approx$ constant at any given instant of time for the linear phase region

ν is a constant.

The field generated by I_{imp} is proportional to it at any given point in space:

$$\phi_r = k_1 L_{imp} I_{imp} e^{j k_2 d_1}$$

where L_{imp} = implants radiating circuit inductance

d_1 = distance between implant and receiving system

k_1, k_2 = constants.

The received signal will then be

$$E_r = N_r \frac{\partial}{\partial t} \phi_r = N_r k_1 L_{imp} e^{j k_2 d_1} N \frac{\partial^2}{\partial t^2} \phi \left| \frac{1}{Z} \right| e^{j\left(\frac{\partial \varphi}{\partial e_m} E_m + \nu\right)}$$

$$E_r = k_1 N_r N L_{imp} \left| \frac{1}{Z} \right| \frac{\partial^2}{\partial t^2} \phi e^{j\left[k_2 d_1 + \frac{\partial \varphi}{\partial e_m} E_m + \nu\right]} \qquad (1)$$

The term in brackets indicates the relative dependency of the phase of the received signal on three factors: the modulation sensitivity $\frac{\partial \varphi}{\partial e_m}$, E_m the applied modulating information voltage, and on the distance d_1. Since the latter is slowly varying, it can be disregarded, with respect to its frequency modulation effects.

The frequency of the output signal of the transmitter at $f_2^{(n)}$ has a definite relation with the input signal at the receiver input as a function of its phase. That is:

$$E_o = k_3 e^{j\left(\frac{\partial \varphi}{\partial f} \Delta f + k_4\right)} = k_3 e^{j\phi_r}$$

which is seen to be dependent only on the phase of the received signal

$$\varphi_r = \left(\frac{\partial \varphi}{\partial f} \Delta f + k_4\right).$$

The field generated by this voltage E_o applied to the radiating system can now be

expressed at the implant in terms of the right hand side of this expression for E_o.

$$\phi(f_i^j) = k_5 \, e^{j\left(\frac{\partial \varphi}{\partial f}\Delta f + k_4 + k_6 d_2\right)} \qquad (2)$$

the k's are constants of proportionality which are determined by fixed phase shifts and amplitude changes about which Δf causes variations; d_2 is the distance between implant and radiating system.

From Equation (1) and (2) we see that their amplitudes play no role in the solution, but are amplitude independent; not so the frequency which is phase dependent. Equating the argument of (1) at the receiver input (signal received) with the argument of (2) transfer function back to implant we get:

$$\nu + k_2 d_1 + \frac{\partial \varphi}{\partial e_m} E_m = \frac{\partial \varphi}{\partial f}\Delta f + k_4 + k_6 d_2$$

$$\Delta f = \frac{1}{\left[\frac{\partial \varphi}{\partial f}\right]_{f_2^{(n)}}} \left[\frac{\partial \varphi}{\partial e_m} E_m + (k_2 d_1 - k_6 d_2 - k_4 + \nu)\right]$$

The magnitudes of d_1 and d_2 vary at slow rates so the above is indicative of the linear dependency of Δf on the modulating input signal E_m and the modulation sensitivity $\frac{\partial \varphi}{\partial e_m}$. That is, the system is an F.M. system where the peak frequency deviation, Δf is proportional to the peak input signal.

One of the important considerations with respect to the Frequency Modulation System is that it can be accurately calibrated. This is due to the fact that the deviation is dependent only on the applied modulation signal, while independent of amplitude variations and noise, as encountered in amplitude modulation systems. In AM, the received amplitude scale becomes highly distance-dependent, unless very complex automatic gain controls (A.G.C.) are used along with good carrier frequency stabilization.

Appendix

PART A

COMPARISON BETWEEN SELF AND MUTUAL INDUCTANCES -- TURNS OF ANTENNA

The self inductance of a rectangular loop of wire carrying uniform current can be expressed by[8]

$$L = .02339\left[(s_1+s_2)\log_{10}\frac{4s_1s_2}{d} - s_1\log_{10}(s_1+g) - s_2\log_{10}(s_2+g)\right]$$

$$+ .01016\left[\mu\delta(s_1+s_2) + 2(g+\frac{d}{2}) - 2(s_1+s_2)\right] \text{ microhenrys} \qquad (A-1)$$

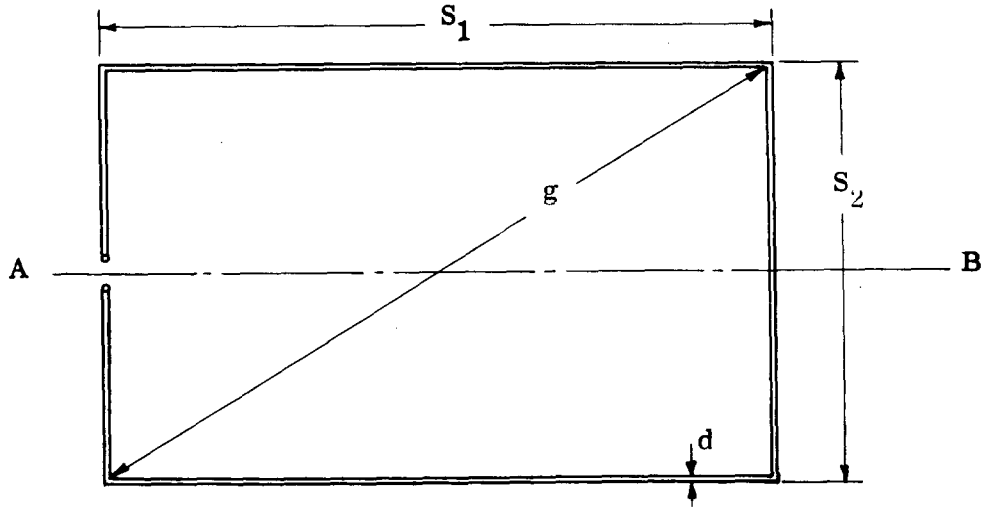

δ = skin effect correction factor (function of d and frequency)

Figure A-1

The distances in (A-1) are in inches, μ = relative permeability of medium, $\delta = .0031$, and $d \ll S_i$, $i = 1,2$. The individual antenna turns which will be constructed for this contract have the following dimensions:

---

8 See for example, Terman, F.E. Radio Engineers Handbook, 1st ed., p. 53.

s_1 = 96 inches

s_2 = 60 inches

g = 113 inches

d = 0.187 inches

The surrounding medium will be air for which $\mu = 1$. Substituting these values in expression (A-1), we get - L = 9.2 microhenrys. The mutual inductance between two loops situated as in Figure A-2 is given by[9]

$$M = .02339 \left[l_1 \log_{10} \frac{\sqrt{l_1^2 + D^2} + l_1}{\sqrt{l_1^2 + l_2^2 + D^2} + l_1} \times \frac{\sqrt{l_1^2 + D^2}}{D} \right.$$

$$\left. + l_2 \log_{10} \frac{\sqrt{l_2^2 + D^2} + l_2}{\sqrt{l_1^2 + l_2^2 D^2} + l_2} \times \frac{\sqrt{l_2^2 + D^2}}{D} \right]$$

$$+ .02032 \left[\sqrt{l_1^2 + l_2^2 + D^2} - \sqrt{l_1^2 + D^2} - \sqrt{l_2^2 + D^2} + D \right] \text{microhenrys} \quad \text{(A-2)}$$

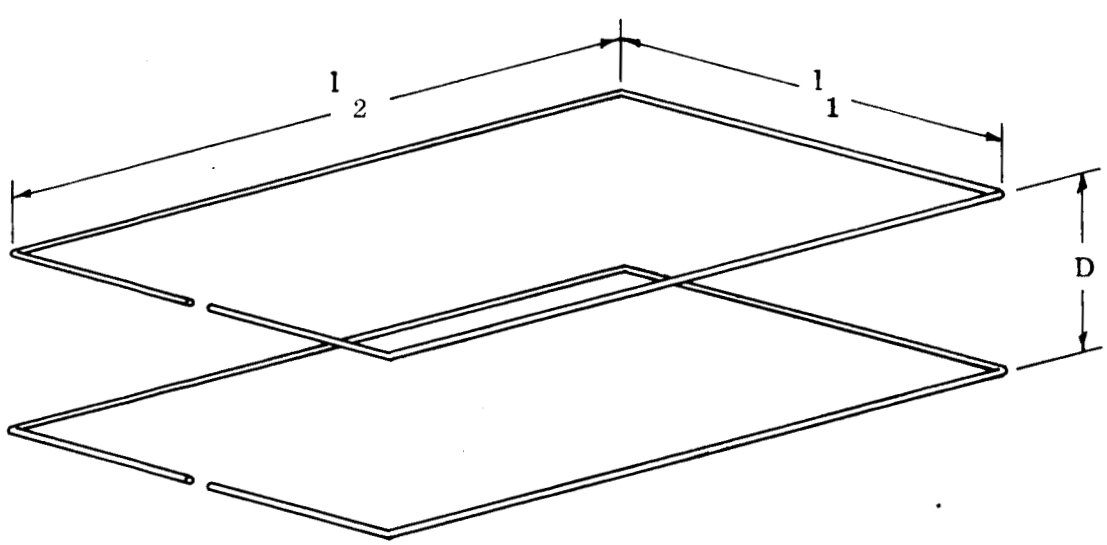

Figure A-2

9 Ibid p. 68

Numerically, with l_1 = 60 inches, l_2 = 96 inches and D = 18 inches, Eq. (A-2) becomes M = 1.5 microhenrys.

PART B

DESIGN ANALYSIS OF SINGLE TURN 3 FREQUENCY RESONATOR ANTENNA

A single turn of the antenna is a symmetrical structure if viewed from the line A-B in Fig. A-1. As such it bears a close resemblance to a balanced two wire transmission line. The exceptions are the ends which are perpendicular to the line of symmetry. However, a symmetrically excited wire like a dipole can be approximated by a balanced transmission line with a spacing equal to twice an average distance of the dipole conductor elements to the excitation point. The length of the "equivalent" transmission line is the distance from the center of the dipole to either end. This approximation is illustrated in Figure A-3.

By utilizing this approximation technique for those elements of the antenna which are perpendicular to the line of symmetry, the entire antenna can be represented by interconnected lengths of different balanced two wire transmission lines.

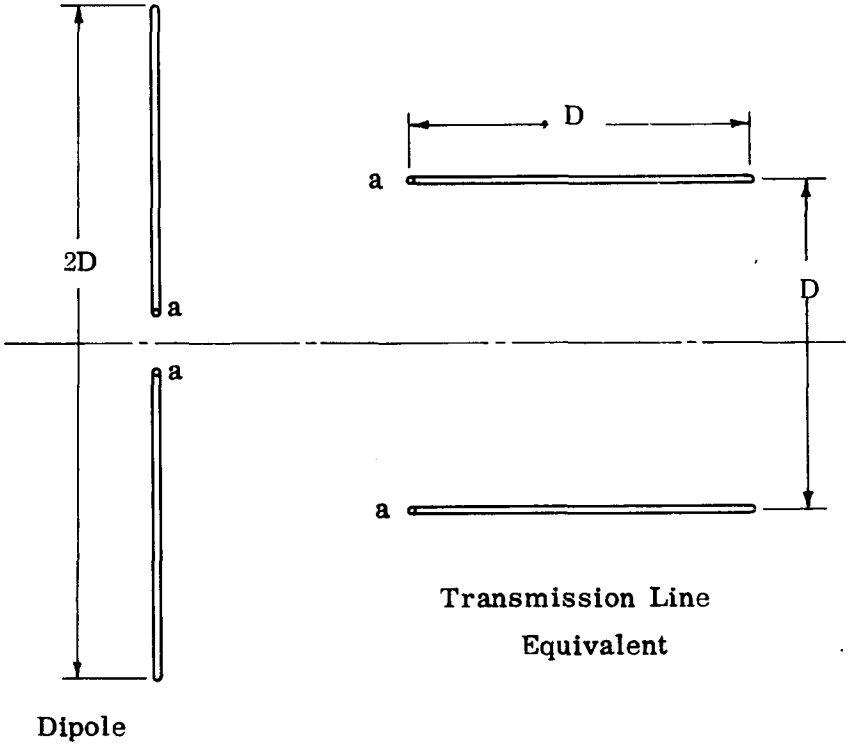

Figure A-3

The resultant approximation to the antenna is shown in Figure A-4. The elements in the approximating network which are perpendicular to the center line are shown just to indicate connection to adjacent lines. The perpendicular element to the far right represents an ideal short circuit.

For each of the three sizes of transmission line pictured in Figure A-4, one can obtain numerical values for characteristic impedance and propagation constant. From these quantities the input impedance of any section may be

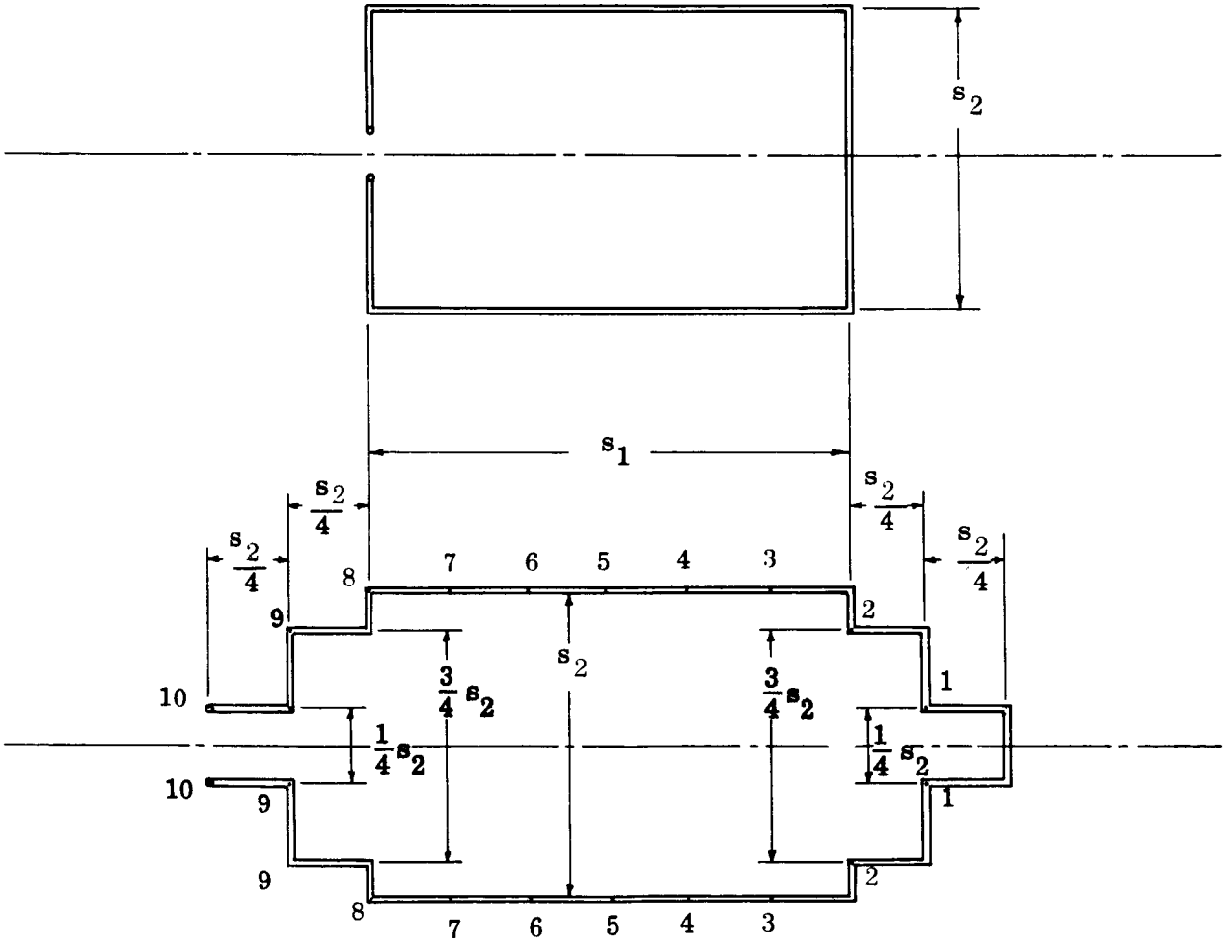

Figure A-4

computed provided the terminating impedance is known. The philosophy of the design can be qualitatively described as follows. The antenna has been broken up into sections as shown in Figure A-4. These sections are short with respect to wavelength to insure constant current distribution across each. The reactance seen at terminals 1-1 can be computed using the lossless transmission line equation:[10]

$$Z = Z_o \frac{j Z_o \sin \beta l + Z_r \cos \beta}{Z_o \cos \beta l + j Z_r \sin \beta l} \qquad \text{A-3}$$

where Z_o = characteristic impedance of line

Z_r = terminating impedance at length l of line

β = phase delay per unit length

Using equation A-3, as applied to section 2-2, it can be determined what reactances (at all three frequencies) would be required at 1-1 in order to reduce the reactance at 2-2 to 0. These values can be combined with the actual values at 1-1 to specify reactances which must be added at 1-1 to reduce the reactance at 2-2 to 0. This procedure is continued along the antenna ending with terminals 10-10, and a theoretical input reactance to the antenna of 0. The numerical design of the antenna is culminated by the design of the reactance networks which supply the required reactances to be added at the various odd numbered sections of the antenna.

Figure A-5 shows the numerical sizes for the different segments of transmission line shown in Figure A-4.

10. See Everitt and Anner, Communication Engineering, Third Edition, p. 339.

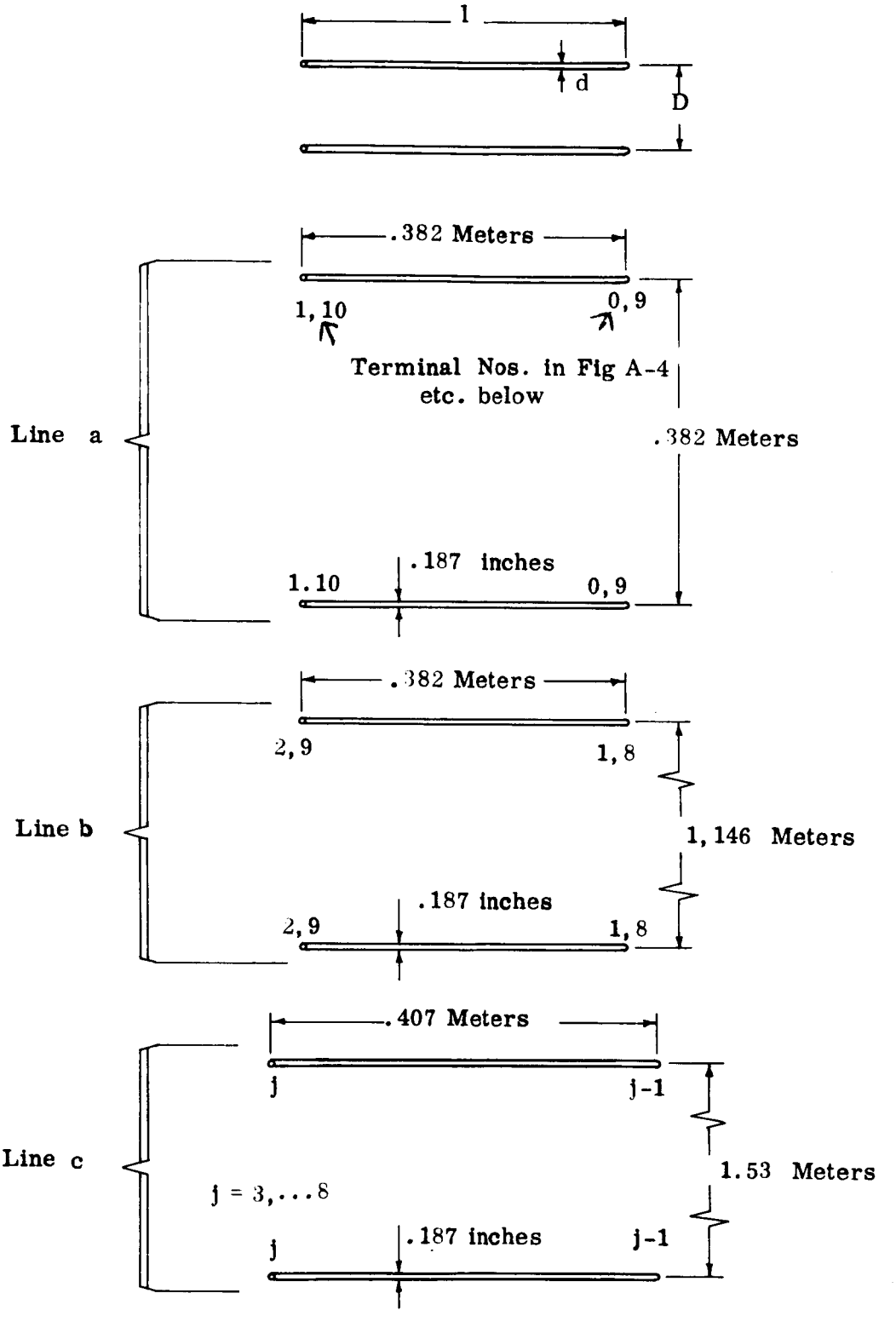

Figure A-5

For each of these lines, the following quantities are computed:

1) Characteristic impedance:

$$Z_o = 276 \log_{10} \frac{2D}{d} \quad [11] \qquad \text{A-4}$$

from which Z_{oa} = 609 ohms (For line a in Fig. A-5) etc. below A-4a

Z_{ob} = 740 ohms A-4b

Z_{oc} = 775 ohms A-4c

2) Loop inductance, L, per unit length of line

$$L = \frac{\mu_o}{4\pi}\left[1 + \frac{4 \log_{10}(\frac{2D}{d})}{\log_{10} \epsilon}\right] \quad [12] \qquad \text{A-5}$$

from which L_a = 2.13×10^{-6} henrys/meter A-5a

L_b = 2.57×10^{-6} henrys/meter A-5b

L_c = 2.68×10^{-6} henrys/meter A-5c

3) Shunt capacitance, C, between wires per unit length of line

$$C = \frac{\pi \epsilon_o \log_{10}(\epsilon)}{\log_{10}(\frac{2D}{d})} \quad [13] \qquad \text{A-6}$$

from which C_a = 5.48×10^{-12} farad/meter A-6a

C_b = 4.51×10^{-12} farad/ meter A-6b

C_c = 4.31×10^{-12} farad/ meter A-6c

11. Reference Data For Radio Engineers, ITT Handbook 4th Edition p. 589
12. Everitt and Anner, op. cit. p. 300
13. Ibid

4) Lossless line propagation constant, γ

$$\gamma = j\omega\sqrt{LC} = j\beta \quad [14] \qquad \text{A-7}$$

From A-5 through A-7, we obtain

$$\gamma_a = j\omega\ 3.42 \times 10^{-9} = j\beta_a \qquad \text{A-7a}$$

$$\gamma_b = j\omega\ 3.40 \times 10^{-9} = j\beta_b \qquad \text{A-7b}$$

$$\gamma_c = j\omega\ 3.39 \times 10^{-9} = j\beta_c \qquad \text{A-7c}$$

5) The phase delay, βl for each line at each of the three frequencies of operation

line a.	8.47 mc: $\beta_a l_a$ =	.0697 radians = 4°	A-8_1
	11.53 mc: $\beta_a l_a$ =	.0948 radians = 5.44°	A-8_2
	20.00 mc: $\beta_a l_a$ =	.165 radians = 9.44°	A-8_3
line b.	8.47 mc: $\beta_b l_b$ =	.0692 radians = 3.96°	A-9_1
	11.53mc: $\beta_b l_b$ =	.0941 radians = 5.40°	A-9_2
	20.00 mc: $\beta_b l_b$ =	.163 radians = .935°	A-9_3
line c.	8.47 mc: $\beta_c l_c$ =	.0735 radians = 4.2°	A-10_1
	11.53 mc: $\beta_c l_c$ =	.100 radians = 5.73°	A-10_2
	20.00 mc: $\beta_c l_c$ =	.173 radians = 9.94°	A-10_3

---

14. Everitt and Anner, op cit p. 301.

The next sequence of operations involves the determination of the reactances which must be added at odd numbered sections in order to reduce to 0 the reactances seen at even numbered sections.

We begin with the section in Figure A-4 farthest to the right. We look between terminals 1-1 and compute the three frequency reactances. Note $Z_r = 0$ for this section in equation(A-3). From (A-3) we get

$$Z_{11} = j\, Z_{oa} \frac{\sin \beta_a l_a}{\cos \beta_a l_a} \qquad \text{A-11}$$

From A-4a, $A\text{-}8_{1\text{-}3}$, A-11, we determine the reactances as viewed to the right of terminals 1-1.

a) 8.47 mc $Z_{11} = j\, 42.5$ $\text{A-}12_1$

11.53 mc $Z_{11} = j\, 57.8$ $\text{A-}12_2$

20.00 mc $Z_{11} = j\, 99.5$ $\text{A-}12_3$

Now we would like to add series reactances at terminals 1-1 such that the net reactance seen looking into terminals 2-2 is 0.at 8.47 mc, 11.53 mc, and 20.00 mc. The reactances which terminals 1-1 should present as a termination to the line 2-2 to 1-1 can be determined by equation (A-3). Let X_1 be the reactance which 1-1 should look like at 8.47 mc, X_2 the reactance which 1-1 should look like at 11.53 mc, and X_3 the reactance which 1-1 should look like at 20.00 mc. By (A-3) we can write,

$$0 = Z_{ob} \frac{j\, Z_{ob} \sin \beta_b l_b + j X_i \cos \beta_b l_b}{Z_{ob} \cos \beta_b l_b - j X_i \sin \beta_b l_b} \quad i = 1, 2, 3 \qquad \text{A-13}$$

This occurs if

$$j X_i \cos \beta_b l_b + j Z_{ob} \sin \beta_b l_b = 0$$

for which

$$X_i = \frac{-Z_{ob} \sin \beta_b l_b}{\cos \beta_b l_b} \qquad \text{A-14}$$

Using $A\text{-}4_b$, $A\text{-}9_{1\text{-}3}$, A-14, the X_i reactances can be computed

8.47 mc	$X_1 = -51.3$	$A\text{-}15_1$
11.53 mc	$X_2 = -70.1$	$A\text{-}15_2$
20.00 mc	$X_3 = -122$	$A\text{-}15_3$

Now the reactances given by $A\text{-}15_{1\text{-}3}$ differ from these given by $A\text{-}12_{1\text{-}3}$. In order to convert the values given by $A\text{-}12_{1\text{-}3}$ to those desired it is necessary to add series reactances Y_i on each side of the symmetry line such that

$$2Y_i + A\text{-}12_i = X_i \qquad i = 1, 2, 3$$

Numerically evaluated, it can be seen that

8.47 mc	$Y_1 = -46.9$	$A\text{-}17_1$
11.53 mc	$Y_2 = -63.9$	$A\text{-}17_2$
20.00 mc	$Y_3 = -111$	$A\text{-}17_3$

Equations $A\text{-}17_{1\text{-}3}$ fix the numerical reactance values required for each of the symmetrically deployed Foster networks at terminals 1-1.

The above procedure is continued along the antenna resulting in the specification of series reactances to be added at the odd numbered terminals such that the net reactance seen ocross the even numbered terminals is 0 at all three frequencies.

Equations A-3, A-4, A-8, A-9, A-10 are used to obtain the following numerical values for added reactances.

Terminals 3, 5, 7:	8.47 mc	$Y_1 = -57.0$	$A\text{-}18_1$
	11.53 mc	$Y_2 = -78.1$	$A\text{-}18_2$
	20.00 mc	$Y_3 = -135.4$	$A\text{-}18_3$
Terminals 9:	8.47 mc	$Y_1 = -47.0$	$A\text{-}19_1$
	11.53 mc	$Y_2 = -64.1$	$A\text{-}19_2$
	20.00 mc	$Y_3 = -114.2$	$A\text{-}19_3$

It now remains to specify the networks which can achieve the reactances required by equations A-17, A-18, and A-19. It should be noted that each set of reactances in these equations calls for increasing capacitive reactances with increasing frequency. Figure A-6 illustrates a sketch of the reactance vs frequency plot of the simplest Foster network which can be used to achieve this effect. The selection of a network of this type is sufficient to specify the analytic form of the sketch of figure A-6:

$$jX = \frac{H}{j\omega} \frac{(f^2 - f_1^2)(f^2 - f_2^2)}{(f^2 - f_3^2)(f^2 - f_4^2)} \quad [15] \qquad A\text{-}20$$

where f is frequency, $\omega = 2\pi f$, and H, f_1, f_2, f_3, f_4 are constants dependent on Co, L_1, L_2, C_1, C_2 in the circuit. The procedure used to determine these circuit parameters is now outlined. Based on the sketch of figure A-6 frequencies f_1, f_2, f_3, f_4 are estimated. Using these values in equation A-20, three separate calculations for the value H are performed, one for each reactance value and frequency combination specified in equations $A\text{-}17_{1\text{-}3}$, $A\text{-}18_{1\text{-}3}$, or $A\text{-}19_{1\text{-}3}$. The frequencies f_1, f_2, f_3, f_4 are readjusted until all three independent calculations for H yield the same value. At this point all the numerical values for the constants in A-20 are known. Now the numerical function is expanded in partial fractions. The resulting expression is compared term by term with the reactance expression

15 Everitt and Anner, op. cit. p. 173.

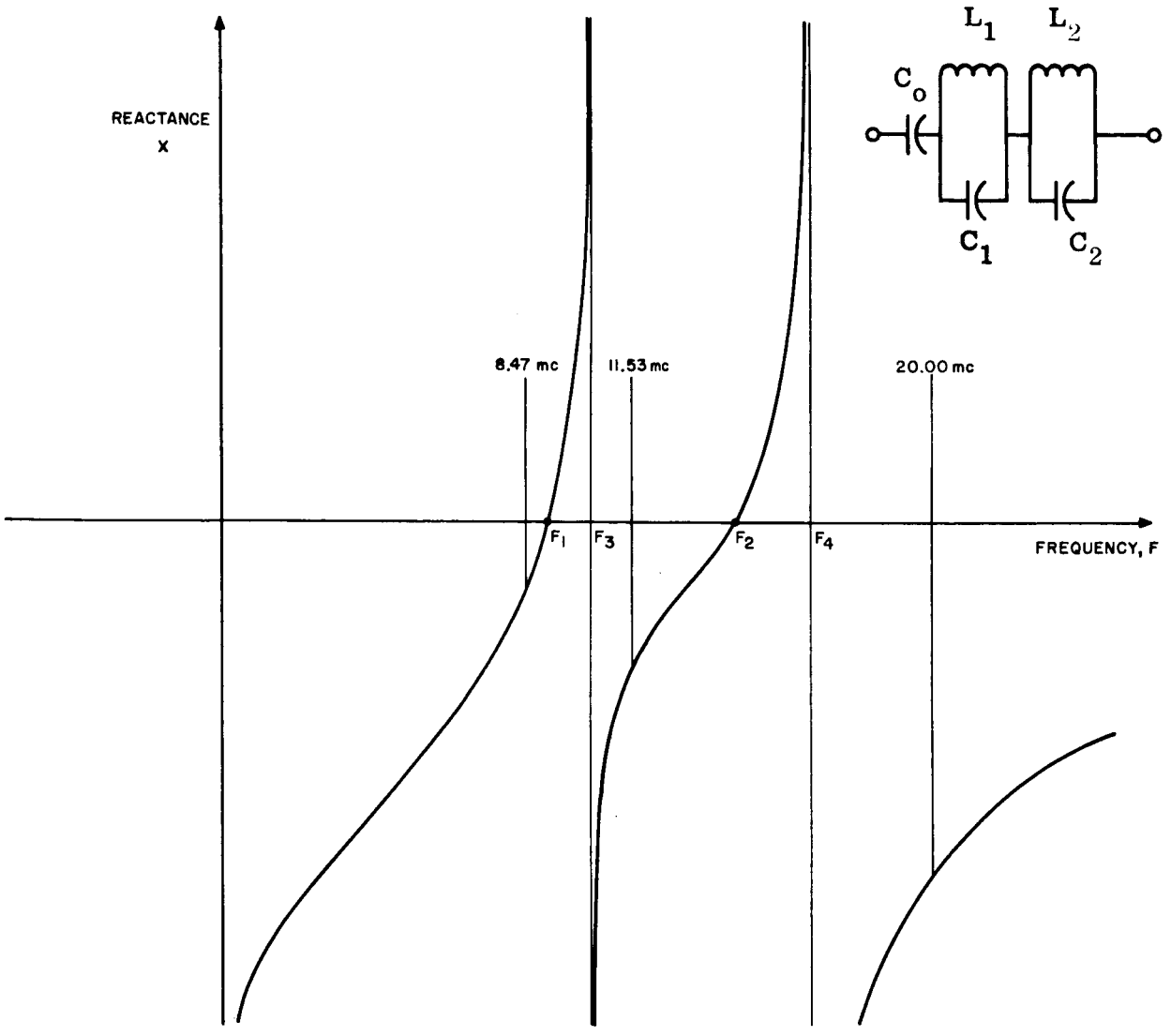

Figure A-6

for the network in terms of Co, L_1, L_2, C_1, C_2:

$$jX = \frac{-j}{\omega Co} - \frac{j\frac{\omega}{C_1}}{(\omega^2 - \frac{1}{L_1C_1})} - \frac{j\frac{\omega}{C_2}}{(\omega^2 - \frac{1}{L_2C_2})} \qquad \text{A-21}$$

The numerical values for the parameters of the network can be obtained from this comparison.

As an example of this procedure, the network design satisfying $A\text{-}17_{1\text{-}3}$ will be shown completely. From figure A-6, we make the following preliminary choices: $f_1 = 9.0$ mc, $f_2 = 14.1$ mc, $f_3 = 9.85$ mc, $f_4 = 17.0$ mc, We substitute these values into Eq. A-20 and evaluate H for each of the three cases of Eqs. $A\text{-}17_{1\text{-}3}$:

$$A\text{-}17_1 \quad -46.9 = \frac{-H\left\{(8.47\times10^6)^2 - (9.0\times10^6)^2\right\}\left\{(8.47\times10^6)^2 - (14.1\times10^6)^2\right\}}{2\pi(8.47\times10^6)\left\{(8.47\times10^6)^2 - (9.85\times10^6)^2\right\}\left\{(8.47\times10^6)^2 - (17.0\times10^6)^2\right\}} \qquad A\text{-}22_1$$

for which $H = 1.14 \times 10^{10}$

$$A\text{-}17_2 \quad -63.9 = \frac{-H\left\{(11.53\times10^6)^2 - (9.0\times10^6)^2\right\}\left\{(11.53\times10^6)^2 - (14.1\times10^6)^2\right\}}{2\pi(11.53\times10^6)\left\{(11.53\times10^6)^2 - (9.85\times10^6)^2\right\}\left\{(11.53\times10^6)^2 - (17.0\times10^6)^2\right\}} \qquad A\text{-}22_2$$

for which $H = .746 \times 10^{10}$

$$A\text{-}17_3\text{:} \quad -111 = \frac{-H\left\{(20.0\times10^6)^2 - (9.0\times10^6)^2\right\}\left\{(20.0\times10^6)^2 - (14.1\times10^6)^2\right\}}{2\pi(20.0\times10^6)\left\{(20.0\times10^6)^2 - (9.85\times10^6)^2\right\}\left\{(20.0\times10^6)^2 - (17.0\times10^6)^2\right\}} \qquad A\text{-}22_3$$

for which $H = .743 \times 10^{10}$

By making the following changes in $f_i \qquad i = 1, 2, 3, 4$

$$f_1 = 9.2 \text{ mc}, \quad f_2 = 14.5 \text{ mc}, \quad f_3 = 9.85 \text{ mc}, \quad f_4 = 17.2 \text{ mc} \qquad A\text{-}23$$

the following more closely matched values of H are obtained using the above procedure.

$A\text{-}17_1$: $H = .747 \times 10^{10}$ $A\text{-}24_1$

$A\text{-}17_2$: $H = .730 \times 10^{10}$ $A\text{-}24_2$

$A\text{-}17_3$: $H = .737 \times 10^{10}$ $A\text{-}24_3$

These values are considered to be close enough. We choose $H = .735 \times 10^{10}$ a compromise value. The numerical value for Eq. A-20 based on the above is,

$$jX = \frac{.735\times10^{10}\left\{f^2 - (9.2\times10^6)^2\right\}\left\{f^2 - (14.5\times10^6)^2\right\}}{j\omega\left\{f^2 - (9.85\times10^6)^2\right\}\left\{f^2 - (17.2\times10^6)^2\right\}} \qquad A\text{-}25$$

It will next be necessary to expand Eq. A-25 in terms of partial fractions. We do it for the general expression (Eq. A-20) first. We set

$$\frac{H}{j\omega}\,\frac{(\omega^2 - \omega_1^2)(\omega^2 - \omega_2^2)}{(\omega^2 - \omega_3^2)(\omega^2 - \omega_4^2)} = \frac{A}{j\omega} + \frac{B\omega}{j(\omega^2 - \omega_3^2)} + \frac{C\omega}{j(\omega^2 - \omega_4^2} \qquad A\text{-}26$$

where A, B, and C are constants to be determined in terms of H, ω_1, ω_2, ω_3, ω_4. When the right hand side of Eq. A-26 is expressed as a single fraction with the same denominator as the left, upon equating the numerators, one gets

$$H(\omega^2 - \omega_1^2)(\omega^2 - \omega_2^2) = A(\omega^2 - \omega_3^2)(\omega^2 - \omega_4^2) + B\omega^2(\omega^2 - \omega_4^2) + C\omega^2(\omega^2 - \omega_3^2)$$

Equating coefficients of the same power of ω, this equation reduces to three equations in A, B, C and the known constants:

$$A + B + C = H \qquad A\text{-}27_a$$

$$A(\omega_3^2 + \omega_4^2) + B\omega_4^2 + C\omega_3^2 = H(\omega_1^2 + \omega_2^2) \qquad A\text{-}27_b$$

$$A\omega_3^2\omega_4^2 = H\omega_1^2\omega_2^2 \qquad A\text{-}27_c$$

We can solve for the unknown constants. The results are

$$A = \frac{H\,\omega_1^2\,\omega_2^2}{\omega_3^2\,\omega_4^2} \qquad \text{A-28}$$

$$B = H\,\frac{(\omega_3^2 - \omega_1^2)\,(\omega_3^2 - \omega_2^2)}{\omega_3^2\,(\omega_3^2 - \omega_4^2)} \qquad \text{A-29}$$

$$C = H\,\frac{(\omega_4^2 - \omega_1^2)\,(\omega_4^2 - \omega_2^2)}{\omega_4^2\,(\omega_4^2 - \omega_3^2)} \qquad \text{A-30}$$

From Eq. A-21, A-26, and the results of A-26 through A-30, the parameters of the circuit can be determined:

$$C_o = \frac{1}{A}$$

$$C_1 = \frac{1}{B} \qquad L_1 = \frac{1}{\omega_3^2 C_1} \qquad \text{A-31}$$

$$C_2 = \frac{1}{C} \qquad L_2 = \frac{1}{\omega_4^2 C_2}$$

Using the numerical data of Eqs. A-23, A-24, and the above analysis, numerical values for the parameters of the filter satisfying $A\text{-}17_{1\text{-}3}$ are

C_o = 220 $\mu\mu$ f

C_1 = 1880 $\mu\mu$ f

L_1 = .139 μ h

C_2 = 442 $\mu\mu$ f

L_2 = .193 μ h

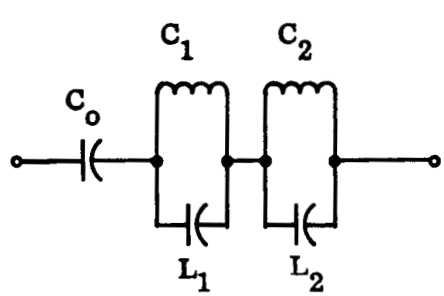

A-32

PART C

CALCULATION OF LOSSES IN THE THREE FREQUENCY RESONATOR ANTENNA

The most important loss contributors will be

1. Ohmic resistance of antenna conductors
2. radiation resistance of the rectangular loops carrying uniform current
3. losses in the reactance networks

The losses due to each of these is considered separately for a single turn. The overall antenna loss resistance is determined by means of the individual turn losses in parallel.

1) The copper losses in the antenna conductors are computed from the following expressions valid for circular conductors:[16]

$$R_{dc} = \frac{8}{\pi d^2 \sigma} \quad \text{ohms/meter} \qquad \text{A-33}$$

$$R_{ac} = \frac{R_{dc}\, d}{4} \sqrt{\pi f \mu_c \sigma} \quad \text{ohms/meter} \qquad \text{A-34}$$

where d = diameter of conductor in meters

σ = conductivity of conductor ($.581 \times 10^8$ mho/meter for copper)

f = frequency in cycles/sec

μ_c = conductor absolute permeability

Applying these expressions to a turn of 3/16" diameter conductor of length 7.94 meters (the perimeter of a single turn of the antenna), one obtains the following loss resistances

8.47mc	.804 ohms	A-35
11.53 mc	.936 ohms	
20.00 mc	1.23 ohms	

16 See Everitt & Anner, op.cit. p. 300

2) The radiation resistance of an electrically small perfect conductor rectangular loop carrying uniform current in a vacuum is given by[17]

$$R_r = 31{,}200 \left(\frac{A}{\lambda^2}\right)^2 \text{ ohms} \qquad \text{A-36}$$

where A = area of loop cross section

λ = free space wavelength at frequency of interest

Each turn of the loop antenna has an area of 3.73 m^2. Using this fact and the wavelengths at 8.47mc, 11.53mc, and 20.00 mc the numerical values for this component of power loss become (per turn)

8.47 mc	R_r	=	0.27 ohms	
11.53 mc	R_r	=	0.97 ohms	A-37
20.00 mc	R_r	=	8.58 ohms	

3) Losses in the reactance networks

The poles, zeroes and reactance values for the Foster networks used in the design of the antenna do not differ appreciably. Therefore the losses from each of these networks (of which there are ten on each turn of the antenna) will be approximately the same. It suffices to consider one network and multiply losses for this by 10 to obtain total losses for a single turn of the antenna. When losses are considered, a reactance network assumes the circuital form of Fig. A-8b.

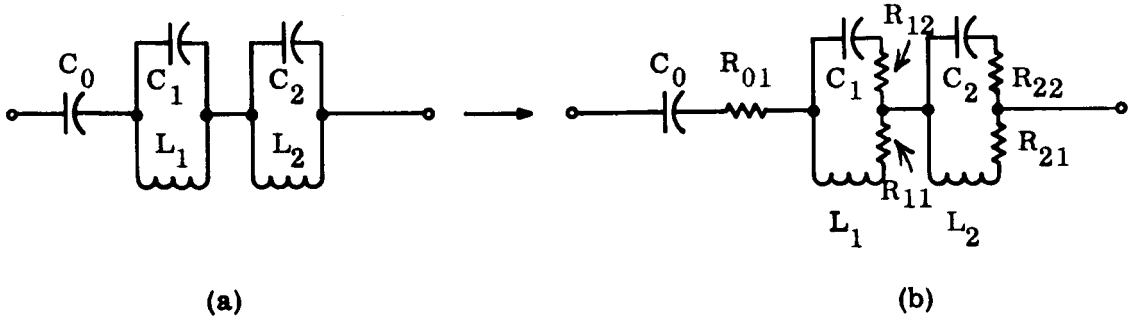

(a) (b)

Figure A-8

17 See, for example, Antennas, Krauss p. 167.

Note that resistance has about 5% error at upper frequency.

Values for the network loss resistances can be determined by the component Q's. Based on laboratory data such as that of Table I the Q's of the coils L_1 and L_2 are assumed to be 200 at 8.47 mc and 11.53 mc and 250 at 20.0 mc. Manufacturer's data on the porcelain capacitors to be used in these networks indicate that a Q of 2500 at 8.47 and 11.53 mc and 2000 at 20 mc are reasonable expectations. A typical antenna reactance network (see Table A-I) has the following component values:

$C_0 = 176\ \mu\mu f$

$C_1 = 1648\ \mu\mu f \qquad L_1 = .158\ \mu h$

$C_2 = 358\ \mu\mu f \qquad L_2 = .239\ \mu h$

Associated with each of these components there is a reactance at 8.47, 11.53, and 20.00 mc. By means of the Q, a numerical series loss resistance can be inferred by the ratio $|\text{Reactance}|/Q$. These values enable calculation of the network series impedance at the three frequencies. The results are:

8.47 mc	0.796 - j 58.3	
11.53 mc	0.798 - j 78.4	A-38
20.00	1.49 - j 136.9	

(Note the reactance values have not changed significantly from the design goals of Table A-I.)

With ten such networks in series with each turn of the antenna, the total series loss resistance due to reactance networks becomes

8.47 mc	7.96 ohms	
11.53 mc	7.98 ohms	A-39
20.00 mc	14.9 ohms	

By combining the results of A-35, A-37, A-39 one obtains total series resistances per turn of antenna;

8.47 mc	9.03 ohms
11.53 mc	9.89 ohms
20.00 mc	24.7 ohms

A-40

The impedance seen by the matching network will consist of three such turns in parallel and will therefore be one third of the values in A-40 provided the antenna is at resonance.

PART D

MINIMAL FLUX DENSITY WITHIN TELEMETRY VOLUME

We neglect the contributions of other turns and calculate the field produced by the current in a single turn of the antenna at its center. Consider the rectangular loop of wire shown in figure A-9 which carries uniformly distributed current $I_m \cos \omega t$. The flux density at a point in space can be determined through the superposition of the contributions of all the current elements of the antenna. The flux density at the center (0) is readily computed in this manner.

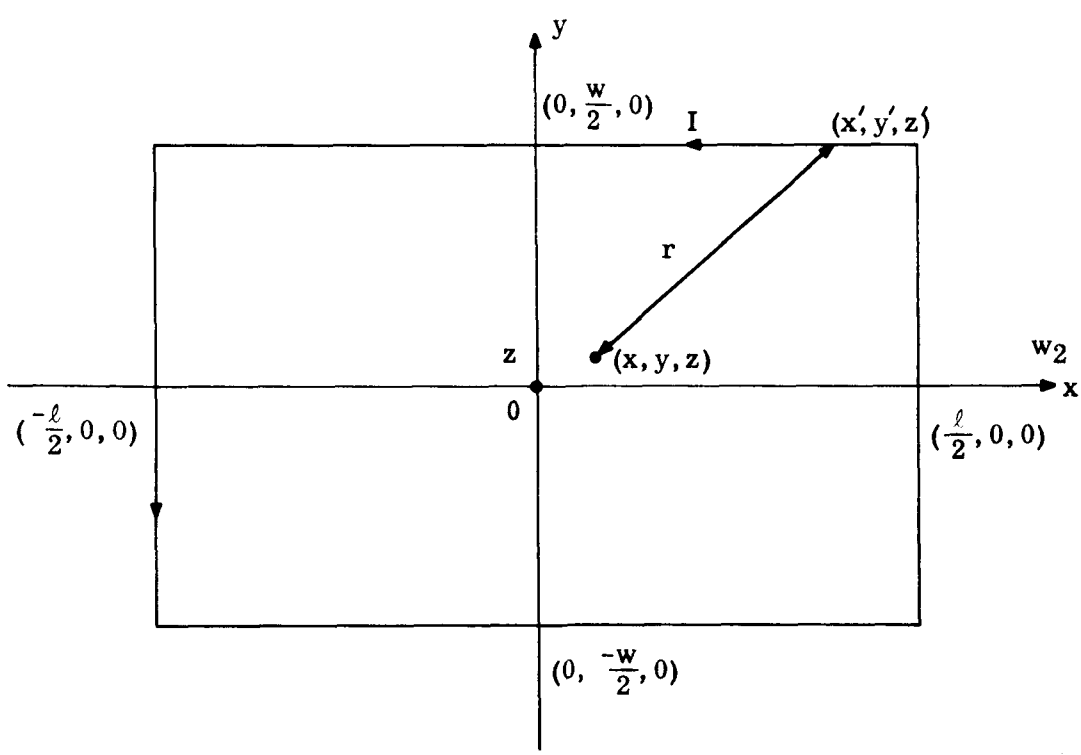

Figure A-9

The magnetic field intensity at a point in space can be determined from the magnetic vector potential from the vector relation[18]

$$\bar{B} = \nabla \times \bar{A} \qquad \text{A-41}$$

in a region where displacement currents can be neglected. The vector potential $\bar{A}$ can be determined from the current density $\bar{j}$ by

$$\bar{A} = \frac{\mu_o}{4\pi} \int_{v^1} \frac{\bar{j}\, dv^1}{r} \qquad \text{A-42}$$

where v^1 is the volume containing the current and r is the distance between the source point and the field point. $\bar{j}\, dv^1$ represents the current moment which can be expressed by $\bar{i}_I\, I\, d\ell$ in the case of linear currents. (Here $\bar{i}_I$ represents a unit vector in the direction of flow of current I. $d\ell$ is an increment of length.) The magnetic vector potential $\bar{A}$ at any point x,y,z in figure A-9 can be regarded as the sum of the contributions due to each of the four sides of the rectangle. Equation A-42 can be written as the sumof four integrals

$$\bar{A} = \frac{\mu_o}{4\pi} \int_{\frac{-\ell}{2}}^{\frac{+\ell}{2}} \frac{-\bar{i}\, I dx^1}{\sqrt{(x-x^1)^2 + (y-\frac{w}{2})^2 + z^2}} \frac{+\mu_o}{4\pi} \int_{\frac{-w}{2}}^{\frac{+w}{2}} \frac{-\bar{j}\, I dy^1}{\sqrt{(x+\frac{\ell}{2})^2 + (y-y^1)^2 + z^2}}$$

$$+ \frac{\mu_o}{4\pi} \int_{\frac{-\ell}{2}}^{\frac{+\ell}{2}} \frac{+\bar{I}\, I\, dx^1}{\sqrt{(x-x^1)^2 + (y+\frac{w}{2})^2 + z^2}} + \frac{\mu_o}{4\pi} \int_{\frac{-w}{2}}^{\frac{+w}{2}} \frac{+\bar{j}\, I\, dy^1}{\sqrt{x-\frac{\ell}{2})^2 + (y-y^1)^2 + z^2}}$$

which can be simplified to,

$$\bar{A} = \frac{\bar{i}\, I\, \mu_o}{4\pi} \int_{\frac{-\ell}{2}}^{\frac{\ell}{2}} \left(\frac{1}{\sqrt{(x-x^1)^2 + (y+\frac{w}{2})^2 + z^2}} - \frac{1}{\sqrt{(x-x^1)^2 + (y-\frac{w}{2})^2 + z^2}} \right) dx^1$$

---

18. See any text on electromagnetic theory, e.g., "Classical Electricity and Magnetism", Panofsky and Phillips, second edition p. 128.

$$+\frac{\bar{j}\, I\mu_o}{4\pi}\int_{-\frac{w}{2}}^{\frac{w}{2}}\left(\frac{1}{\sqrt{(x-\frac{\ell}{2})^2+(y-y^1)^2+z^2}}-\frac{1}{\sqrt{(x+\frac{\ell}{2})^2+(y-y^1)^2+z^2}}\right)dy^1 \qquad \text{A-43}$$

But

$$\bar{B}=\nabla X\,\bar{A}=\bar{k}\left[\frac{\partial Ay}{\partial x}-\frac{\partial Ax}{\partial y}\right] \text{ since } Az=0 \qquad \text{A-44}$$

and

$$\frac{\partial Ay}{\partial z}\to 0,\ \frac{\partial Ax}{\partial z}\to 0 \text{ as } z\to 0$$

Therefore, by differentiating A-43 we get,

$$\bar{B}=\frac{\bar{k}\,\mu_o}{4\pi}\left[\int_{-\frac{w}{2}}^{\frac{w}{2}}\left(\frac{I(-\frac{1}{2})\,(2)(x-\frac{\ell}{2})}{\left[(x-\frac{\ell}{2})^2+(y-y^1)^2+z^2\right]^{3/2}}+\frac{I(\frac{1}{2})\,(2)\,(x+\frac{\ell}{2})}{\left[(x+\frac{\ell}{2})^2+(y-y^1)^2+z^2\right]^{3/2}}\right)dy^1\right.$$

$$\left.-\int_{-\frac{\ell}{2}}^{\frac{\ell}{2}}\left(\frac{I\,(-\frac{1}{2})\,(2)\,(y+\frac{w}{2})}{\left[(x-x^1)^2+(y+\frac{w}{2})^2+z^2\right]^{3/2}}+\frac{I\,(\frac{1}{2})\,2\,(y-\frac{w}{2})}{\left[(x-x^1)^2+(y-\frac{w}{2})^2+z^2\right]^{3/2}}\right)dx^1\right] \qquad \text{A-45}$$

Now we are interested in the point x = y = z = 0 (i.e. the center of the loop) at this point A-45 becomes

$$\bar{B}=\frac{\bar{k}\,\mu_o}{4\pi}\int_{-\frac{w}{2}}^{\frac{w}{2}}\left(\frac{\frac{\ell I}{2}}{\left[(\frac{\ell}{2})^2+(y^1)^2\right]^{3/2}}+\frac{\frac{\ell I}{2}}{\left[(\frac{\ell}{2})^2+(y^1)^2\right]^{3/2}}\right)dy^1$$

$$+\int_{-\frac{\ell}{2}}^{\frac{\ell}{2}}\left(\frac{\frac{w}{2}\,I}{\left[(\frac{w}{2})^2+(x^1)^2\right]^{3/2}}+\frac{\frac{w}{2}\,I}{\left[(\frac{w}{2})^2+(x^1)^2\right]^{3/2}}\right)dx^1 \qquad \text{A-46}$$

or

$$\bar{B} = \frac{\bar{k}\mu_o}{4\pi}\left(\int_{-\frac{w}{2}}^{\frac{w}{2}} \frac{\ell\, I\, dy^1}{\left[(\frac{\ell}{2})^2 + (y^1)^2\right]^{3/2}} + \int_{-\frac{\ell}{2}}^{\frac{\ell}{2}} \frac{w\, I\, dx^1}{\left[(\frac{w}{2})^2 + (x^1)^2\right]^{3/2}} \right)$$

by symmetry in the integrals,

$$\bar{B} = \frac{\bar{k}\mu_o}{4\pi}\left(\int_0^{\frac{w}{2}} \frac{2\,\ell\, I\, dy^1}{\left[(\frac{\ell}{2})^2 + (y^1)^2\right]^{3/2}} + \int_0^{\frac{\ell}{2}} \frac{2\, w\, I\, dx^1}{\left[(\frac{w}{2})^2 + (x^1)^2\right]^{3/2}} \right) \qquad \text{A-47}$$

These integrals can be converted to the following trigonometric integrals:

$$\bar{B} = \frac{\bar{k}\mu_o}{4\pi}\left(\int_0^{\arctan \frac{w}{\ell}} \frac{8I}{\ell} \cos\theta\, d\theta + \int_0^{\arctan \frac{\ell}{w}} \frac{8I}{w} \cos\theta\, d\theta \right) \qquad \text{A-48}$$

Integrating,

$$\bar{B} = \frac{\bar{k}\mu_o}{4\pi}\ 8I\left[\frac{w}{\ell\sqrt{w^2 + \ell^2}} + \frac{\ell}{w\sqrt{w^2 + \ell^2}} \right]$$

$$\bar{B} = \frac{\bar{k}\,\mu_o\, 8I}{4\pi\sqrt{w^2 + \ell^2}}\left[\frac{w}{\ell} + \frac{\ell}{w} \right] = \frac{\bar{k}\, 2\mu_o\, I\sqrt{w^2 + \ell^2}}{\pi\, w\, \ell} \qquad \text{A-49}$$

In our case I = 1 amp {see p.

$\mu_o = 4\pi \times 10^{-7}$ henrys/meter

w = 5 feet = 1.53 meters

ℓ = 8 feet = 2.44 meters

Substituting these numerical values in equation A-49 the rms flux density at the center of the loop evaluates to

$$\bar{B} = \bar{k}\ 6.16 \times 10^{-7}\ \frac{\text{webers}}{\text{meter}^2} = 6.16 \times 10^{-3}\ \text{gauss} \qquad \text{A-50}$$

PART E - MATCHING NETWORK DESIGN

Figure A-10 shows a generator inductively coupled to a resistive load.

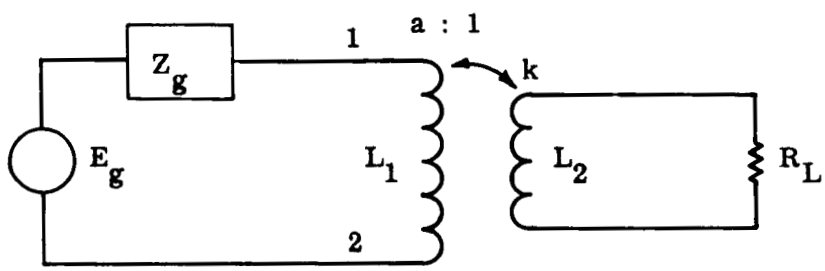

FIGURE A-10

The turns ratio between the "primary inductor" and the "secondary inductor" is a and the coefficient of coupling between primary and secondary is k. It can be shown that the impedance seen looking into terminals 1 - 2 with the generator disconnected is

$$Z_p = \frac{R_L k^2 \omega^2 L_1 L_2}{R_L^2 + \omega^2 L_2^2} + \frac{j\omega L_1 \left[1 + \left(\frac{\omega L_2}{R_L}\right)^2 (1-k^2)\right]}{1 + \left(\frac{\omega L_2}{R_L}\right)^2} \qquad \text{A-51}$$

The matching network is required to couple maximum power from transmitters at 8.47 mc and 11.53 mc to the antenna and from the antenna side to a receiver

at 20.00 mc. The requirement for this maximum power transfer is that the impedance seen looking into the primary be conjugate matched to the impedance seen looking into the transmitter or receiver as the case may be.

The load impedance which the antenna presents at each of the frequencies of interest has been computed in Part C of this Appendix. Dividing the values of equation A-40 by 3 one obtains, as in Table II

$$R_L = 3.01 \text{ ohms at } 8.47 \qquad (A\text{-}52)_1$$

$$R_L = 3.30 \text{ ohms at } 11.53 \text{ mc} \qquad (A\text{-}52)_2$$

$$R_L = 8.23 \text{ ohms at } 20.00 \text{ mc} \qquad (A\text{-}52)_3$$

The matching network pictured in Figure 3 can be treated as the network of Figure A-10 for each of the three frequencies due to the fact that each of the series bandpass filters possesses a high impedance (pole) at the two frequencies other than that which is to be passed. Under these conditions the loading effects of the circuits can be neglected. We therefore consider each case separately. First 8.47 mc. The primary inductance L_1 must be chosen such that the voltage across it is not excessive when carrying rated currents. At 8.47 mc a 10 μh coil having a reactance of 532 ohms has been chosen as a design goal. In order to produce the matched condition we are after, the real part of Z_p in A-51 must match the real part of the generator impedance. In the case of a 50 ohm generator such as the one available we have -

$$\frac{R_L k^2 \omega^2 L_1 L_2}{R_L^2 + \omega^2 L_2^2} = 50 \qquad (A\text{-}53)$$

The coefficient of coupling k is a function of geometry and may be assumed equal to 0.5 in this case. Therefore, with numerical values of R_L, $\omega = 2\pi f$, L_1, k, it is easy to obtain a value for L_2 the secondary (antenna side) self inductance of the matching network. Solving A-53 numerically one obtains, upon solving a resulting quadratic equation

$$L_2 = 0.125 \ \mu\text{h or } 0.025 \ \mu\text{h} \qquad (A\text{-}54)$$

The higher value is accepted for practical reasons. Thus, a primary self inductance of 10 μh and a secondary self inductance of 0.125 μh have been specified for the matching network at 8.47 mc. As a result the real part of the primary impedance will be matched to the real part of the transmitter output impedance. In order to obtain conjugate matching a negative reactance in series with the transmitter output impedance must be added to match the imaginary part of Z_p given by A-51. This negative reactance is estimated by means of the design values determined above

$$X_t = \frac{-\omega L_1 \left[1 + \left(\frac{\omega L_2}{R_L}\right)^2 (1-k^2)\right]}{1 + \left(\frac{\omega L_2}{R_L}\right)^2} = \frac{-532 \left[1 + \left(\frac{6.65}{3.01}\right)^2 (1-.25)\right]}{1 + \left(\frac{6.65}{3.01}\right)^2}$$

$$= -421 \text{ ohms} \qquad \text{(A-55)}$$

At 8.47 mc this reactance implies a capacitance of 44.6 $\mu\mu$f. This completes the design of the 8.47 mc portion of the matching network. The secondary is the winding to be connected to the antenna terminals and should be the same for all three frequencies. Thus, with the secondary self inductance specified at 8.47 mc it is specified at 11.53 mc and 20.00 mc also. We therefore next determine the required primary inductance at 11.53 mc assuming a knowledge of the secondary inductance { 0.125 μh}. The output resistance of the transmitter is again nominally 50 ohms and equation A-52 holds. We assume the following numerical values in computing L_1 for 11.53 mc.

$k = .55$ (slightly higher than earlier because of better linkage in this case)

$\omega = 2\pi(11.53 \times 10^6)$

$R_L = 3.30$ ohms from A-52)$_2$

$L_2 = .125 \times 10^{-6}$ henrys from A-54

from which we get

$$L_1 = 7.15 \ \mu\text{h} \qquad \text{(A-56)}$$

Repeating A-55 for the 11.53 mc case, the required conjugate tuning reactance, X_t at 11.53 mc is obtained:

$$X_t = -380 \text{ ohms which implies a series capacitance } C = 36.2\ \mu\mu f \qquad \text{(A-57)}$$

The design of the section which couples 20 mc energy to the receiver is similar to that above except that a separate primary has been added to avoid ground loop problems at the receiver. However it is coupled by the same secondary inductance of 0.125 μh. Equation A-53 is employed to determine the 20 mc primary (receiver side) inductance, L_1;

$$50 = \frac{R_L k^2 \omega^2 L_1 L_2}{R_L^2 + \omega^2 L_2^2}$$

With

$R_L = 8.23$ ohms from A-52)$_3$

$k = 0.6$

$\omega = 2\pi\ (20) \times 10^6$

$L_2 = .125\ \mu$h from A-54

we get

$$L_1 = 2.68\ \mu\text{h} \qquad \text{(A-58)}$$

Repeating A-55 for the 20.00 mc case, the required conjugate tuning reactance, X_t at 20.00 mc is obtained;

$$X_t = -241 \text{ ohms} \qquad \text{(A-59)}$$

which implies a series capacitance

$$C = 32.9\ \mu\mu f$$

A schematic diagram of the matching network resulting from the foregoing considerations is shown in Figure A-11.

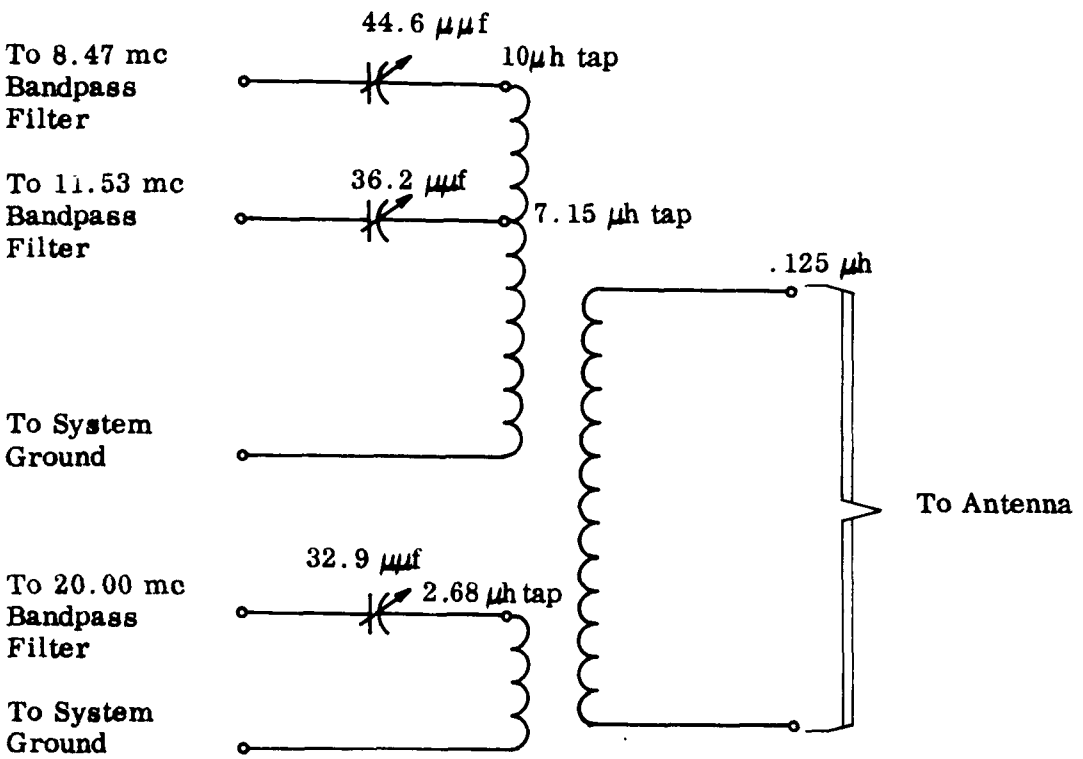

Figure A-11

Matching Network Schematic Diagram

The coefficients of coupling called for in the above design are rather high for air core coupled coils. The technique which has been employed to increase primary - secondary coupling consists of utilizing a current sheet for the secondary inductor. The transmitting primary inductances are situated within the current sheet and the receiving primary is constructed around the outside of the current sheet. Figure 4 shows photographs of the matching network.

PART F. DESIGN OF BANDPASS FILTERS

As mentioned in earlier sections, the bandpass filters are to be series Foster reactance networks having a zero at the pass carrier frequency and a pole at each of the other two carrier frequencies in the three frequency system. Figure A-12 shows sketches of the reactance functions, analytic representations of the reactance functions, and circuital configurations of the reactance networks which are required in the three transmission channels of the subject system.

In each case some or all of the poles and zeroes are predetermined. The problem of design becomes one of choosing H and the undefined poles and zeroes such that the parameters in the resulting circuit are reasonable values from a practical standpoint. As with the antenna reactance networks the reactance expressions are expanded in partial fractions and the circuit components identified with coefficients in the expansion.

Thus, for the network of Figure A-12(a), we equate

$$jX = \frac{1}{j\omega C_0} + \frac{\frac{\omega}{C_1}}{j\left(\omega^2 - \frac{1}{L_1C_1}\right)} + \frac{\frac{\omega}{C_2}}{j\left(\omega^2 - \frac{1}{L_2C_2}\right)} = \frac{H}{j\omega}\frac{\left(\omega^2-\omega_1^2\right)\left(\omega^2-\omega_2^2\right)}{\left(\omega^2-\omega_3^2\right)\left(\omega^2-\omega_4^2\right)} = \frac{A}{j\omega} +$$

$$\frac{B\omega}{j\left(\omega^2-\omega_3^2\right)} + \frac{C\omega}{j\left(\omega^2-\omega_4^2\right)} \qquad \text{A-60}$$

Solving for A, B, C in terms of H, ω_1, ω_2, ω_3, ω_4, one obtains the following

$$A = \frac{H\left(\omega_1^2\right)\left(\omega_2^2\right)}{\omega_3^2\ \omega_4^2} \qquad \text{A-61)}_1$$

(a)

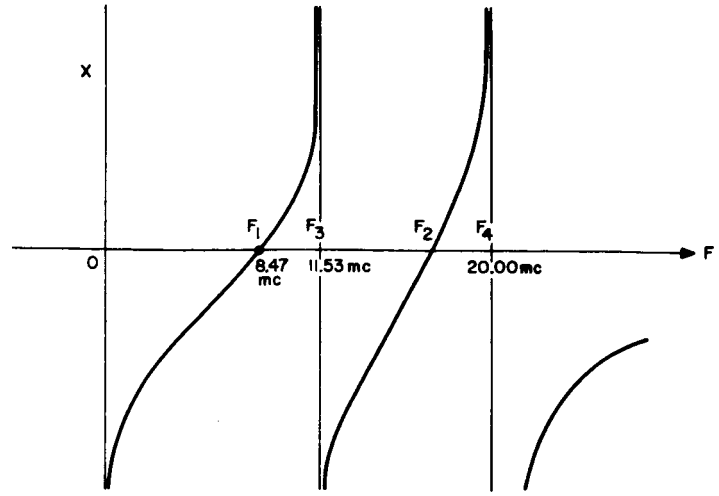

$$jX = \frac{H}{j\omega} \frac{(\omega^2-\omega_1^2)(\omega^2-\omega_2^2)}{(\omega^2-\omega_3^2)(\omega^2-\omega_4^2)}$$

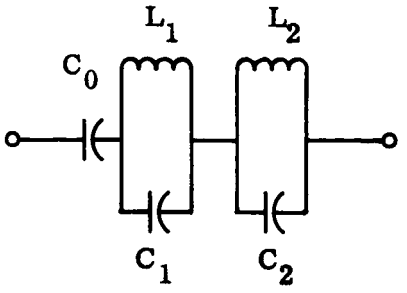

a) Network for 8.47 mc transmission channel

(b)

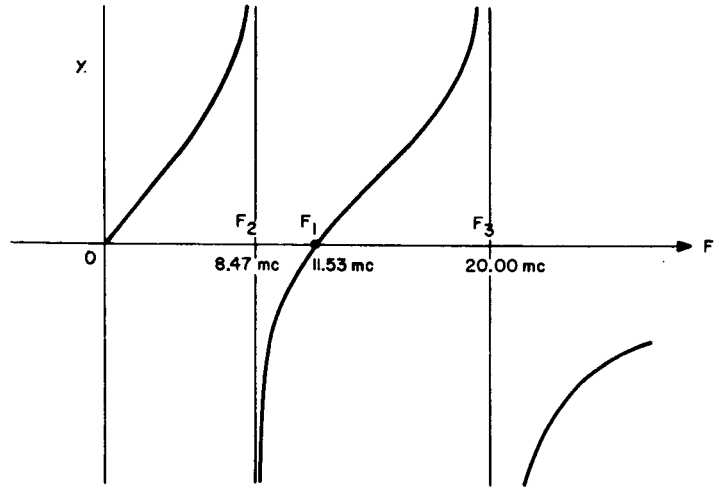

$$jX = \frac{j\omega H(\omega^2-\omega_1^2)}{(\omega^2-\omega_2^2)(\omega^2-\omega_3^2)}$$

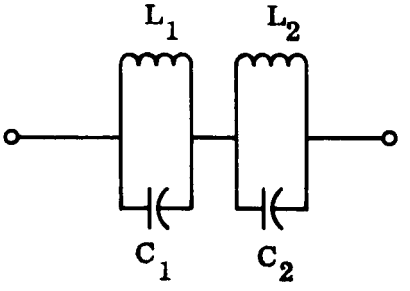

b) Network for 11.53 mc transmission channel

(c)

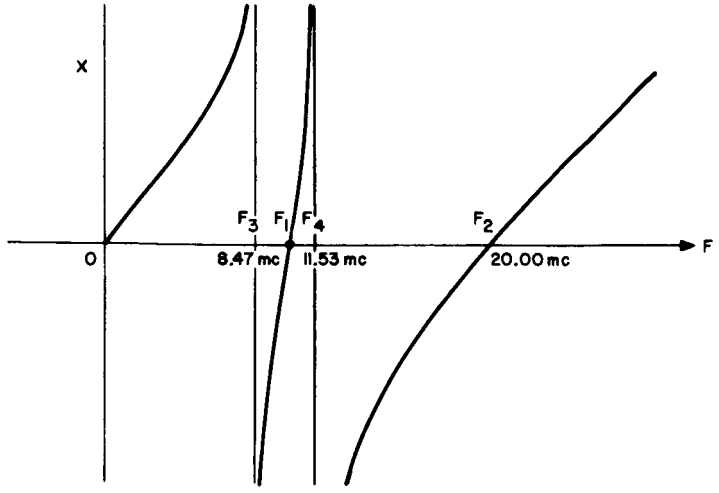

$$jX = \frac{j\omega H(\omega^2-\omega_1^2)(\omega^2-\omega_2^2)}{(\omega^2-\omega_3^2)(\omega^2-\omega_4^2)}$$

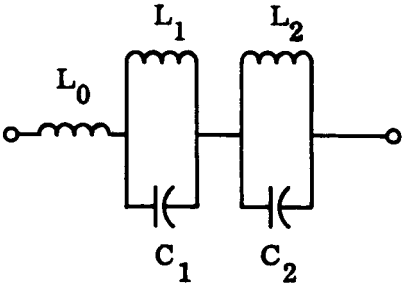

c) Network for 20.0 mc receive channel

Figure A-12

$$B = \frac{H\left(\omega_3^2-\omega_2^2\right)\left(\omega_3^2-\omega_1^2\right)}{\omega_3^2\left(\omega_3^2-\omega_4^2\right)} \qquad \text{A-61)}_2$$

$$C = \frac{H\left(\omega_4^2-\omega_2^2\right)\left(\omega_4^2-\omega_1^2\right)}{\omega_4^2\left(\omega_4^2-\omega_3^2\right)} \qquad \text{A-61)}_3$$

Now ω_1, ω_3, ω_4 are predetermined. Numerical selection of H and ω_2 completely determines coefficients A, B, and C and (by equation A-60) the values for the circuit components. The design of the networks of b) and c) in Figure A-12 is similar although A-60 takes a slightly different form in each case. Figure A-13 shows the numerical results of these design procedures.

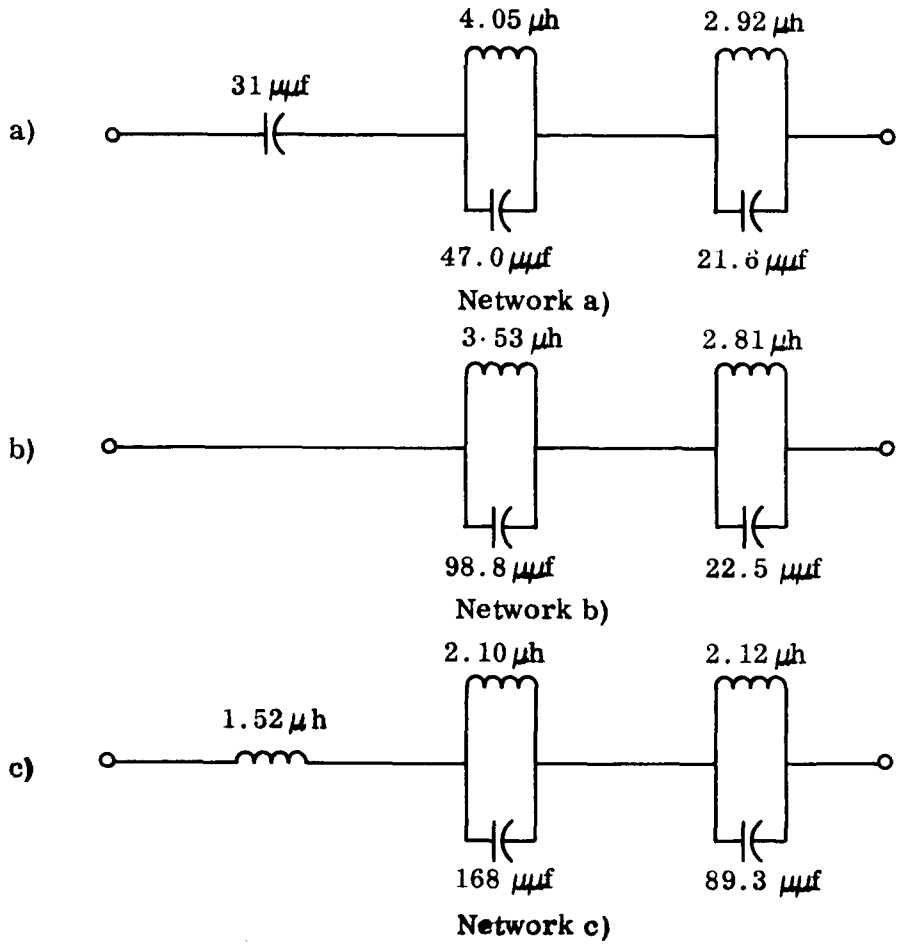

Figure A-13

Bandpass Filters

Part G

EVALUATION OF RATE OF CHANGE OF ANTENNA CURRENT PHASE

If a unit voltage taken at 0 phase is applied across the terminals of the system antenna a current will flow which is given by

$$I = \frac{1}{Z} \qquad \text{A-62}$$

where Z is the complex impedance of the antenna. In complex notation we can associate a phase angle $\Phi(\omega)$ with the current as follows:

$$I = I_o \epsilon^{j\Phi(\omega)} \qquad \text{A-63}$$

It is important to relate the rate of change of this phase with respect to frequency. From A-63 we can see

$$\frac{\partial I}{\partial \omega} \cong j I_o \frac{\partial \Phi(\omega)}{\partial \omega} \epsilon^{j\Phi(\omega)} \qquad \text{A-64}$$

provided the rate of change of amplitude, (I_o) with respect to frequency is small. We can solve for $\left|\frac{\partial \Phi(\omega)}{\partial \omega}\right|$. From A-63, A-64

$$\left|\frac{\partial \Phi(\omega)}{\partial \omega}\right| = \left|\frac{\partial I}{\partial \omega}\right| \cdot \frac{1}{|I|} \qquad \text{A-65}$$

From A-62 $\frac{\partial I}{\partial \omega} = -\frac{\partial Z}{\partial \omega} / Z^2$

$$\left|\frac{\partial I}{\partial \omega}\right| = \left|\frac{\frac{\partial Z}{\partial \omega}}{Z^2}\right| \qquad \text{A-66}$$

$$|I| = \frac{1}{|Z|}$$

Therefore $\left|\frac{\partial \Phi(\omega)}{\partial \omega}\right| = \left|\frac{\partial Z}{\partial \omega}\right| \frac{1}{|Z^2|} |Z| = \left|\frac{\partial Z}{\partial \omega}\right| \frac{1}{|Z|}$ A-67

In evaluating the numerical value of A-67 it is necessary to consider the losses in the antenna for otherwise at the reactance zeroes the derivative would be infinite. In Part C of this appendix it was determined that the predominant loss contributors to the antenna are the Foster reactance networks. The following analysis therefore neglects other losses in evaluating A-67 numerically. It is also possible to restrict the investigation to one turn since the expression A-67 is unchanged for three identical turns in parallel.

The procedure is to break an antenna turn into sections as shown in Figure A-14. Then the impedance and its first derivative are evaluated across each symmetrical pair of terminals starting with the terminals at the far right. Each section of transmission line is terminated in an impedance formed by the preceding section and, for most sections, series Foster networks. In terms of pair-terminals and network nomenclature of Figure A-14 the desired impedance calculation proceeds are as follows.

Evaluate $Z_{1,1}$ and $\frac{\partial Z_{1,1}}{\partial \omega}$

using the appropriate transmission line equation.

Now $Z_{2,2} = 2 Z_{N1} + Z_{1,1}$ A-68

thus

$$\frac{\partial Z_{2,2}}{\partial \omega} = 2 \frac{\partial Z_{N1}}{\partial \omega} + \frac{\partial Z_{1,1}}{\partial \omega} \quad \text{A-69}$$

Then knowing $Z_{2,2}$, $\frac{\partial Z_{2,2}}{\partial \omega}$ we can evaluate $Z_{3,3}$, $\frac{\partial Z_{3,3}}{\partial \omega}$ from the transmission line equation. (Eq. A-3). This procedure is continued along the antenna until the terminal impedance $Z_{13,13}$ and its derivative are obtained. This is the impedance in equation A-67. Thus, the phase shift derivative will be determined.

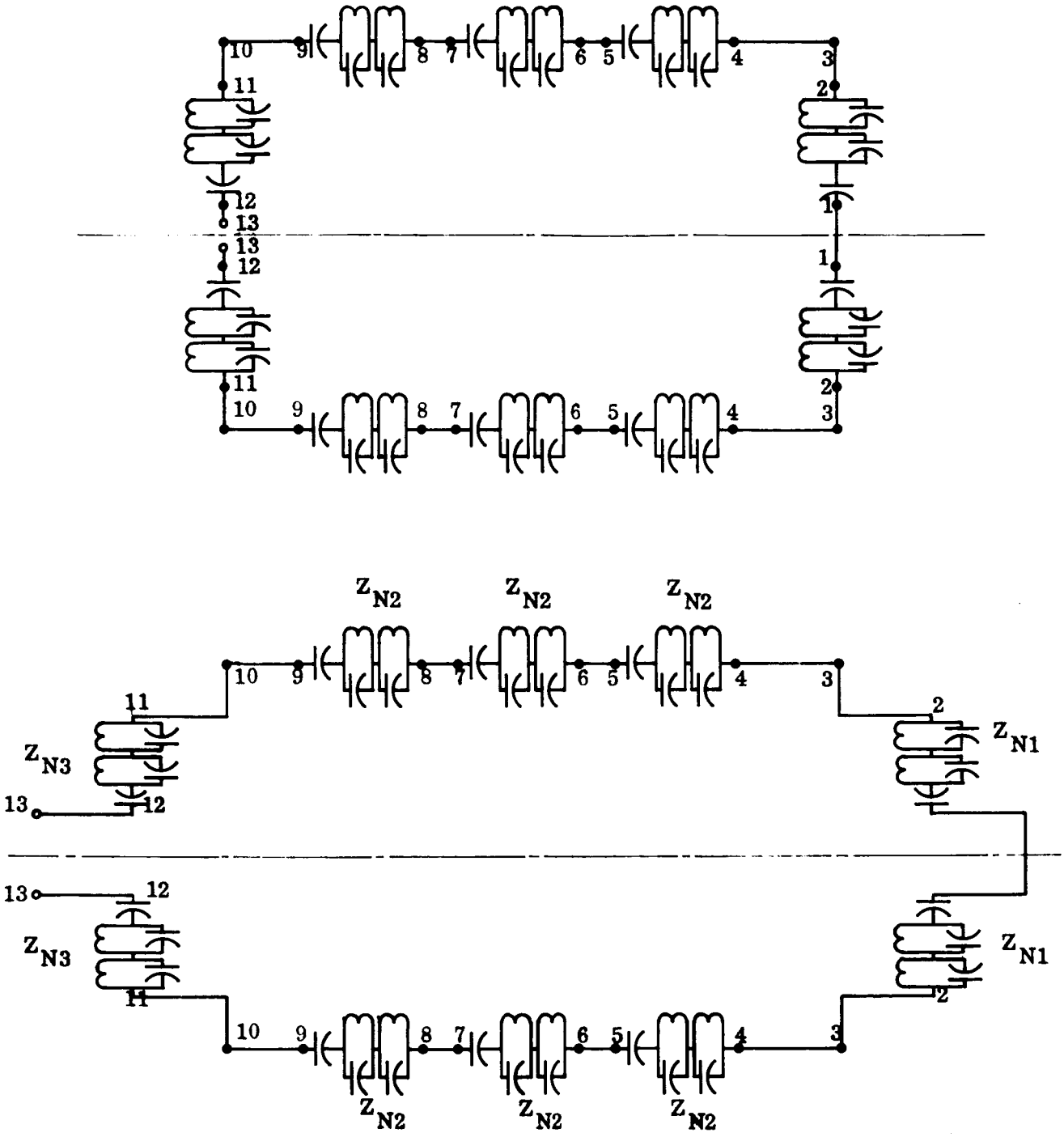

FIGURE A-14

Breakup of Antenna for Evaluating Phase Change Velocity

The details of the computation are lengthy but straightforward. A computational order has been established for numerical determination of $Z_{13,13}$, $\frac{\partial Z_{13,13}}{\partial \omega}$ at any frequency ω. The frequencies at which it will be necessary to specify these quantities for the subject contract will be 8.47 mc and 20.00 mc, the two frequencies to be tracked in the phase lock loop.

Elaboration of Computational Order

1) From the impedance expression for a short circuited lossless transmission line (see Eq. A-3 with $Z_{r=0}$) we can evaluate $Z_{1,1}$

$$Z_{1,1} = j Z_{oa} \tan k_1 \omega \qquad \text{A-70}$$

Where from Eq. A-4a, Z_{oa} = 609 ohms, and from Eq. A-7a and Fig. A-5a, $\gamma_a \ell_a = j\omega 1.31 \times 10^{-9}$ and $k_1 = 1.31 \times 10^{-9}$ rads/rad/sec.

2) Differentiating A-70 with respect to ω, we obtain

$$\frac{\partial Z_{1,1}}{\partial \omega} = j Z_{oa} k_1 \sec^2 k_1 \omega \qquad \text{A-71}$$

3) It is now required to specify the complex impedance of the network Z_{N1} in Fig. A-14 as a function of frequency. The circuit will be specified as shown in Fig. A-15

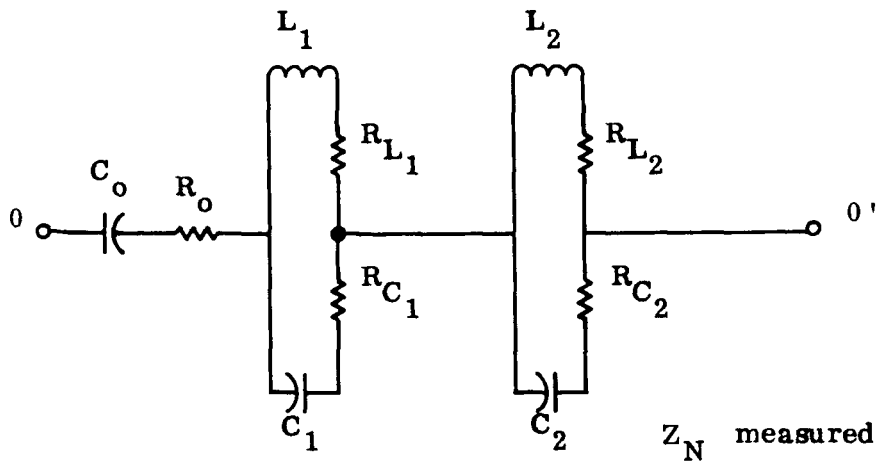

Z_N measured across terminals 0-0'

Figure A-15

It can be easily shown that the impedance of Z_N in Fig. A-15 is expressible by

$$Z_N = \frac{a_N}{\omega} + \frac{b_N \omega}{b_n \omega^2 + b_m} + \frac{C_N \omega}{C_n \omega^2 + C_m} \qquad \text{A-72}$$

where $a_N = \left(\frac{1}{Q_o} - j\,1\right)\frac{1}{C_o}$

$$b_N = \left(\frac{1}{Q_{L1}} + j\,1\right)\left(\frac{1}{Q_{C_1}} - j\,1\right)\frac{L_1}{C_1}$$

$$b_n = L_1\left(\frac{1}{Q_{L_1}} + j\,1\right)$$

$$b_m = \frac{1}{C_1}\left(\frac{1}{Q_{C_1}} - j\,1\right)$$

$$C_N = \frac{L_2}{C_2}\left(\frac{1}{Q_{L_2}} + j\,1\right)\left(\frac{1}{Q_{C_2}} - j\,1\right)$$

$$C_n = L_2\left(\frac{1}{Q_{L_2}} + j\,1\right)$$

$$C_m = \frac{1}{C_2}\left(\frac{1}{Q_{C_2}} - j\,1\right)$$

$$Q_o = \frac{1}{\omega C_o R_o}$$

$$Q_{L_1} = \frac{\omega L_1}{R_{L_1}} \qquad Q_{L_2} = \frac{\omega L_2}{R_{L_2}}$$

$$Q_{C_1} = \frac{1}{\omega C_1 R_{C_1}} \qquad Q_{C_2} = \frac{1}{\omega C_2 R_{C_2}}$$

The changes in circuital Q's with respect to frequency will be small compared to the overall impedance variations at the antenna terminals. Therefore the coefficients of ω and $1/\omega$ in Eq. A-72 can be assumed constant under the differentiating process. Moreover, numerical values for these coefficients has been obtained (in the laboratory for the coils and from the manufacturer for the capacitors)of the three different networks shown in Fig. A-14.

From Eq. A-72 there follows:

$$\frac{\partial Z_N}{\partial \omega} = \frac{a_N}{\omega^2} + \frac{b_N b_m - b_N b_n \omega^2}{(b_n \omega^2 + b_m)^2} + \frac{C_N C_m - C_N C_n \omega^2}{C_n \omega^2 + C} \qquad \text{A-73}$$

The foregoing analysis can be applied to the network Z_{N1} in Fig. A-14 thus determining numerical values for $Z_{N1}, \frac{\partial Z_{N1}}{\partial \omega}$ at any frequency of interest

4) From 1) and 3) calculate

$$Z_{2,2} = 2 Z_{N1} + Z_{1,1} \qquad \text{A-74}$$

5) From 2) and 4) calculate

$$\frac{\partial Z_{2,2}}{\partial \omega} = 2 \frac{\partial Z_{N1}}{\partial \omega} + \frac{\partial Z_{1,1}}{\partial \omega} \qquad \text{A-75}$$

6) The transmission line impedance equation A-3 as applied to the line beginning at terminals 3, 3 and ending at terminals 2, 2 is now employed:

$$Z_{3,3} = Z_{ob} \frac{j Z_{ob} \tan k_2 \omega + Z_{2,2}}{Z_{ob} + j Z_{2,2} \tan k_2 \omega} \qquad \text{A-76}$$

Numerically from Eq. A-4b $Z_{ob} = 740$ ohms and from Eq. A-7b and Fig. A-5b $\gamma_b \ell_b = j\omega 1.30 \times 10^{-9}$ and $k_2 = 1.30 \times 10^{-9}$ rad/rad/sec.

Thus, with Equation A-74, $Z_{3,3}$ can be computed.

7) From 4), 5), 6) calculate the numerical value of

$$\frac{\partial Z_{3,3}}{\partial \omega} = Z_{ob}\left\{ \frac{(Z_{ob}+jZ_{2,2}\tan k_2\omega)(jZ_{ob}k_2\sec^2 k_2\omega + \frac{\partial Z_{2,2}}{\partial \omega})}{[Z_{ob}+j\,Z_{2,2}\tan k_2\,\omega]^2} \right.$$

$$\left. - \frac{(j\,Z_{ob}\tan k_2\,\omega + Z_{2,2})(jk_2Z_{2,2}\sec^2 k_2\,\omega + j\tan k_2\,\omega\,\frac{\partial Z_{2,2}}{\partial \omega})}{[Z_{ob}+j\,Z_{2,2}\tan k_2\,\omega]^2} \right\} \qquad \text{A-77}$$

8) We next obtain the impedance seen from the terminals 4, 4 assuming a terminating impedance at terminals 3, 3 of $Z_{3,3}$. Again applying Eq. A-3 as in A-76

$$Z_{4,4} = Z_{oc}\left[\frac{jZ_{oc}\tan k_3\,\omega + Z_{3,3}}{Z_{oc}+j\,Z_{3,3}\tan k_3\,\omega}\right] \qquad \text{A-78}$$

Numerically from Eq. A-4c, $Z_{oc} = 775$ ohms and from Eq. A-7c and Fig. A-5c $\frac{\nu_c l_c}{2} = j\,\omega\,1.03 \times 10^{-9}$ and $k_3 = 1.03 \times 10^{-9}$ rad/rad/sec.

9) From 6), 7), 8) calculate the numerical value of

$$\frac{\partial Z_{4,4}}{\partial \omega} = Z_{oc} \left\{ \frac{(Z_{oc}+jZ_{3,3}\tan k_3\omega)(jZ_{oc}k_3\sec^2 k_c\omega + \frac{\partial Z_{3,3}}{\partial \omega})}{[Z_{oc}+jZ_{3,3}\tan k_3\omega]^2} \right.$$

$$\left. - \frac{(jZ_{oc}\tan k_3\omega + Z_{3,3})(jk_3\sec^2 k_3\omega + j\tan k_3\omega \frac{\partial Z_{3,3}}{\partial \omega})}{[Z_{oc}+jZ_{3,3}\tan k_3\omega]^2} \right\} \qquad \text{A-79}$$

10) Calculate the numerical values of Z_{N2}, $\frac{\partial Z_{N2}}{\partial \omega}$ from Equations A-70 and A-71, utilizing known values for the circuit parameters.

11) From the results of 8), 10) calculate the impedance seen to the right of terminals 5,5 in Figure A-14.

$$Z_{5,5} = 2Z_{N2} + Z_{4,4} \qquad \text{A-80}$$

12) From 9), 10) calculate

$$\frac{\partial Z_{5,5}}{\partial \omega} = 2\frac{\partial Z_{N2}}{\partial \omega} + \frac{\partial Z_{4,4}}{\partial \omega} \qquad \text{A-81}$$

13) Analogously to 6), 8), obtain

$$Z_{6,6} = \frac{Z_{oc}(jZ_{oc}\tan k_4\omega + Z_{5,5})}{(Z_{oc}+jZ_{5,5}\tan k_4\omega)} \qquad \text{A-82}$$

where from Equation A-7c and Figure A-5c $\gamma_c l_c = j\omega 2.06 \times 10^{-9}$ and $k_4 = 2.06 \times 10^{-9}$ rad/rad/sec.

14) Calculate, from 11), 12), 13) the numerical value of

$$\frac{\partial Z_{6,6}}{\partial \omega} = Z_{oc} \left\{ \frac{(Z_{oc} + jZ_{5,5} \tan k_4\omega)(jZ_{oc} k_4 \sec^2 k_4\omega + \frac{\partial Z_{5,5}}{\partial \omega})}{[Z_{oc} + jZ_{5,5} \tan k_4\omega]^2} \right.$$

$$\left. - \frac{(jZ_{oc} \tan k_4\omega + Z_{5,5})(jZ_{5,5} k_4 \sec^2 k_4\omega + j \tan k_4\omega \frac{\partial Z_{5,5}}{\partial \omega})}{[Z_{oc} + j Z_{5,5} \tan k_4\omega]^2} \right\} \quad \text{A-83}$$

15) We next compute the impedance seen to the right of terminals 7,7 in Figure A-14. From 10), 13)

$$Z_{7,7} = 2Z_{N2} + Z_{6,6} \quad \text{A-84}$$

16) From 10), 14) calculate

$$\frac{\partial Z_{7,7}}{\partial \omega} = 2 \frac{\partial Z_{N2}}{\partial \omega} + \frac{\partial Z_{6,6}}{\partial \omega} \quad \text{A-85}$$

17) As in 13) we determine next

$$Z_{8,8} = \frac{Z_{oc} (j Z_{oc} \tan k_4\omega + Z_{7,7})}{[Z_{oc} + j Z_{7,7} \tan k_4\omega]} \quad \text{A-86}$$

18) Calculate, from 15), 16), 17)

$$\frac{\partial Z_{8,8}}{\partial \omega} = Z_{oc} \left\{ \frac{(Z_{oc} + jZ_{7,7} \tan k_4\omega)(jZ_{oc} k_4 \sec^2 k_4\omega + \frac{\partial Z_{7,7}}{\partial \omega})}{[Z_{oc} + jZ_{7,7} \tan k_4\omega]^2} \right.$$

$$\left. - \frac{(jZ_{oc} \tan k_4\omega + Z_{7,7})(jZ_{7,7} k_4 \sec^2 k_4\omega + j \tan k_4\omega \frac{\partial Z_{7,7}}{\partial \omega})}{[Z_{oc} + j Z_{7,7} \tan k_4\omega]^2} \right\} \quad \text{A-87}$$

19) We next compute the impedance seen to the right of terminals 9,9 in Figure A-14. From 10), 17)

$$Z_{9,9} = 2 Z_{N2} + Z_{8,8} \quad \text{A-88}$$

20) From 10), 18) calculate

$$\frac{\partial Z_{9,9}}{\partial \omega} = 2\frac{\partial Z_{N2}}{\partial \omega} + \frac{\partial Z_{8,8}}{\partial \omega} \qquad \text{A-89}$$

21) Analogous to 17) we determine

$$Z_{10,10} = \frac{Z_{oc}\,(j\,Z_{oc}\tan k_3\omega + Z_{9,9})}{Z_{oc} + j\,Z_{9,9}\tan k_3\omega} \qquad \text{A-90}$$

where it should be noticed that between 10, 10 and 9, 9 the line is half as long as the immediately preceding sections. Therefore k_3 as in 8) above must be used in A-90.

22) From, 19), 20), 21) we can calculate

$$\frac{\partial Z_{10,10}}{\partial \omega} = Z_{oc}\left\{\frac{(Z_{oc}+jZ_{9,9}\tan k_3\omega)(jZ_{oc}k_3\sec^2 k_3\omega + \frac{\partial Z_{9,9}}{\partial \omega})}{[Z_{oc} + jZ_{9,9}\tan k_3\omega]^2}\right.$$

$$\left. - \frac{(jZ_{oc}\tan k_3\omega + Z_{9,9})(jZ_{9,9}k_3\sec^2 k_3\omega + j\tan k_3\omega\frac{\partial Z_{9,9}}{\partial \omega})}{[Z_{oc} + jZ_{9,9}\tan k_3\omega]^2}\right\} \qquad \text{A-91}$$

23) From 21) we calculate next the impedance seen across terminals 11, 11 in Figure A-14 looking to the right, Proceeding as in A-90 we see here

$$Z_{11,11} = \frac{Z_{ob}\,(j\,Z_{ob}\tan k_2\omega + Z_{10,10})}{[Z_{ob} + j\,Z_{10,10}\tan k_2\omega]} \qquad \text{A-92}$$

where line dimensions are as in 6) above

24) From 21), 22), 23) we calculate, -

$$\frac{\partial Z_{11,11}}{\partial \omega} = Z_{ob}\left\{\frac{(Z_{ob}+jZ_{10,10}\tan k_2\omega)(jZ_{ob}k_2\sec^2 k_2\omega + \frac{\partial Z_{10,10}}{\partial \omega})}{[Z_{ob} + jZ_{10,10}\tan k_2\omega]^2}\right.$$

$$\left. - \frac{(jZ_{ob}\tan k_2\omega + Z_{10,10})(jZ_{10,10}k_2\sec^2 k_2\omega + j\tan k_2\omega\frac{\partial Z_{10,10}}{\partial \omega})}{[Z_{ob} + jZ_{10,10}\tan k_2\omega]^2}\right. \qquad \text{A-93}$$

25) Calculate the numerical values of Z_{N3}, $\frac{\partial Z_{N3}}{\partial \omega}$ from Equations A-72 and A-73, utilizing known values for the circuit parameters.

26) From 23) and 25) compute

$$Z_{12,12} = Z_{11,11} + 2Z_{N3} \qquad \text{A-94}$$

27) From 24), 25), and 26) determine

$$\frac{\partial Z_{12,12}}{\partial \omega} = \frac{\partial Z_{11,11}}{\partial \omega} + 2\frac{\partial Z_{N3}}{\partial \omega} \qquad \text{A-95}$$

We can now determine the overall antenna terminal quantities $Z_{13,13}$ and $\frac{\partial Z_{13,13}}{\partial \omega}$

28) From the transmission line Equation (A-3) applied to the final section of the antenna, -

$$Z_{13,13} = \frac{Z_{oa}(jZ_{oa}\tan k_1\omega + Z_{12,12})}{[Z_{oa} + jZ_{12,12}\tan k_1\omega]} \qquad \text{A-96}$$

where line dimensions are as in 1) above.

29) Calculate from 26), 27), 28)

$$\frac{\partial Z_{13,13}}{\partial \omega} = Z_{oa}\left\{\frac{(Z_{oa}+jZ_{12,12}\tan k_1\omega)(jZ_{oa}K_1\sec^2 k_1\omega + \frac{\partial Z_{12,12}}{\partial \omega})}{[Z_{oa} + jZ_{12,12}\tan k_1\omega]^2}\right.$$

$$\left. - \frac{(jZ_{oa}\tan k_1\omega + Z_{12,12})(jZ_{12,12}k_1\sec^2 k_2\omega + j\tan k_1\omega \frac{\partial Z_{12,12}}{\partial \omega})}{[Z_{oa} + jZ_{12,12}\tan k_1\omega]^2}\right\} \qquad \text{A-97}$$

The impedance Z, in Equation A-67 can be considered equal to $Z_{13,13}$ as determined through the above computational procedure. Substituting the numerical values obtained in Equations A-96 and A-97 in Equation A-67, $\left|\frac{\partial \phi(\omega)}{\partial \omega}\right|$ can be readily computed.

APPENDIX III

REPORT ON MEASUREMENT OF COUPLING IN AND THROUGH SEA WATER

A series of measurements were performed to determine the effects of sea water (which has electromagnetic properties similar to blood on the magnetic coupling between two coils. The results were interesting but as yet unexplained.

The first approach which was tried consisted in the construction of a metal box approximately 13 x 145 x 20 inches with an 5 x 9 inch opening in one face for the purpose of coupling energy into the box. It was anticipated that a coil would be mounted within the box, and energy would be coupled into the box through the opening only (the rest of the box acting as a shield). The induced voltage in the coil would be measured by coaxial connection to a receiver. When a body of Sea water was placed in the opening a new induced voltage would be measured the change directly attributable to the presence of the sea water. However, when a cover was placed on the box opening to observe its shielding properties, it was found that a large signal was coupled through the box when totally enclosed. This kind of coupling and its magnitude would invalidate the anticipated measurements. In order to ascertain if welding the joints on the metal box would help, a measurement was performed of the attenuation offered by a standard completely enclosed box with a 2 turn miniature loop antenna on its inside. It was found that the RFI box attenuated the signal 52 db with respect to the coupling of two similar coils in air. The RFI box measurements were approximately 4 x 5 x 3 inches.

On the basis of the above results, and the time allotted, it was decided to abandon the large shielded enclosure approach and seek a simpler measurement which may offer some clues on the attenuation problem and whether it is a problem in a minimum amount of time.

The setup arrived at consists of two identical single turn circular coils spaced a fixed distance apart with their planes parallel and centers in line. These coils were constructed of formvar coated wire so that no direct connection would occur between the coil conductors and the sea water if immersion were tried.

The first set of measurements was made as a comparison of coupling between the coils for a) both coils in air and b) both coils immersed in a vessel of sea water. It was found that from 7.5 mc to 30 mc (the entire band tested) a larger signal was coupled from the transmitter coil to the receiver coil in sea water than in air with the greatest coupling improvement being observed at 20 mc (an improvement factor of nearly 7 to 1).

In the next setup, one of the coils was removed from the sea water for all measurements and the other was immersed at several depths into the sea water with the outside coil being moved to maintain the same geometric relative positioning of the two coils. For this method of measurement markedly different relative attenuation effects were observed as a function of frequency. For example, the following attenuation effects were noted. At 10 mc the greatest attenuation measurement {about (in voltage) 2.5:1} occurred with the receiver coil at the greatest depth in the sea water {about 6 inches } with a gradual lessening as the deceiving coil was brought closer to the edge of the vessel facing the transmitting coil.

At 15 mc however the position of greatest attenuation {about (in voltage) 5.5:1} did not occur at the position of greatest depth of the receiving coil, but at a point 3/4-inch from the far side of the vessel. Signal level increased in the received coil for depths greater than this point.

It was found that this position of greatest attenuation moved toward lesser depths at frequency was increased. At 18 mc it was located 4-3/8-inches in from the far side of the vessel and was about 2.5:1 in voltage (with respect to coupling through the air). Also, at 18 mc the greatest signal coupling was for the receiving coil immersed at the greatest depth in the sea water being about 2.5 times greater (in voltage) than the coupling in air. An additional test was performed where the coil in the sea water was covered by a 1/8-inch waterproof coating in order to simulate conditions with a silastic covered implant and markedly reduce the capacitance between the receiving coil and the sea water in which it was immersed. In this experiment attenuation due to the water could not be detected. In fact, at 10-20 mc, coupling between the coils increased as the fraction of the space between the coils occupied by sea water increased. At this point with the uncertainties posed by these measurements and the attendant current time limitations, measurements were halted.

For the purpose of the above measurements the immersed coils were deliberately chosen to have low self inductance {with reactance << 50 ohms} so that the voltage recorded by the receiver would be that due to the mutual coupling impedance changes and not self inductance changes. Referring to Figure III-1 the following equations can be written.

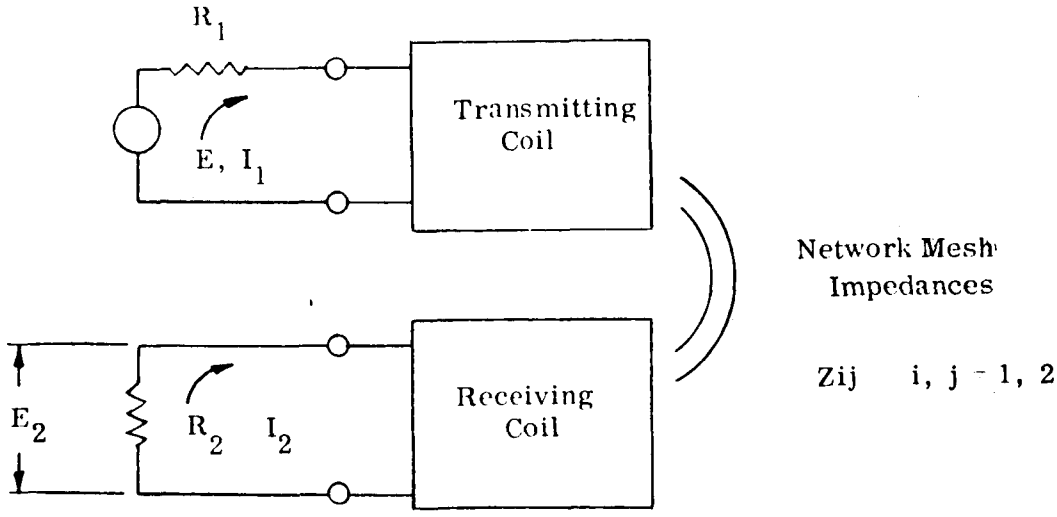

Figure III-1. General Mutually Coupled Networks

$$E_1 = I_1(R_1 + Z_{11}) + I_2 Z_{12}$$

$$O = I_1 Z_{21} + I_2(R_2 + Z_{22})$$

from which we obtain

$$I_2 = \frac{- E_1 Z_{21}}{(R_1 + Z_{11})(R_2 + Z_{22}) - Z_{12} Z_{21}}$$

Now if

$$R_1 >> Z_{11}, \quad R_2 >> Z_{22}$$

$$R_1, R_2 >> Z_{12}, Z_{21}$$

then

$$I_2 \approx \frac{- E_1 Z_{21}}{R_1 R_2}$$

Since E_i is measured and R_1, R_2 are fixed {50 ohms}, the voltage recorded at the receiver is proportional to the mutual coupling between the two coils.

However, the inconclusiveness of the tests can be partially explained by the fact that Z_{21} in the above expression can itself be expressed in terms of the self impedances of the coils as well as the coefficient of coupling between the coils; i.e. for inductive coupling

$$Z_{21} \approx j\omega M = j\omega k \sqrt{L_1 L_2}$$

Thus changes in the induced voltages can indeed be due to changes in the self impedances $j\omega L_1$ and $j\omega L_2$, especially for the cases of immersion of one or both of the coils. This consideration leads to a more refined measurement approach which could be tried if more time were available. For any particular configuration, the self impedances of both coils would be measured in order to ascertain the extent to which they are changing and producing the observed results. Then, too, the effect of R-C coupling between the transmitting and receiving coils should be measured to determine the contribution of this possible coupling effect to the observed results, and more important, to explain the mechanism behind this possible coupling effect.